ADDIS ABABA UNIVERSITY SCHOOL OF EARTH SCIENCES

SEDIMENTOLOGICAL AND GEOCHEMICAL ANALYSIS OF SEDIMENTS IN THE EXCAVATED ROCK SHELTER AT FINCHA HABERA SECTION, BALE MOUNTAIN, SOUTHEASTERN ETHIOPIA: IMPLICATIONS ON PROVENANCE (SOURCE) AND DEPOSITIONAL HISTORY

By

Trhas Hadush Kahsay

Advisor: **Dr. Balemwal Atnafu**

Co-advisor: **Prof. Asfawossen Asrat**

A Thesis Submitted to School of Graduate Studies of Addis Ababa University as Partial Fulfillment of the Degree of Master of Earth Sciences in Sedimentology and Stratigraphy.

ADDIS ABABA UNIVERSITY

SCHOOL OF GRADUATE STUDIES

SCHOOL OF EARTH SCIENCES

Sedimentological and geochemical analysis of sediments in the excavated rock shelter at Fincha Habera Section, Bale Mountain, Southeastern Ethiopia: Implications on Provenance (source) and Depositional history

By

Trhas Hadush Kahsay

Advisor: **Dr. Balemwal Atnafu**

Co-advisor: **Prof. Asfawossen Asrat**

A Thesis Submitted to School of Graduate Studies of Addis Ababa University as Partial Fulfillment of the Degree of Master of Earth Sciences in Sedimentology and Stratigraphy

January, 2019

ADDIS ABABA, ETHIOPIA

ADDIS ABABA UNIVERSITY

SCHOOL OF GRADUATE STUDIES

SCHOOL OF EARTH SCIENCES

Sedimentological and geochemical analysis of sediments in the excavated rock shelter at Fincha Habera Section, Bale Mountain, Southeastern Ethiopia: Implications on Provenance (source) and Depositional history

By

Trhas Hadush Kahsay

Approved by Examining Committee:

Name	Position	Signature	Date
Dr. Balemwal Atnafu	**Head, SES**	_____	_____
Dr. Balemwal Atnafu	**Advisor**	_____	_____
Prof. Asfawossen Asrat	**Co-Advisor**	_____	_____
Prof. Dereje Ayalew	**Examiner**	_____	_____
Dr. Mulugeta Feseha	**Examiner**	_____	_____

January, 2019
ADDIS ABABA, ETHIOPIA

Declaration of originality

I hereby declare that this is my original work prepared for the partial fulfillment of the Degree of Master of Science in the graduated School of Earth Sciences, Addis Ababa University during 2018 under the supervision of Dr. Balemwal Atnafu and Prof. Asfawossen Asrat. I certify that this thesis work contains no materials which has been accepted for award of any other degree in any university and not does it contains any materials which previously published and written by any other persons, except where due reference is made in the reference list and there citations in the text.

		Signature	**Date**
Trhas Hadush Kahsay		_____	_____
Dr. Balemwal Atnafu	**Advisor**	_____	_____
Prof. Asfawossen Asrat	**Co-Advisor**	_____	_____

January, 2019
ADDIS ABABA, ETHIOPIA

ABSTRACT

This study is about the provenance and depositional history of clastic sediments deposited in a rock shelter at the Bale Mountains, Southeastern Ethiopia. The sediment section has been excavated for archaeological study. Sedimentological and geochemical characteristics of the sediments in the Fincha Habera section, at the excavated rock shelter site have been investigated. A total of 22 sediment samples have been collected and analyzed, and the analysis results are used to determine the provenance (source) and depositional history of the sediments. The grain size analyses of the unconsolidated sediments show that the sediments range from fine to coarse (silt to silty sand) with mean particle size ranging from 11.97 to 140 µm, poorly to very poorly sorted, with standard deviation of most samples ranging from 1.829 to 5.12 µm; very fine skewed to very coarse skewed with skewness ranging from -0.378 to 0.396 µm, and platykurtic to very leptokurtic with kurtosis ranging from 0.709 to 1.537µm. The relationship between the mean grain size and sorting suggests that sedimentation took place in high energy, open fluvial depositional environments. The integrated data from the field (lithofacies associations), sedimentological analysis (grain size and magnetic susceptibility measurement), and geochemical analysis (elemental and mineralogical compositions) of the sediments has been used as a combined proxy for provenance determination. Accordingly, the integrated data suggest that the materials/sediments that are deposited in the rock shelter have a mixture of three sources: geogenic (either as endogenic or exogenic), biogenic or human induced (anthropogenic) origins. The grain size analysis (sorting), the log ratio of major elements (low log (SiO_2/Al_2O_3) value), the less mobile major elements (Al_2O_3 and TiO_2) ratio, and the mineralogical composition (i.e., predominantly of plagioclase feldspars, particularly anorthite and albite) suggests that the geogenic materials are texturally as well as chemically immature and derived predominantly from mafic source rocks. The magnetic susceptibility of the sediments is indicative of either the anthropogenic sources of some layers in the section, or significant accumulation of organic matter, as the combustion/heating of the sediments by anthropogenic activities or occurrence of sizable quantity of organic matter such as ash and charcoal deposits, respectively, can affect the magnetic susceptibility value. Furthermore, the magnetic susceptibility value of the sediments can be correlated with the Ca and P concentrations (indicators of biogenic materials).

Key words: Bale Mountain, Fincha Habera, sedimentology, provenance, depositional environment, grain size distribution

ACKNOWLEDGMENTS

I would like to acknowledge Addis Ababa and Mekelle Universities for providing me the opportunity to study my MSc in the field of Sedimentology and Stratigraphy. I would like to express my deepest thanks and gratitude to my advisors who supervised the work presented in this thesis. Professor Asfawossen Asrat has been supportive throughout the project starting from proposal writing up to the completion of my thesis. He allocated considerable amount of time for technically commenting on my methodologies, results and interpretation of results and on the write up of the thesis. He has encouraged me and shared his valuable knowledge throughout the thesis work. His door was always open whenever I needed help and he answered my questions respectfully. Thank you again! I have no enough words to express my gratitude. Dr. Balemawal Atnafu spent a lot of time to help me on a lot of technical problems and respectfully discussed and answered many of my questions. Thank you both for your patience, encouragements and guidance throughout my thesis. This thesis would not have been possible without your support.

I would also like to thank the Collaborative Research Center (CRC806) of Cologne University and the Bale Project for financially supporting me to travel to the University of Köln, Germany, and conduct my analysis in their laboratories. I would like to express my great gratitude to Dr. Ralf Vogelsang in particular, who invited me to work on my thesis within his project in the collaborative research center. He arranged field training in the Sodicho rock shelter site in southern Ethiopia, and he dedicated his valuable time for arranging all my travels to Germany, accommodation in Cologne and facilitated my laboratory work at the University of Köln. I would like also to thank Ms. Elena (PhD student at Köln University) who helped me both at Sodicho fieldwork and in the Geography Laboratory Center of Köln University. She gave me valuable information on the sampling and preparation techniques of unconsolidated sediments.

I express also my immense gratitude to Dr. Goetz, and Mr. Minassie who helped me in the fieldwork and during technical works in Köln. I would also like to thank all members of the Köln University, especially to the society of the Geography Institute of Köln University, Dr. Stefan and Ms. Marie for letting me to use their laboratories with all the organized equipment, computers and various types of softwares and for supporting me during sample preparation and analysis.

TABLE OF CONTENTS

LIST OF FIGURES

LIST OF TABLES

LIST OF ACRONYMS

a.s.l: Above sea level

BMNP: Bale Mountain National Park

cm: cent meter

CMER: Central Main Ethiopian Rift

CSa: Coarse sand

CS: Coarse silt

CS: Coarse skewed

D_{50}: Median

DEM: Digital elevation model

EARS- East African Rift System

FHL-01 to 09: Fincha Habera lithofacies 01 to 09

FHS: Fincha Habera Section

FH SS 01 to 22: Fincha Habera sediment samples 01 to 22

FoM: Figure of merit

FSa: Fine sand

FS: Fine silt

FS: Fine skewed

H_2O_2: Hydrogen per oxide

HCl: Hydro choleric acid

HE: High energy

HF: Magnetic susceptibility measurement at high frequency

K-Ar: Potassium argon dating

K_G: Kurtosis

khf: High frequency susceptibility

kHZ: Kilohertz

klf: Low frequency susceptibility

LE: Low energy

LF: Magnetic susceptibility measurement at low frequency

LK: Leptokurtic

LS13320: Beckmann Coulter Laser particle Analyzer

m: meter

MER: Main Ethiopian rift

MK: Mesokurtic

MS2B: Dual frequency magnetic susceptibility sensor

MS3: magnetic susceptibility meter

MSa: Medium sand

MS: Medium silt

MS: Medium sorted

Mz_G: Geometric mean

Na_2PO_4: sodium pentaphosphate

NITON XL3: thermo scientific Niton Xl3t analyzer

NMER: Northern Main Ethiopian Rift

NNE: North north east

PK: Platykurtic

ppm: parts per million

PS: Poorly sorted

PSDC: Particle size distribution classification

P_x: Grain diameter

Safar: Southern Afar

SD_G: Standard deviation (sorting)

SI: Standard international unit

SK_G: Skewness

SMER: Southern Main Ethiopian Rift

SY: Symmetrical

VCSa: Very coarse sand

VCS: Very coarse silt

VCS: Very coarse skewed

VFSa: Very fine sand

VFS: Very fine silt

VFS: Very fine skewed

VLK: Very leptokurtic

VPK: Very platykurtic

VPS: Very poorly sorted

Wt%: Weight percent

µm: micro meter

XRD: X-ray diffraction analyzer

XRF: X-ray fluorescence analyzer

CHAPTER ONE

1. INTRODUCTION

1.1. BACKGROUND AND JUSTIFICATION OF THE STUDY

The opening of the Main Ethiopian Rift marks the incipient plate boundary between Nubia and Somalia which was formed long after the flood basaltic magmatism (Wolfenden et al., 2004) it forms part of the roughly NE-trending East African Rift System, extending from the Afar to the Kenyan rift (Bonini et al., 2005). New petrological, structural and geochronological data indicate that the evolution of Main Ethiopian Rift and the adjoining plateaus, such as the Arsi-Bale massif, have complex structural pattern consisting of three rift segments as southern, central and northern (Bonini et al., 2005).

The Bale Mountains are situated in the southeastern highlands of Ethiopia along the eastern edge of the southern segment of Main Ethiopian Rift. These high rising mountain chains are built of Pliocene-trachytes underlain by basalt erupted from central sources subsequent to the formation of the Main Ethiopian Rift (Workineh Haro et al., 2014). The Bale massifs are bordered by some extensional grabens to the west such as the Galana graben, which represents the eastern branch of the rift, filled with sedimentary rocks, and the Ganjuli graben containing Quaternary cinder cones and fissural basaltic flows interspersed with sediments containing paleontological and paleoantroplogical evidences (Ebinger et al., 1993 cited in Gidey Woldegabriel, 2009). The main part of the massif forms a flat-topped highland of late Cenozoic volcanic rock marked by nearly E-W oriented watershed, and the two major rivers: the Wabe Shebele and the Genale, originate from this massif (Gobena et al., 1997).

The lava beds were forming the peaks and gorges on the Bale massif have been continuously carved by erosional processes (including, water, wind and glacier actions) forming some rock shelters. Subsequent erosional and depositional processes accumulated sediments including conglomeratic deposits (rounded, smooth, clast supported and poorly sorted). Preliminary excavations of such deposits and subsequent ^{14}C dating indicate the presence of archaeological records from the late Pleistocene (45.5±971 ka BP) to Holocene (Hood, 2018).

The main objective of the study is to delineate the source and depositional history of the sediments in the excavated rock shelters using sedimentological and geochemical approaches. The study includes detailed field description and subsequent laboratory analysis (grain size, magnetic susceptibility, XRD and XRF) of the sediments in order to understand the specific characteristics preserved within each sampled layer and deduce the provenance (source) and depositional processes that shaped the deposits.

1.2. General description of the study area

1.2.1 Location

The study area where the excavated rock shelter is found is located at the Bale massif, southeastern Ethiopia around 450 km southeast of Addis Ababa in the Oromiya National Region State, which is bounded between longitude of 39°40'46" to 39°48'48"E and latitudes 06°54'03" to 07°02'05"N (Fig. 1.1) and lies at 2500 m above sea level. The area lies within five woredas of Adaba (west), Dinsho (north), Goba (northeast), Delo-Mena-Angetu and Harena-forest (southeast) (Anteneh et al., 2013) (Fig.1.1).

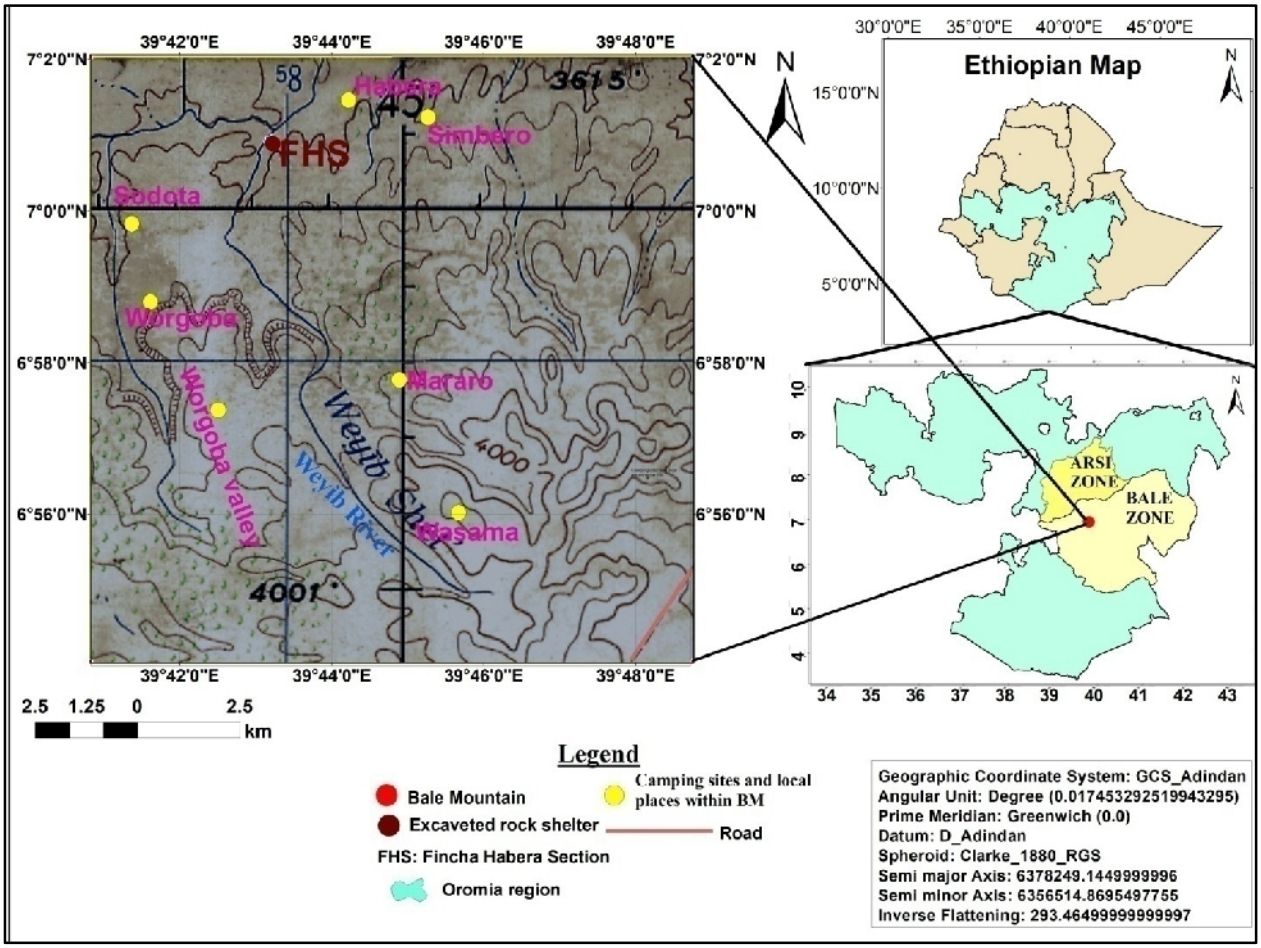

Figure 1.1. Location map of the study area.

1.2.2 Accessibility

The area is characterized by rugged topography but the study area can be accessed by good networks of footpaths, which are made for tourists within the Bale Mountain National Park boundaries. The tributaries of the two major rivers: the Wabe Shebelle and Genale rivers are located within the vicinity of the study area.

.

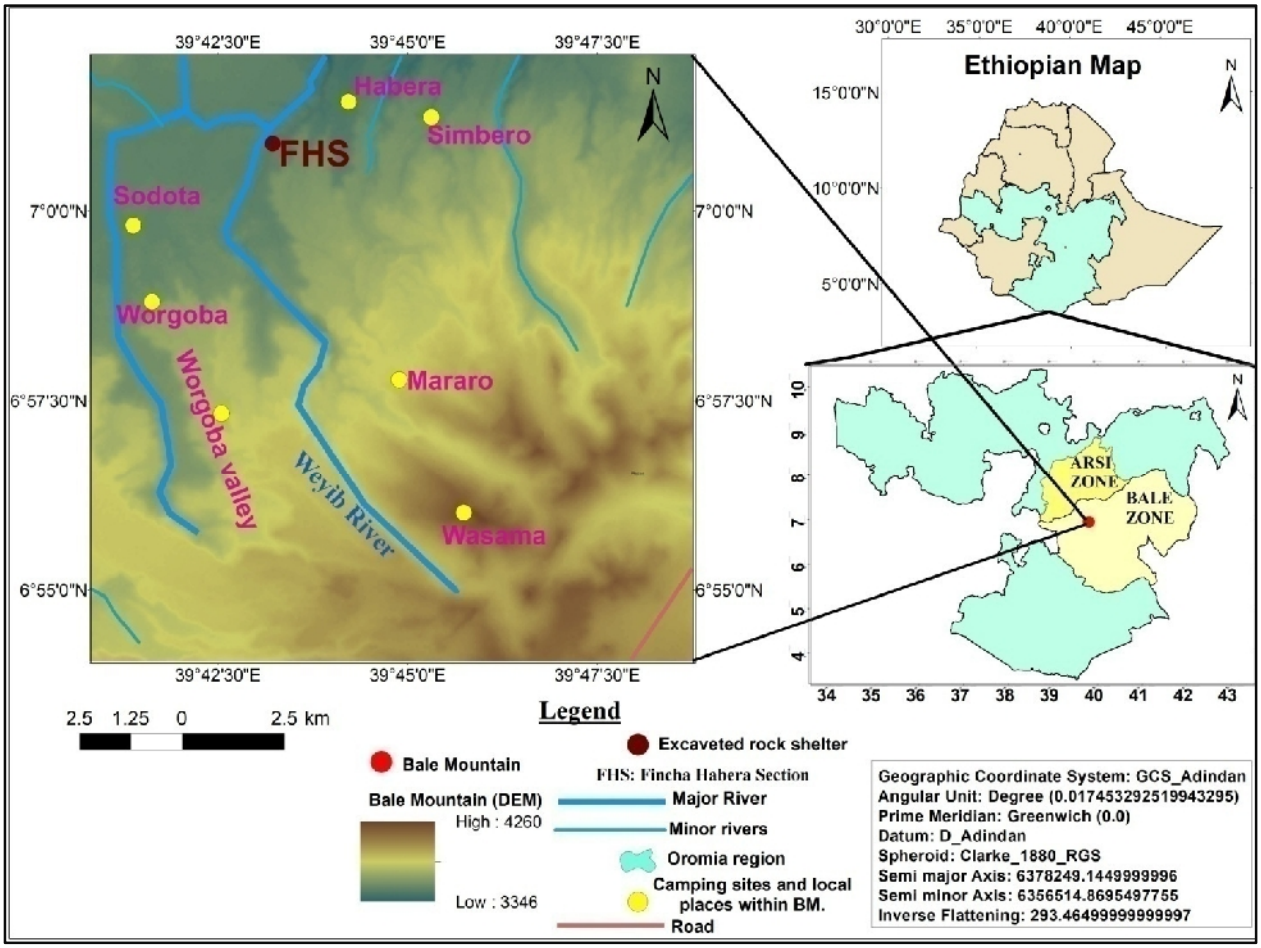

Figure 1.2. Accessibility map on a Digital Elevation Model of the study area. Note that the study area is not accessible by any roads.

1.2.3 Physiography

The study area is located on the southeastern highlands of Ethiopia, and the altitude varies from less than 3500m at the Finicha Habera (the first excavation site) to > 4000m at the highest peaks of the area: Tullu Dimtu (4377 m) and Kara Deema (4205 m). Both peaks rise from the Sanetti plateau which is located east of the shoulder of the southern segments of Main Ethiopian Rift (Gobena et al., 1997). These flat-topped highlands are built of various types of Tertiary volcanic rocks (Eberz et al., 1988; Seife Michael Berhe et al., 1987).

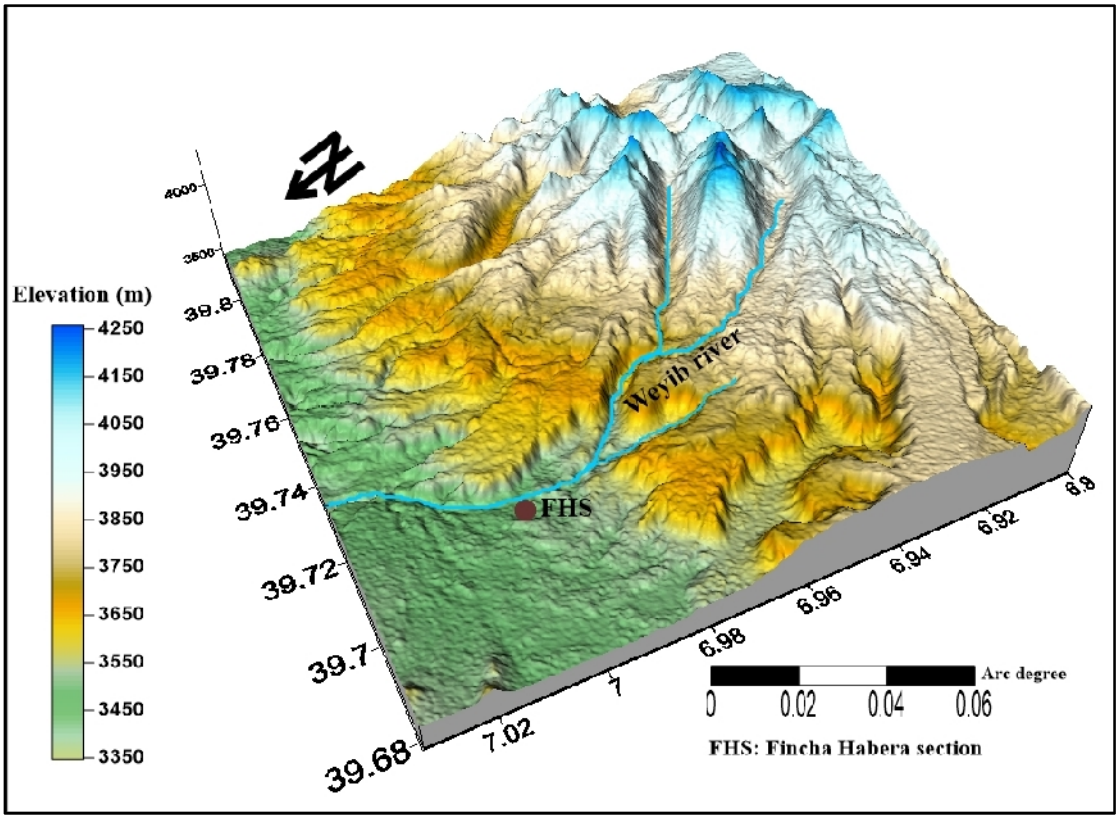

Figure 1.3. Physiographic map of Bale area.

1.2.4 Drainage pattern

The head waters of tributaries of two major rivers which rise from the Bale massif are located within the study area. These are the Wabe Shebele river to the north and its tributaries flowing northeast wards, and the Genale river flowing to the south, and one of its major tributaries, the Weyib river, flowing southeast wards. The area consist different types of drainage patterns: radial, dendritic, and sub-parallel; and consists numerous springs which originate from the volcanic centers (Gobena et al., 1997; Workineh Haro et al., 2014).

1.2.5 Climate

The Bale massif is a tropical highland with great variation in altitude and topographic features, leading to highly variable climatic conditions. The area receives rain from two sources, the equatorial Atlantic and Indian Ocean (Gobena et al., 1997). The rainfall is highly seasonal with heavy rains from July to October and small rains from March to June (Addisu Assefa et al., 2011) and the annual precipitation rises with elevation from 925mm at 2720m to 1086mm at

3500m (Umer et al., 2007). The warmest month of the year is June with an average temperature of 16.5°C and November has the lowest average temperature of the year with 14.1°C. According to Koppen and Geiger Global Climatic Classification System, this is classified as subtropical highland (oceanic) climate (Belda et al., 2014; http://en.climate-data.org/location/).

1.2.6 Vegetation

The difference in rainfall "seasonality" between the northern and southern slopes (Umer et al., 2007), the composition and mineralogical constituents of the dominant rock which are exposed in the area (i.e., basalt), and the variation in climate, altitude, and topography of the region led to the development of distinct and unique types of "plant communities" (Siebert, 2004). The Bale Mountains National Park (BMNP) is characterized by five distinct vegetation zones (Addisu Assefa et al., 2011). The Northern part of the park which has an altitude from 2600m- 3000m above sea level (a.s.l) is covered by grassland; the southeastern part (i.e., Harenna Montane Forest: 1450m– 3200m a.s.l) is covered by woodland habits. The area between 3500m and 4000m is covered by Erica shrub on the ridges and moorlands in the valley. The northern end of the park is covered by dry evergreen "montane" forests. The central massif of the park consists of an Afro-Alpine plateau (from 3200m to 4377m) covered by Erica (Umer et al., 2007).

1.3. Objectives

1.3.1 General objective

The primary objective of the study is to determine the depositional history of sediments including the provenance or source and depositional processes of the sediments accumulated in a rock shelter on the Bale Mountains, using sedimentological and geochemical approaches.

1.3.2 Specific objectives

The specific objectives include:

- Constructing detailed stratigraphic log of the excavated sections;
- Detail in-situ recording of the sedimentological features
- Detail in-situ description of all observable sedimentary features and structures
- Sedimentological analysis (grain size, magnetic susceptibility, etc.)

- Geochemical analysis (elemental and mineralogical composition of the sediments using XRF and XRD).

1.4. Basic Research Questions

In order to achieve the objectives, this research will try to address the following key questions:

- ✓ What major indices and criteria will be used to transfer the sedimentological and geochemical characteristics (i.e., magnetic susceptibility, elemental and mineralogical composition, texture, color, anthropogenic components, and other relevant physical properties) of sediments to the source (provenance) and depositional histories of the sedimentary sequence?
- ✓ How does the field data (in-situ descriptions) relate to laboratory analysis data of the sediments?

1.5. Methodology

To successfully accomplish the above mentioned objectives, the following activities and methods have been applied:

1.5.1. Pre-field work

The primary activities conducted before the fieldwork and laboratory analysis were review of previous works on the study area in particular and the region in general, including review of published and unpublished research articles, reports, other secondary data, geological maps, and satellite image interpretation. These were used to prepare base maps in order to determine the accessibility and regional geological setting. Materials and equipment for fieldwork were also identified and prepared.

1.5.2. Fieldwork

The fieldwork was conducted during two seasons: on Nov. 08-26/2017 for general survey and subsequent sampling and on Feb/Mar 2018 for verification. The main activities conducted during the actual fieldwork include:

- accessing the excavated rock shelter sites

- selecting the appropriate sections with undisturbed, unlithified, representative and fresh sediments where sedimentological information are believed to be well preserved
- graphic/stratigraphic logging of the section along with detailed observation and description of every layer: these included identification of different sedimentary features such as general observation on the textural distribution of the framework grains (determine the grain sizes visually), identification of different natural (geological) and anthropogenic components preserved within the sediment, and delineation of the contact relationships between the sediment layers
- collecting sediment samples from the northern profile of the Fincha Habera section (FHS): twenty two sediment samples were collected with a sampling interval of 1-2cm, depending on the lithological variation. The samples were collected in properly labeled plastic bags, and dully cross-recorded in a separate note book (Fig. 1.4). These samples were collected for sedimentological and geochemical analysis.

Figure 1.4. Field photograph of sediment samples collection and description from Fincha Habera section (Northern profile). Tooth picks are used as scale (i.e., to take a sample based on two centimeters), and materials used to collect the sediments include brush, shovel, plaster, plastic

sample bag, GPS, Burton compass, hand lens, camera, ruler, field notebook, pen, pencil, color pencil, eraser, and marker.

1.5.3. Sample preparation and sample analysis

After fieldwork, all collected samples were shipped to the University of Cologne, Germany. Sample preparation and all sedimentological and geochemical analyses have been conducted at the Institute of Geography, Köln University, Germany.

The dry sediment samples were first gently crushed using mortar and pestle, then sieved on a 2mm mesh size in order to separate the grains having a size of greater than 2mm (Fig.1.5). The <2mm size fraction of the sediment samples were then divided into two parts. One part is used for particle size analysis and magnetic susceptibility measurement of the sediments. Another portion was powdered and used for X-ray diffractometer (XRD) and X-ray fluorescence (XRF) analysis for the determination of the mineralogical and elemental composition of sediments, respectively. A summary of the methodologies used for sedimentological and geochemical analysis is given in Fig. 1.6.

Figure 1.5. Equipment used to sieving and grinding the sediment samples.

.

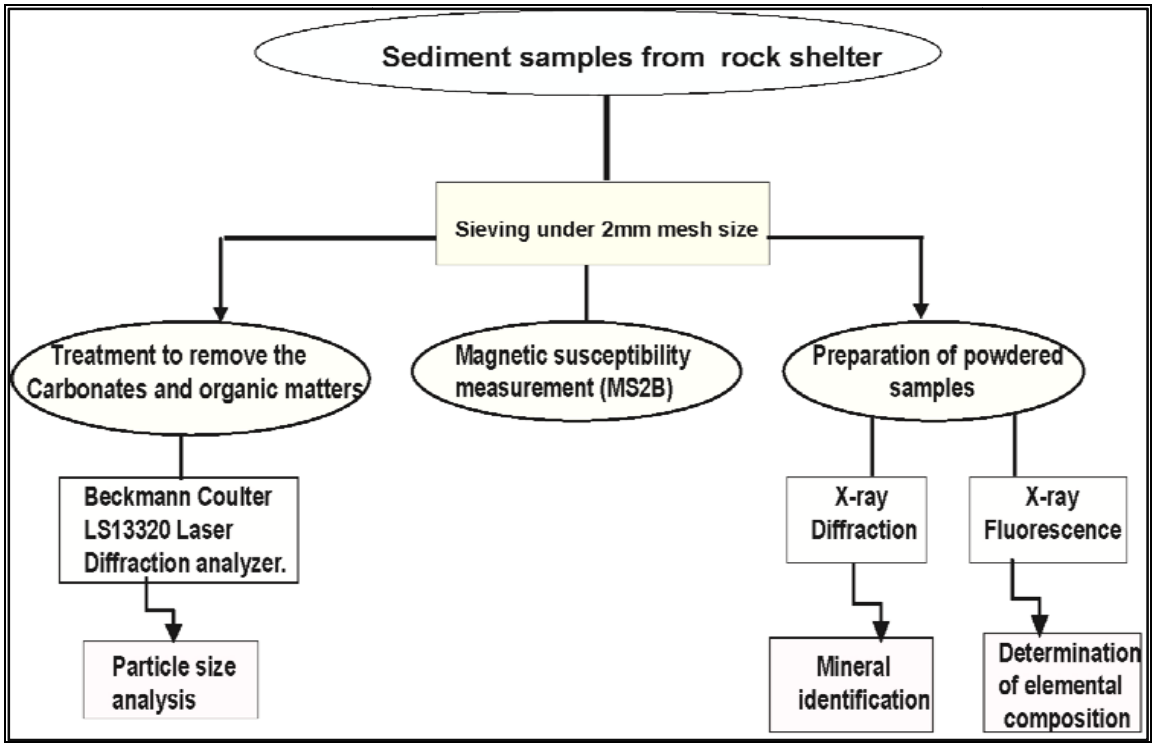

Figure 1.6. Flow chart showing summery on the different methodologies used for sedimentological and geochemical analysis of the sediments.

1.5.3.1. Grain size analysis

Laser diffraction analysis provides a determination of grain size distribution within the sediment with a wide range of particle sizes (0.04-2000µm) (Gamboa et al., 2017) and has an ability to differentiate and compare different types of sedimentary environments (Lopez, 2017).

Preparation: The ideal concentration for measuring the grain size distribution of sediments using Beckmann Coulter Laser particle Analyzer (LS13320) is between 6-20%. If the results do not fit with the ideal concentration repeat the measurement again and again. However, to avoid numerous measurements, it is helpful to perform pre-tests on the samples. This is conducted by dividing the sediment samples into different groups with quite similar grain sizes (i.e., visually and with finger testing) into clay and fine silt, silt, sandy silt-fine sand and sand, and the corresponding weights are 0.2-0.35g, 0.3-0.5g, 0.5-0.8g and 1g, respectively (Stephan Opitz: Laboratory Manual, Köln University, Germany). Then weigh the sediment samples (<2mm) on Sartorius-QM system and label them carefully. Remove the organic matter by treating the sample using 15% hydrogen peroxides (H_2O_2). After two weeks, wash and separate the sediment samples from the liquid (acid) by ROTINA 420R centrifuge machine for seven minutes with

speed (RPM) of 3500 (Fig.1.7). The sample is further treated with 10% dilute hydrochloric acid (HCl) to eliminate carbonate components. Then separate and wash it repeatedly. Further treat each sample with 1ml Na_2PO_5 and add distilled water, which is used as dispersant and prevents the sediment from coagulation. Put the samples over the Rotator (SB3) for three days. Finally the particle size analysis was done with Beckmann Coulter Laser particle Analyzer (LS13320) and data displayed with the supporting software (Fig. 1.8).

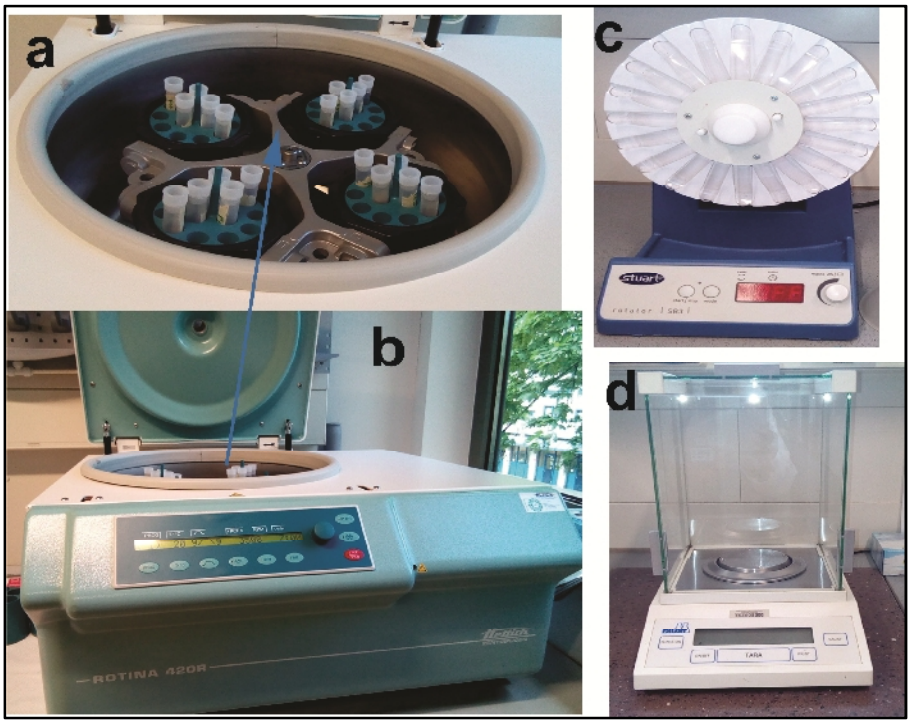

Figure 1.7. Equipment used to prepare sediment samples for Beckmann Coulter Laser particle Analyzer (LS13320): (a) the top view of image (b) ROTINA 420R Bench top centrifuge; used to wash and separate the sediment samples from liquid (acid);(c) Rotator (SB3) for effective mixing of grains within the sediment; and (d) Sartorius-QM system, used to weighing the samples.

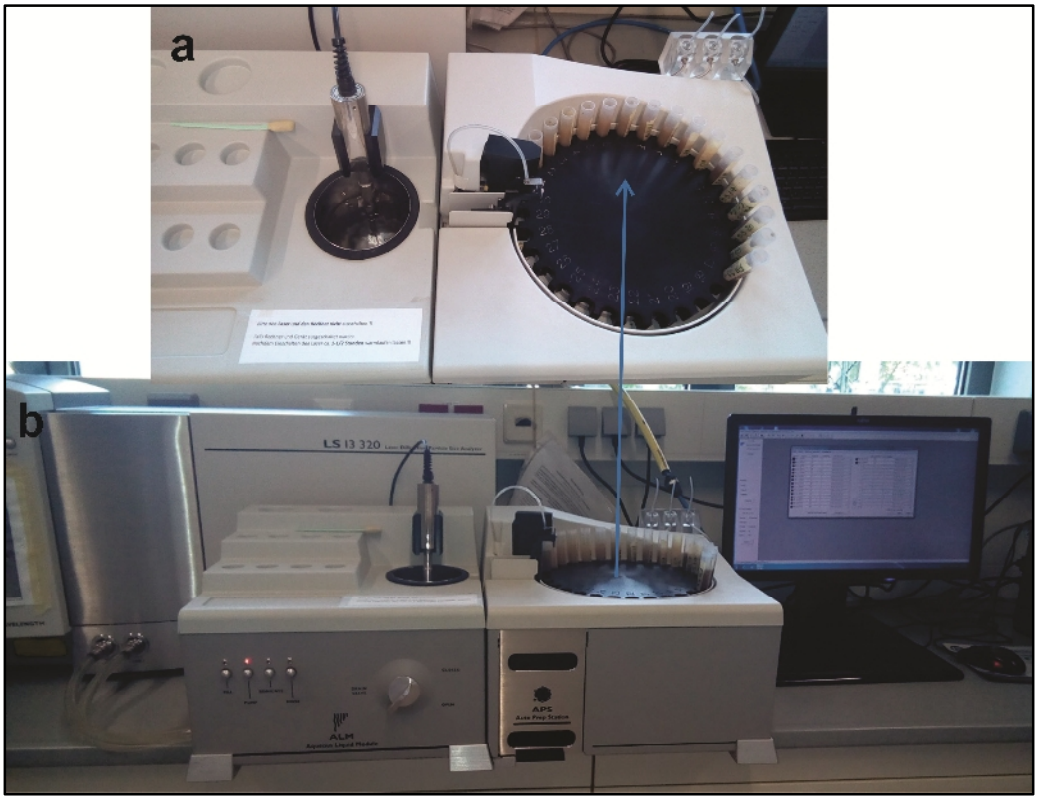

Figure 1.8. Beckmann Coulter Laser particle Analyzer (LS13320) while, image (a) is the top view of (b).

1.5.3.2. Magnetic Susceptibility

The magnetic susceptibility of sediments was measured using the Bartington Susceptibility Dual Frequency (MS2B) sensor with a low (0.465 kHz; klf) and high (4.65 kHz; khf) frequencies and the capacity allows the detection of important very fine super-paramagnetic particles within the sediments (Dearing, 1999; Gamboa et al., 2017).

Preparation and analysis: the MS2B sensor is connected to the meter (MS3), which expresses the magnetic susceptibility in the standard international unit (SI), and to the reader (computer) which displays measurements using the Bart Software. Measurement is conducted with the 1.9cm^3 ferromagnetic cassette tape. This is used to check the long-term calibration of the MS3 meter (Fig.1.9). The mass concentration (g) of the sediment samples is measured on the Sartorius-QM system. The magnetic susceptibility measurements of sediments on the MS2B dual frequency sensor are given as the average value of 3 successive measurements.

Figure 1.9. Equipment used to prepare and measure the magnetic susceptibility of sediment samples: (a) sediments sample and sample container; (b) computer with Bartsoft instrumentation Software; (c) MS2B sensor, d) cassette tape used to calibrate the sensor, (e) USB cables, and (f) MS3 meter.

1.5.3.3. Elemental composition

X-ray fluorescence is a particular well studied geochemical analytical technique to analyze the bulk chemical composition of major and trace elements (Varghese, 2004).

Preparation and analysis: the sample preparation procedure starts with sieving the sediment sample on 2mm mesh size. For the X-ray analysis the sediments were crushed with compact Retsch Mini Mill (MM 400) machine with frequency of 301/s and grinding time ranging from 30sec to 2min (i.e., depending on the strength of the sample) in order to obtain a homogeneous powder sediment, and the samples were gently pressed in small pellets. The XRF measurements were done on the pressed powder pellets with NITON Data transfer programs; this allows the NITON XL3 Analyzer to interface with the computer and use the NDT Modules to download the data from the XRF Analyzer. The mean of three successive XRF measurements is recorded (Fig. 1.10).

Figure 1.10. Equipment and analytical instruments used to measure the elemental composition of sediments: (a) different tools used to prepare the sediment samples including polypropylene thin films which helps to detect the lighter elements, notebook, plastic, pressed powder pellets, sample holder, and powdered sediment samples; (b) machine used to press the sediment samples and make it harder; (c) computer display with NITON and NDT program; (d) test stand used to hold the NITON XL3 Analyzer; (e) NITON XL3 Analyzer which is used to analyze the elemental composition of sediment samples.

1.5.3.4. Mineralogical composition

X-ray powder diffraction is a fast and reliable analytical technique particularly used to identify fine-grained minerals within the sediment (Crain, 2015). This gives a diffraction pattern of each crystalline substances and this is useful to identify and compare the components (i.e., minerals) within the sediment. This is conducted by looking on the peak of the pattern and relating it with the amount of the phase present within the sediment samples (Zou, 2016).

Preparation and analysis: the X-ray diffraction samples were prepared in the same way as for the X-ray fluorescence, except that the samples are not pressed into pellets, instead the

homogenized and powdered sediment samples are pressed on a sample holder until it shows a smooth and flat surface (Fig. 1.11, d).

Figure 1.11. Equipment used to prepare and analyze the mineralogical composition of sediments: (a) Retsch Mini Mill (MM 400), used to mill the sediments; (b) sample holder, note book, sediment samples, and isopropanol, beach sand and de-mineralized water; all used to to clean the equipments; (c) materials used to prepare sediment samples for the XRD analysis including sample holder pellets, plaster, powdered sediments sample, small shovel, brush, and marker pen; (d) prepared sample for XRD analysis; (e) X-ray diffractometer D5000 Analyzer and computer.

1.6. Significance of the research

Construction of detailed stratigraphic logs and sedimentological analysis of the sediments provide detailed information on the relationship of the logged sequence with the depositional processes. Furthermore, detailed laboratory analyses of sediments provide useful sedimentological information which help to determine the origin, physical characteristics, and processes that preserved within the sediment during and after deposition. All these could be used as input for cultural studies of the archeological remains buried within the sediments.

1.7. Review of previous works

Previous geological works in the area mostly focused on the evolution of the volcanic rocks, while there have been a considerable amount of paleo-environmental reconstruction using lake sediments, glacial deposits and peat bogs. The major regional geological studies include: lithological development, the frequency of the volcanic centers, the age of effusion, and type of activity in the area (Abbate and Saggri, 1979; Abbate et al., 2015); regional geological mapping of Cenozoic volcanic rock of Dodola area which classified rocks based on variation in lithological composition, structure, and mode of an eruption (Belay, 1978; Gobena et al., 1997); geochronological (K-Ar) dating with detailed geological mapping to distinguish the flood basalt and the shield volcano in western and southeastern Ethiopia (Seife Michael Berhe et al., 1987); and the geological mapping, geochemical analysis of stream sediment, and gravity survey of the Assela area (Workineh Haro, 2014). Sedimentological and glacial characteristics of lake sediments at Bale Mountain has been carried out (Umer et al., 2007; Tiercelin et al., 2008), who indicated the Holocene age sediments that are deposited on the high mountain ranges of the Bale massif marked the change of sedimentation from clastic to organic lake deposits in response to increase in moisture and temperature.

Understanding the depositional history and provenance of the sediments in the rock shelters will, therefore, add further insight into the climate history of the period covered by the sedimentary record, in addition to shedding light on the local depositional and environmental history.

CHAPTER TWO

REGIONAL GEOLOGICAL SETTING

2.1. THE CENOZOIC VOLCANIC HISTORY OF ETHIOPIA

According to Merla et al. (1979) and Abbate et al. (2015), the volcanic rocks of Ethiopia have been classified into five major provinces: (i) volcanites of the Northern Ethiopian plateau; (ii) southwestern Ethiopia volcanites; (iii) volcanites of the Somali plateau ;(iv) southern Ethiopian volcanites; (v) Afar and Main Ethiopian Rift volcanites. These all are classified based on their difference in lithological development, frequency of their eruption, and age of their effusions.

2.1.1. Geology and volcanites of the Somali plateau

The Ethiopian plateau volcanites also collectively called as “traps” are the first major volcanic activity during the Cenozoic characterized by fine-grained stratoid volcanites (Merla et al., 1979). The huge Plio-Quaternary volcanic complex of the Bale Mountain is a typical morphological feature in the Somali plateau (Abbate et al., 2015) rested on the Arussi and Bale basalts (upper Oligocene-upper Miocene) (Merla et al., 1979) and this massif is covered in some localities by Pleistocene glacial deposits (Abbate et al., 2015).

2.1.2. Geology of Southeastern Ethiopia

The volcanically and seismically active Main Ethiopian Rift (MER) system divides the 1000km wide uplifted Ethiopian volcanic province asymmetrically into the northwest and southeast plateaus (Gidey Woldegabriel et al., 1990; Ebinger et al., 1993). The Ethiopian flood basalt erupted in three major stages and one localized episode; stage one mainly covered southwestern Ethiopia and it is older than 40Ma, which was separated from the second stage (34Ma-30Ma) by an unconformity. Cenozoic volcanism on the plateau on eastern side of the Main Ethiopian Rift commenced with the third stage and ranges in age from 30-26Ma (Seife Michael Berhe et al., 1987) (Fig. 2.1).

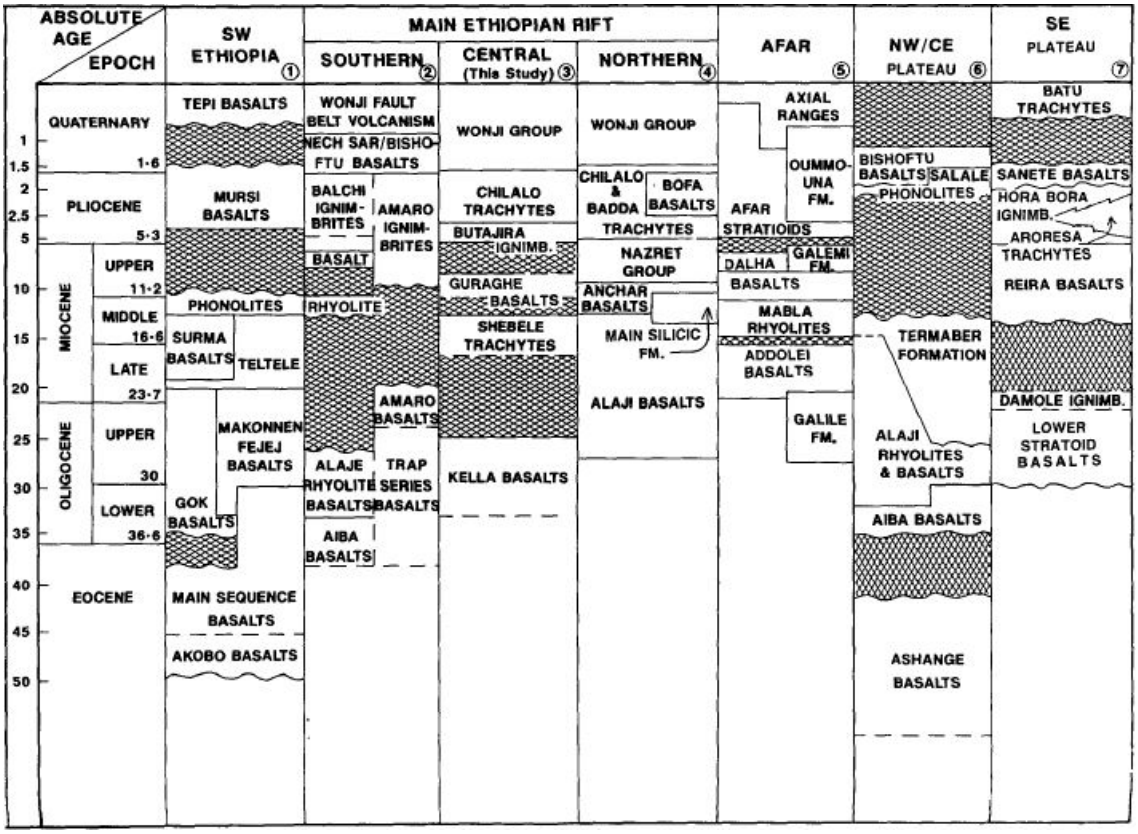

Figure 2.1. Correlation chart of Cenozoic volcanic rocks in Ethiopia; the volcanic succession of southeastern Ethiopia plateau is marked in the last column (from Gidey Wolde Gabriel et al., 1990).

According to Seife Michael Berhe et al. (1987), K-Ar dating with detailed geological mapping enabled to distinguish the flood basalt and the shield volcano in western and southeastern Ethiopia. The Cenozoic volcanic province of the Bale area is characterized by a succession of basalt and trachytes with thickness of up to 2300m (Fig. 2.1 and 2.3). These are from the oldest to the youngest: The Lower Stratoid Basalts, the Reira Basalts, the Dodola and Aroresa Trachytes; the Sanete Basalts; and the Batu Trachytes.

In addition, Gobena et al. (1997) recognized eight major volcanic map units from the 2400m thick Bale massif volcanic succession, from older to younger: (i) aphyric (aphanitic) to porphyritic basalt (composed of plagioclase and opaque oxides) and lesser occurrence of vesicular basalt; (ii) ankaramite (porphyritic basalt with 5 to 10mm long pyroxene phenocrysts); (iii) alkali trachyte flows with some plugs (the plug forming alkali trachyte has well cleaved phenocrysts of sanidine minerals); (iv) aphanitic basalt (the dominant rock type in the area); (v)

trachytic tuff with minor basalt and alkali trachyte flow;(vi) inter layered alkali trachyte and basaltic flows, (vii) alkali trachyte flow and minor plugs (this occur as both flows and plugs and the highest peak of the area, Tulu Dimtu,is formed of this type of rocks); and (viii) the scoriaceous basalt (the youngest volcanic unit of the area). Vertical to sub vertical trachytic and to a lesser extent basalt dikes commonly cut across the various layers of the older basalts (Workineh Haro, 2014). The rock shelters are formed under such dikes within the younger sequence of the lava flows.

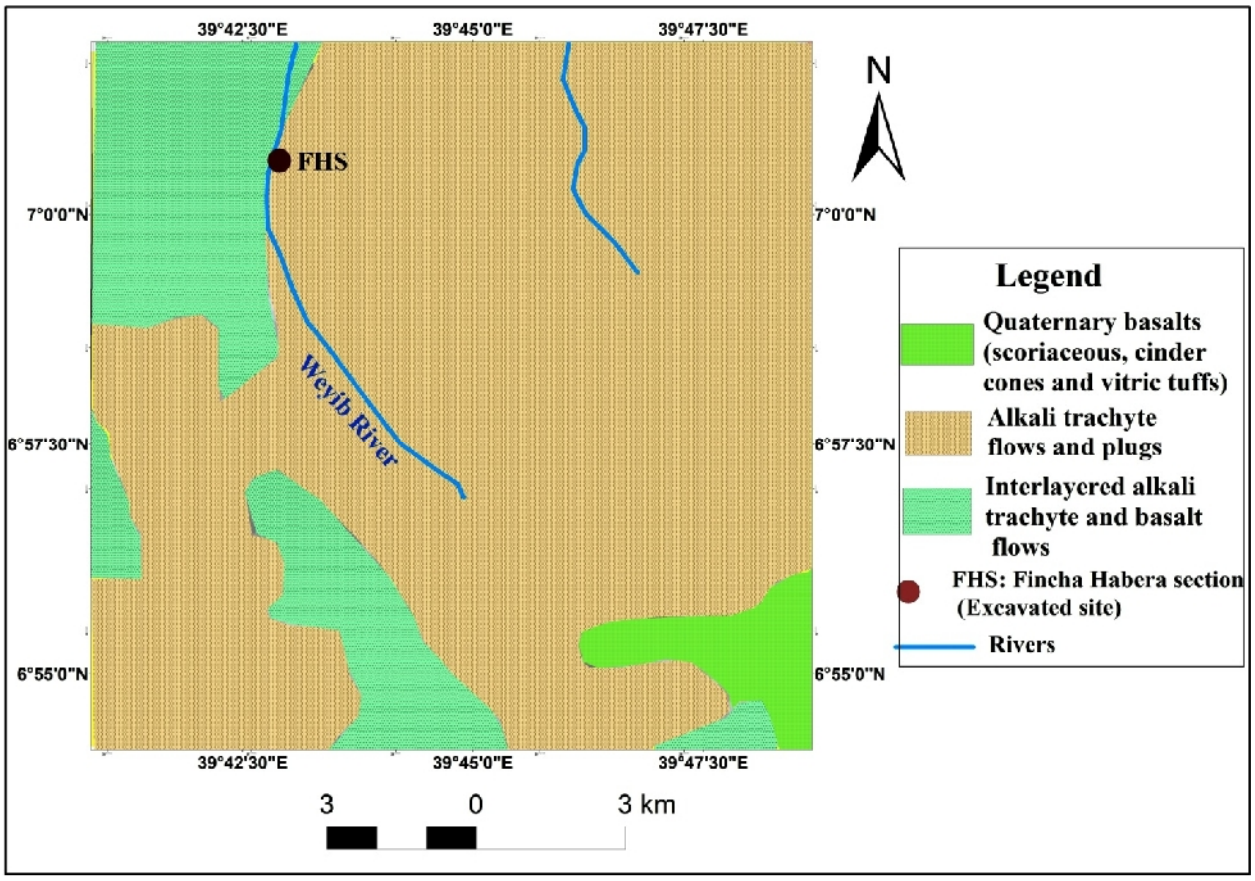

Fig. 2.2. Simplified geological map of the Bale Mountains, southeastern Ethiopia Highlands (Gobena et al., 1997) (modified from Asfawossen Asrat, 2016).

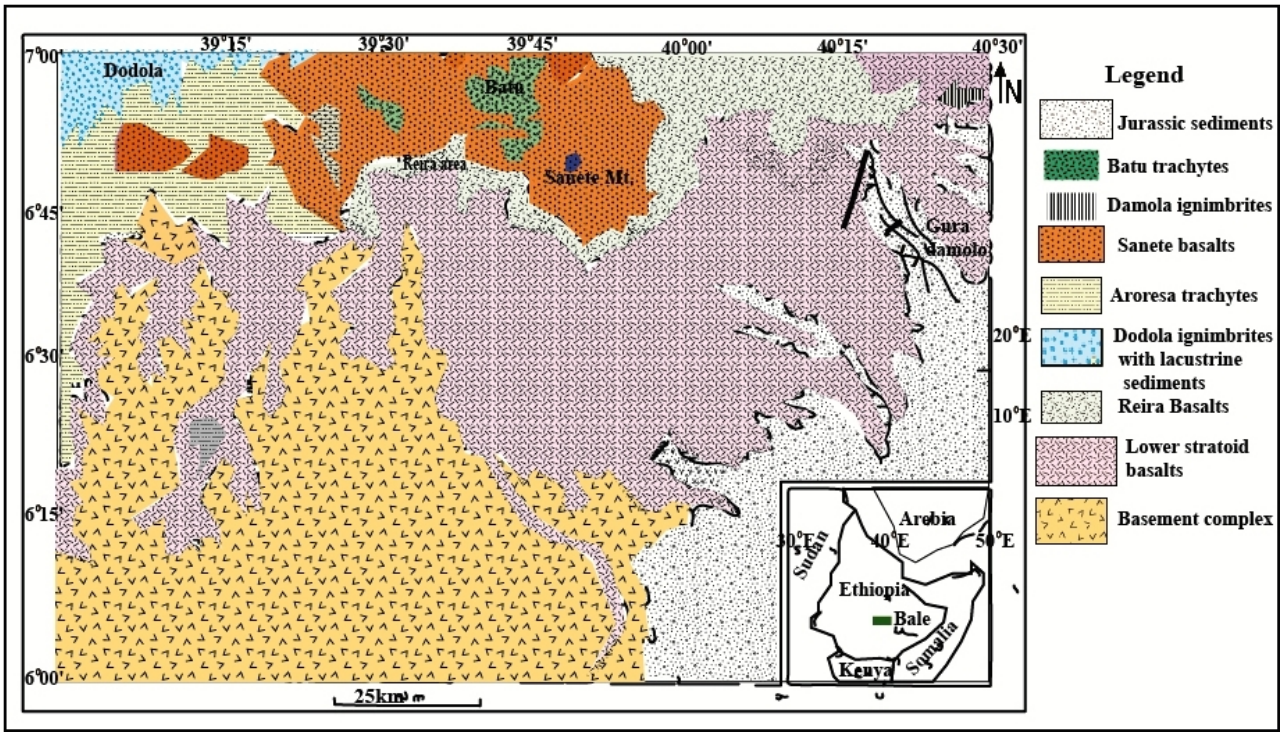

Figure 2.3 Simplified geological map of Cenozoic volcanic rocks of the Bale area, SE Ethiopia (modified from Seife Michael Berhe et al., 1987)

There have been some studies on lake sediments from the Bale Mountain area which could be used as reference framework for comparison with sedimentological analysis from the sediments in the rock shelters. Such lake records indicate evidence of Quaternary glaciations in which the accommodation spaces are filled by monogenic sediments which originated from the erosion of trachytic tuff (Tiercelin et al., 2008).

2.2. Tectonic Evolution and volcanism of the Main Ethiopian Rift

The East African Rift System (EARS) is an active continental rift which began to develop around the onset of the Miocene (22-25Ma) and marks the incipient plate boundary between Nubia and Somalia from Djibouti to Mozambique (Bonini et al., 2005). The Ethiopian rift is part of the EARS and consists two main physiographic segments, namely the northeastern sector (the Main Ethiopian Rift: MER) and the southern Afar sector (SAfar) (Corti, 2009) (Fig. 2.4).

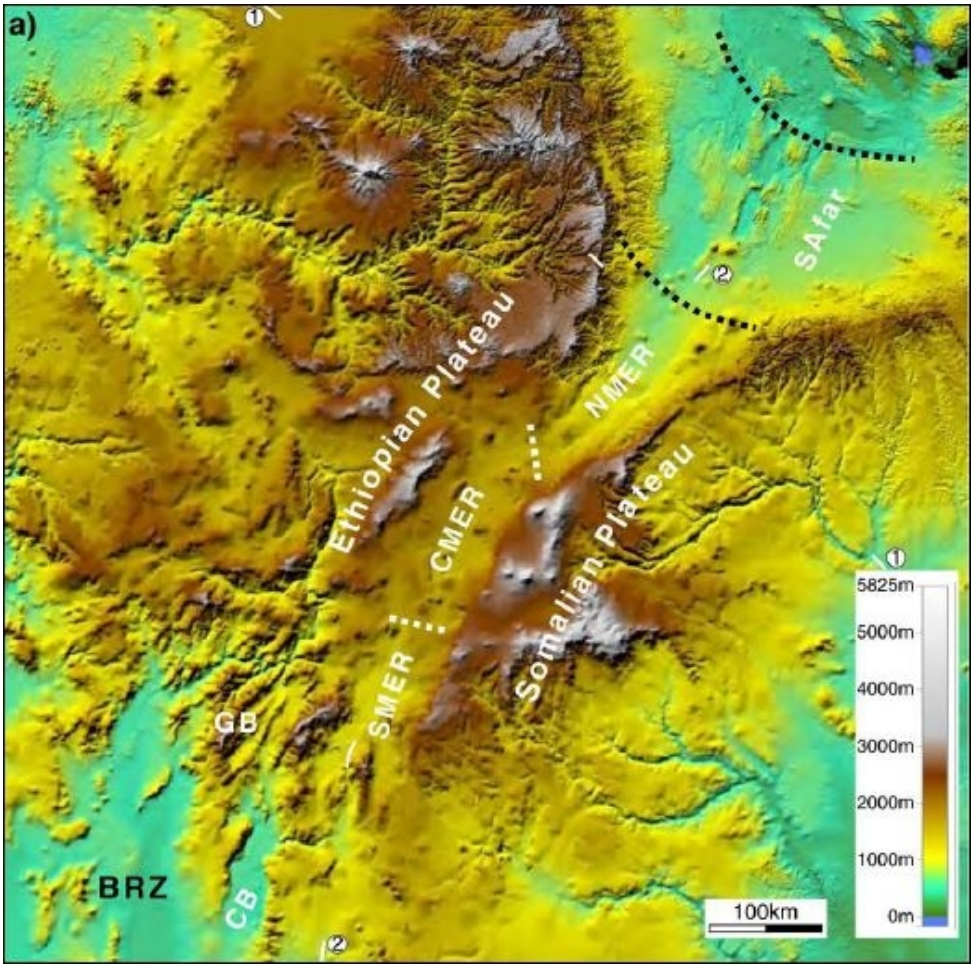

Figure 2.4 Digital elevation model (SRTM data) of the Main Ethiopian Rift (MER) showing the main rift segments: Southern Afar (SAfar), Northern MER (NMER), Central MER (CMER) Southern MER (SMER), and the adjoining plateaus (from Corti, 2009).

New stratigraphic, structural and chronological data indicate that the MER marks the early plate boundary between Nubia and Somalia which is formed long after the flood basaltic magmatism (Wolfenden et al., 2004) and this region represents the northernmost branch of the EARS (Kurz et al., 2007; Kurkura Kabeto et al., 2009) which trends NE across the Ethiopian plateau (Keranen and Klemperer, 2008). The MER is a magmatic rift that records all stages of rift evolution from rift initiation to breakup and incipient oceanic spreading (Corti, 2009).

The change in age, geochemical character as well as the complex history and nature of the MER reflects the tectonic evolution of the rift (Boccaletti et al., 1999). The MER and the adjoining plateaus, such as the Arsi-Bale massif have a complex structural pattern and can be divided into

three rift segments: the southern (SMER), central (CMER) and northern (NMER) (Fig. 2.4) with varying morphology and tectonic evolutions (Gidey Woldegabriel, et al., 1990; Bonini et al., 2005).

The southern MER is affected by extension in the early Miocene (21-20Ma) due to northern propagation of the Kenyan rift related deformation (Bonini et al., 2005). Reconstruction of fault geometry indicates that the minimum extension of the rift is approximately 12km (Ebinger et al., 1993) and the extensional basin is bounded by fault escarpment and uplift flanks (Hayward and Ebinger, 1996). The central sector of the MER on the other hand was formed in two stages: an early stage from late Oligocene to early Miocene of series of alternating half grabens with major faults replaced in late Miocene to early Pliocene by the present stage of mostly symmetrical and synthetic rift margins with increment of the rate and diversity of volcanism (Gidey Woldegabriel et al., 1990). The maximum age (10Ma) of tectono-magmatic activity represents the onset of modern rift margin development and rift shoulder volcanism in the northern segment of the MER (Tadiwos Chernet et al., 1998).

CHAPTER THREE

FIELD DESCRIPTION OF SEDIMENTS

3.1. General description of the rock shelter site at Fincha Habera section

Fincha Habera rock shelter (7°00'17"N latitude; 39°43'12"E longitude; 3467m a. s. l.) is located close to a tourist camping site of the same name in the Bale Mountains National Park, south of Dinsho town. The rock shelter is formed in the aphanitic basalt flow (black to gray colored depending on degree of weathering), under which are deposited smooth, rounded to spherical, platty, clast-supported conglomeratic sediments (Fig. 3.1). The rock shelter, opened towards east, is exposed by the north-south flowing Weyib River. The sedimentary deposits are of late Pleistocene to Holocene age (based on ^{14}C dating of charcoal recovered from the deposits) (Hood, 2018). First excavation of the site started on the 08/11/2017.

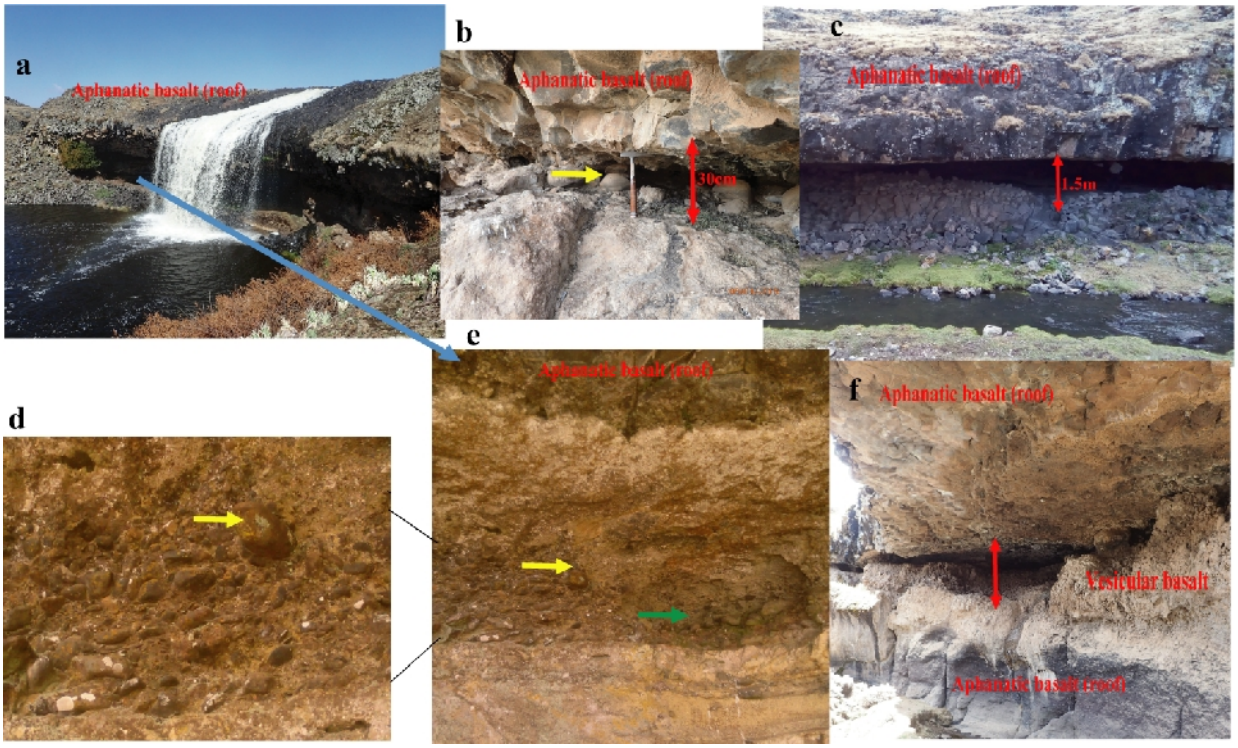

Figure 3.1. Field photographs of the Fincha Habera rock shelter (a) Fincha Habera waterfall and rock shelter site, view towards west; (b) closer view of the rock shelter and the conglomeratic deposits (height of the opening is ~30cm); (c) the excavated rock shelter site (Fincha Habera: 7°00'17"N latitude; 39°43'12"E longitude); the height of the opening is ~1.5m while the thickness

of the sediment deposits is ~55cm); (d) and (e) rounded, smooth, massive, clast (pebbles)-supported, poorly sorted conglomeratic deposits found between the lava beds; rounded gravel (marked by yellow arrow) indicates long distance of transportation; small grooves in the deposit (marked by green arrow) indicate erosion of the pebble clasts; and (f) signs of progressive deepening of the rock shelter due to rock fall from the roof and walls of the lava beds.

3.1.1. Lithofacies description of the profile

Recording of sedimentary litho facies involves visual description of textural features (i.e., grain size, shape, and sorting), the contact relationship between layers, and color of the sediments in vertical profile. These all give some clues about the depositional history of the sequence (Davies, 2008; Silva et al., 2017), and are used for comparison and correlation of different sections (Wright et al., 2017).

The following physical properties were used to define the profile of the sedimentary succession in the field: texture (i.e., visual description of grain sizes and distribution), color, thickness, and the contact relationship between the sedimentary layers. However, irregular distribution and varying thickness of the vertical profile is apparent and this could be related to the type of parent material, topography, cultural activity, and the sensitivity of the deposits against different types of weathering agents (Silva et al., 2017).

In this study, the northern profile of the excavated Square E8 (1×1m) of the Fincha Habera section (Fig.3.2.) was described and sampled. The vertical sequence of this profile, with a total thickness of 55 cm, consists more or less rock free succession and is less affected by anthropogenic activities. The following sedimentary facies were identified from younger to older (from top to bottom) (Fig.3.2):

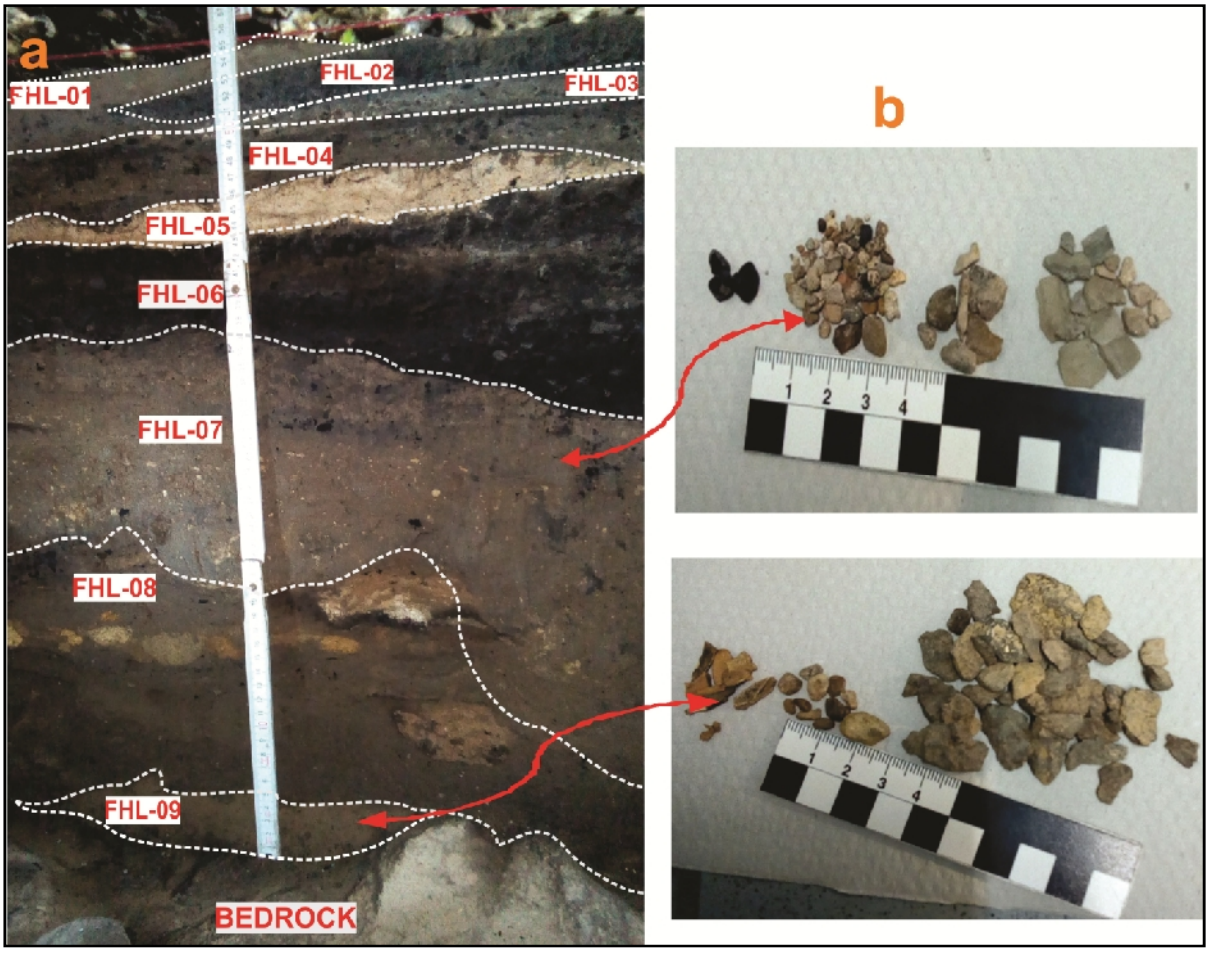

Figure 3.2. Field photograph of lithofacies association from the northern profile; Fincha Habera Section; Square E8: (a) FHL: Fincha Habera Layers/lithofacies and 01 to 09: number of layers (lithofacies) from younger to older (from top to bottom), respectively, (b) gravel size (i.e., size >2mm) sediments recovered from sieving on 2mm mesh size of some of the layers.

Lithofacies-01 (FHL-01)

The sediment in this layer appears as young topsoil with a thickness of about 3cm, fine grain size, dark grayish brown (10YR4/2), very loose soil, highly weathered, and disturbed by human and animal trampling.

Lithofacies-02 (FHL-02)

Macroscopically this layer is characterized by burned, black (10YR2/1), fine grain size sediments which incorporate boulders of ecofacts (i.e., charcoal). This unit has an average vertical thickness of 3cm and shows a pinching out lateral contact.

Lithofacies-03 (FHL-03)

This unit has a thickness of about 1cm, and is laminated, clay size, dark brown (10YR3/3), and moderately compact than the upper two layers. This unit shows gradual contact with the lower and the upper layers.

Lithofacies-04 (FHL-04)

This tabular unit with thickness of 3cm is dark gray (10YR4/1), silt size, and with a small amount of ecofacts (i.e., charcoal). It is moderately compact, bedded, and shows a gradual contact with the upper layer and sharp planar contact with the lower layer.

Lithofacies-05 (FHL-05)

This unit has a vertical thickness of about 3cm and distinguished by its brown (7.5YR5/3) color, highly altered sediments and consists of sizable quantity of burned and broken bones with charcoal. This unit shows a sharp planer contact with the upper and lower layers.

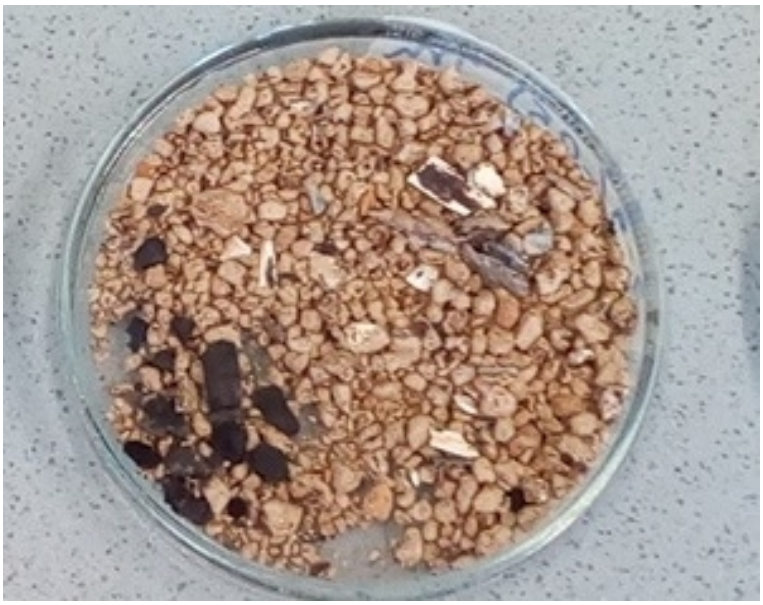

Figure 3.3. Highly altered brown color sediments with charcoal and burned broken bones recovered from sieving on 2mm mesh size of sediments (FH SS-05).

Lithofacies-06 (FHL-06)

The vertical thickness of this layer is wide-ranging and increases laterally from 6cm to 10cm toward NNE. In the field, the sediment of this layer is difficult to recognize, because it is highly

affected by anthropogenic activity and consists black (10YR2/1), burned sediments with a maximum amount of charcoals.

Lithofacies-07 (FHL-07)

This stratified unit has a varying lateral thickness from 18cm to 24cm to ward NNE. It is composed of compact, poorly sorted, wet, and light brown (10YR6/2) sediments with a variety of rock fragments (Fig 3.4). This unit has sharp planer contact with the above layer, whereas it is disconformably deposited over the lower layer. This unit has a maximum amount of obsidian artifacts, bone, and coprolites.

Figure 3.4. Rock fragments and ecofacts (charcoal) recovered from sieving on 2mm mesh size of sediments from lithofacies FHL-07 (FH SS 07 & FH SS 08). While, (a) charcoal, (b) different source (mixed) of rounded and poorly sorted grains, (c) black color, angular shaped fine grained rock fragments (i.e. aphanatic basaltic), (d) light color, fine-grained, angular shape rock fragments (trachytic).

Figure 3.5. Different organic remains and artifacts occurred within the sediment deposits. (a) Coprolites (i.e., trace fossils (ichofacts) indicate the repeated occupation of the shelter by spotted hyenas), (b) bone and teeth of small animals (i.e., rodents: which might have been eaten by humans or dead and buried within the sediment deposits), (c) obsidian artifacts recovered from lithofacies FHL-07 and top part of lithofacies FHL-08 (i.e., indicates of human settlement inside the rock shelter) (image from Goetz and Minassie, 2018).

Lithofacies-08 (FHL-08)

This layer has varying vertical thickness from 16cm to 6cm laterally towards NNE. It consists of grayish brown (10YR5/2) sand size sediments with a significant number of fragments of obsidian artifacts. This unit has a sharp and planer contact with the lower layer. Its distinctive property is the inclusion of brown colored rounded shape burned sediment deposits.

Lithofacies-09 (FHL-09)

This unit is the oldest succession and has a thickness of 4 cm, brownish yellow (10YR6/6), poorly sorted gravely and sand size sediment deposits. It has a sharp and planar contact relationship with the upper layer and lies over the aphanitic basalt bedrock.

Figure 3.6. Rock fragments and bones recovered from sieving on 2mm mesh size of sediments from lithofacies FHL-09. Where, (a) broken bone (b) highly rounded and poorly sorted mixed grains, (c) black color, angular shape and fine grained volcanic rock fragments (i.e. aphanatic basalt).

CHAPTER FOUR

RESULTS

4.1. SEDIMENTOLOGICAL CHARACTERISTICS OF THE SEDIMENTS

4.1.1. Grain size analysis

Grain sizes and their distributions are the fundamental property of unconsolidated sediments, and grain size analysis is used to classify different types of sediments, to determine the depositional environments, and to explain the energy associated with the transporting mechanisms at the time of depositions (Blott and Pye, 2001; 2012; Varghese, 2014; Switzer and Pile, 2015; Lopez, 2017).

In this study, grain size analysis of 22 treated sediment samples was performed using Laser Diffraction Analyzer. The particle size detection limit of the analyzer ranges from 0.04-2000µm. The analysis of grain size parameters including mean (the average size), sample sorting (the standard deviation of the grain size distribution), skewness (deviation of grain size distribution from symmetrical), and kurtosis (degree of curvature near the mode of the grain size distribution) of sediments are calculated on the GRADISTAT (Version-8) Microsoft excel spread sheet program using the Folk and Ward (1957) graphical methods (Table 4.1). The sediments are polymodaly distributed in nature (i.e., indicates more than two modes/populations of grains) and the grain size distribution curves are non-uniform (i.e., show more than two peaks at the curve) (Fig.4.1). However, the Folk and Ward graphic measures of grain size parameters were adopted based on two or three points read from the cumulative curves. The parameters calculated geometrically and the result is expressed in metric units (µm) (Table 4.3 and Table 4.5). The GRADISTAT program also allows the classification, description and naming of unconsolidated sediments based on the relative proportion of sand and silt size percentages of sediment samples (Blott and Pye, 2001) (Table 4.3, Table 4.4, and Table 4.5). In terms of graphical out put the program provides grain size classifications on ternary diagrams (Fig. 4.4).

Mean	Standard Deviation
$M_G = \exp\frac{\ln P_{16} + \ln P_{50} + \ln P_{84}}{3}$	$\sigma_G = \exp\left(\frac{\ln P_{16} - \ln P_{84}}{4} + \frac{\ln P_5 - \ln P_{95}}{6.6}\right)$
Skewness	**Kurtosis**
$Sk_G = \frac{\ln P_{16} + \ln P_{84} - 2(\ln P_{50})}{2(\ln P_{84} - \ln P_{16})} + \frac{\ln P_5 + \ln P_{95} - 2(\ln P_{50})}{2(\ln P_{95} - \ln P_5)}$	$K_G = \frac{\ln P_5 - \ln P_{95}}{2.44(\ln P_{25} - \ln P_{75})}$

Sorting (σ_G)		Skewness (Sk_G)		Kurtosis (K_G)	
Very well sorted	< 1.27	Very fine skewed	$^{-}$0.3 to $^{-}$1.0	Very platykurtic	< 0.67
Well sorted	1.27 – 1.41	Fine skewed	$^{-}$0.1 to $^{-}$0.3	Platykurtic	0.67 – 0.90
Moderately well sorted	1.41 – 1.62	Symmetrical	$^{-}$0.1 to $^{+}$0.1	Mesokurtic	0.90 – 1.11
Moderately sorted	1.62 – 2.00	Coarse skewed	$^{+}$0.1 to $^{+}$0.3	Leptokurtic	1.11 – 1.50
Poorly sorted	2.00 – 4.00	Very coarse skewed	$^{+}$0.3 to $^{+}$1.0	Very leptokurtic	1.50 – 3.00
Very poorly sorted	4.00 – 16.00			Extremely leptokurtic	> 3.00
Extremely poorly sorted	> 16.00				

Table 4.1. Geometric Folk and Ward (1957) graphical measures and statistical formulas used to calculate the grain size parameters. Where Px: is grain diameter in metric (µm) at the cumulative percentile value of x (Blott and Pye, 2001).

Grain size Phi	mm	Descriptive term	
>-6	>64	Boulder	
-5	32	Very coarse	Gravel
-4	16	Coarse	
-3	8	Medium	
-2	4	Fine	
-1	2	Very fine	
0	1	Very coarse	Sand
Micron			
1	500	Coarse	
2	250	Medium	
3	125	Fine	
4	63	Very fine	
5	31	Very coarse	Silt
8	16	Coarse	
7	8	Medium	
8	4	Fine	
9	2	Very fine	
		Clay	

Table 4.2. The Udden (1914) and Wentworth (1922) Grain size scale for clastic sediments used in the GRADISTAT program. Where, millimeter and micron used to different sizes on scale and phi value is $-\log_2$ of the grain diameters (modified from Blott, 2010).

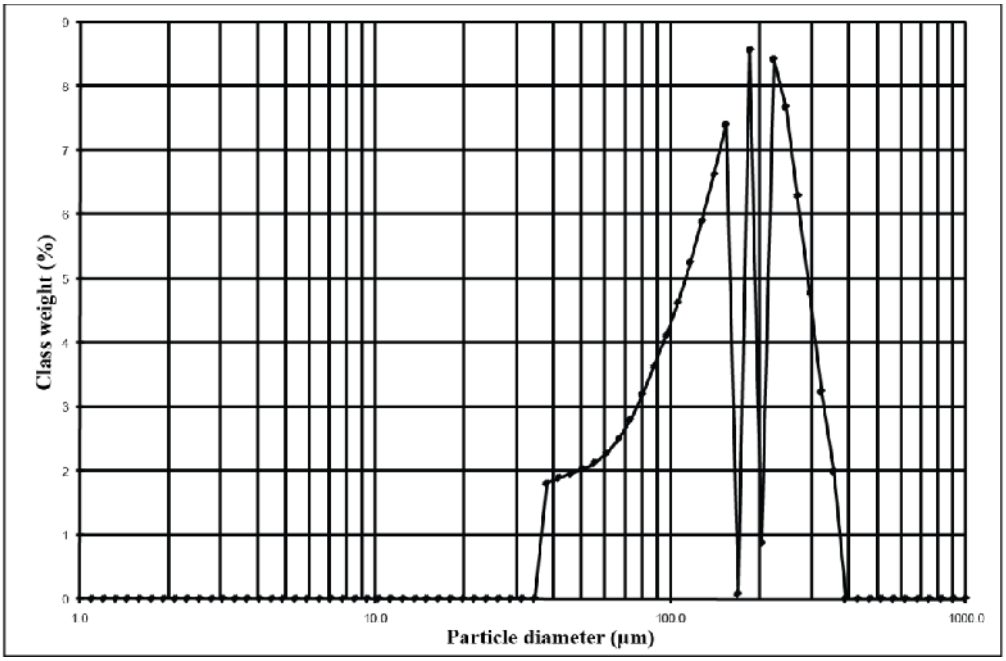

Figure 4.1. Frequency curve of sediment sample FH SS 22 with several peaks indicating the presence of more than one population (mode) of grains (i.e., polymodal distributed sediments) (Folk and Ward, 1957; Switzer and Pile, 2015).

Table 4.3. Grain size analysis of sediments at Fincha Habera Section.

Sample Id	Depth (cm)	Lithofacies	Sand (%)	Silt (%)	Mz_G (µm)	SD_G (µm)	SK_G (µm)	K_G (µm)	D_{50} (µm)	PSDC
FH SS 01	0-2	FHL-01	0	100	11.97	2.383	-0.004	0.92	11.86	Silt
FH SS 02	2-4	FHL-02	17.00	83	19.9	3.432	0.281	1.097	16.28	Sandy silt
FH SS 03	4-5	FHL-03	15.5	84.5	17.6	3.941	0.36	1.537	23.56	Sandy silt
FH SS 04	5-7	FHL-04	31.2	68.8	35.41	4.983	0.356	0.862	15.25	Sandy silt
FH SS 05	7-9	FHL-05	23.3	76.7	27.28	2.878	0.135	0.884	25.07	Sandy silt
FH SS 06	9-17	FHL-06	42.8	57.2	45.87	4.702	0.067	0.777	43.74	Sandy silt
FH SS 07	17-19	FHL-07	20.8	79.2	19.89	4.226	0.284	0.931	14.67	Sandy silt
FH SS 08	19-21	FHL-07	23.1	76.9	22.37	4.381	0.279	0.895	16.04	Sandy silt
FH SS 09	21-23	FHL-07	22.6	77.4	20.76	4.139	0.277	0.89	15.49	Sandy silt
FH SS 10	23-25	FHL-07	24.8	75.2	22.64	4.21	0.293	0.887	16.41	Sandy silt
FH SS 11	25-27	FHL-07	29.4	70.6	25.89	4.244	0.217	0.769	20.11	Sandy silt
FH SS 12	27-29	FHL-07	23.6	76.4	21	3.973	0.272	0.828	15.62	Sandy silt
FH SS 13	29-34	FHL-07	26.7	73.3	25.89	3.683	0.131	0.841	23.14	Sandy silt
FH SS 14	34-36	FHL-08	29.3	70.7	28.97	4.212	0.202	0.709	22.88	Sandy silt
FH SS 15	36-39	FHL-08	21.1	78.9	25.86	3.378	0.396	1.225	17.8	Sandy silt
FH SS 16	39-41	FHL-08	38.5	61.5	38.16	4.457	0.133	0.762	32.74	Sandy silt
FH SS 17	41-43	FHL-08	28.3	71.7	26.74	3.893	0.094	0.799	24.67	Sandy silt

FH SS 18	43-45	FHL-08	38.2	61.8	39.74	4.105	0.073	0.754	36.46	Sandy silt
FH SS 19	45-47	FHL-08	66.8	33.2	121.4	5.198	-0.281	0.734	175.3	Silty sand
FH SS 20	47-49	FHL-08	65.6	34.4	85.56	4.292	-0.311	0.858	123.9	Silty sand
FH SS 21	49-51	FHL-09	65.6	34.4	83.86	2.572	-0.378	0.849	104.9	Silty sand
FH SS 22	51-53	FHL-09	88.3	11.7	140	1.829	-0.145	0.864	145.5	Silty sand

Note: FH SS 01-09: sediment samples from 01-09 respectively, FHL-01-09: lithofacies from 01-09 (from younger to older respectively). **Mz_G**: geometric mean, **SD_G**: standard deviation (sorting), **SK_G**: skewness, **K_G**: kurtosis, **D_{50}**: (median) Particle diameter representing the 50% of the grain in the sediment samples is finer than the D_{50} grain size (in microns) and **PSDC**: particle size distribution classification of sediments based on the relative proportion of sand-silt size percentage.

Table 4.4. Grain size description of sediments at Fincha Habera Section.

Sample Id	Lithofacies	Descriptions	Sediments name
FH SS 01	FHL-01	Poorly sorted, symmetrical, and mesokurtic	Medium silt
FH SS 02	FHL-02	Poorly sorted, coarse skewed, and mesokurtic	Very fine sandy medium silt
FH SS 03	FHL-03	Poorly sorted, very coarse skewed, and very leptokurtic	Coarse sandy medium silt
FH SS 04	FHL-04	Very poorly sorted, very coarse skewed, and platykurtic	Coarse sandy medium silt
FH SS 05	FHL-05	Poorly sorted, coarse skewed, and platykurtic	Very fine sandy coarse silt
FH SS 06	FHL-06	Very poorly sorted, symmetrical, and platykurtic	Fine sandy coarse silt
FH SS 07	FHL-07	Very poorly sorted, coarse skewed, and mesokurtic	Fine sandy medium silt
FH SS 08	FHL-07	Very poorly sorted, coarse skewed, and platykurtic	Fine sandy medium silt
FH SS 09	FHL-07	Very poorly sorted, coarse skewed, and platykurtic	Fine sandy fine silt
FH SS 10	FHL-07	Very poorly sorted, coarse skewed, and platykurtic	Fine sandy medium silt
FH SS 11	FHL-07	Very poorly sorted, coarse skewed, and platykurtic	Fine sandy medium silt
FH SS 12	FHL-07	Poorly sorted, coarse skewed, and platykurtic	Fine sandy medium silt
FH SS 13	FHL-07	Poorly sorted, coarse skewed, and platykurtic	Fine sandy medium silt
FH SS 14	FHL-08	Very poorly sorted, coarse skewed, and platykurtic	Fine sandy medium silt
FH SS 15	FHL-08	Poorly sorted, very coarse skewed, and leptokurtic	Fine sandy medium silt
FH SS 16	FHL-08	Very poorly sorted, coarse skewed, and platykurtic	Fine sandy medium silt
FH SS 17	FHL-08	Poorly sorted, symmetrical, and platykurtic	Very fine sandy medium silt
FH SS 18	FHL-08	Very poorly sorted, symmetrical, and platykurtic	Fine sandy coarse silt
FH SS 19	FHL-08	Very poorly sorted, fine skewed, and platykurtic	Medium silty medium sand
FH SS 20	FHL-08	Very poorly sorted, very fine skewed, and platykurtic	Medium silty fine sand
FH SS 21	FHL-09	Poorly sorted, very fine skewed, and platykurtic	Very coarse silty fine sand
FH SS 22	FHL-09	Moderately sorted, fine skewed, and platykurtic	Very coarse silty fine sand

Table 4.5. Grain size analysis of sediments at Fincha Habera Section.

Sample Id	Litho-facies	VFS %	FS %	MS %	CS %	VCS%	VFSa%	FSa %	MSa%	CSa %	VCSa %	Cumul weight %	Sediment (sample) type
FH SS 01	FHL-01	10.7	19.7	33.3	21.4	14.9	0.0	0.0	0.0	0.0	0.0	100.0	Polymodal
FH SS 02	FHL-02	5.0	16.5	26.9	19.0	15.5	7.6	4.6	3.5	1.4	0.0	100.0	Polymodal
FH SS 03	FHL-03	1.5	14.5	22.0	17.0	13.8	7.6	8.1	4.7	10.7	0.0	100.0	Polymodal
FH SS 04	FHL-04	3.7	19.0	28.3	20.1	13.4	5.0	0.0	0.0	6.1	4.4	100.0	Polymodal
FH SS 05	FHL-05	0.0	10.7	22.7	24.1	19.3	14.1	9.2	0.0	0.0	0.0	100.0	Polymodal
FH SS 06	FHL-06	0.2	13.1	13.8	15.4	14.7	12.8	13.7	9.2	7.1	0.0	100.0	Polymodal
FH SS 07	FHL-07	10.5	19.8	21.9	13.8	13.3	7.0	9.7	4.0	0.0	0.0	100.0	Polymodal
FH SS 08	FHL-07	9.2	16.1	23.9	16.8	10.9	5.6	13.3	4.2	0.0	0.0	100.0	Polymodal
FH SS 09	FHL-07	8.0	22.0	20.3	16.0	11.1	8.1	10.4	4.1	0.0	0.0	100.0	Polymodal
FH SS 10	FHL-07	7.2	20.2	21.2	15.8	10.9	8.2	11.3	4.1	1.2	0.0	100.0	Polymodal
FH SS 11	FHL-07	6.4	15.1	22.2	13.7	13.2	11.0	12.8	5.6	0.0	0.0	100.0	Polymodal
FH SS 12	FHL-07	8.2	18.8	23.0	13.4	13.0	9.7	13.0	0.9	0.0	0.0	100.0	Polymodal
FH SS 13	FHL-07	3.8	15.0	20.0	19.1	15.4	11.4	11.9	2.1	1.2	0.0	100.0	Polymodal
FH SS 14	FHL-08	3.8	17.2	21.4	14.1	14.3	8.5	14.0	4.0	2.7	0.0	100.0	Polymodal
FH SS 15	FHL-08	0.2	12.5	30.4	27.5	8.3	6.8	10.7	3.7	0.0	0.0	100.0	Polymodal
FH SS 16	FHL-08	2.8	12.0	19.5	14.6	12.6	12.7	14.0	8.4	3.3	0.0	100.0	Polymodal
FH SS 17	FHL-08	5.0	16.2	18.7	16.4	15.4	12.8	11.2	4.2	0.0	0.0	100.0	Polymodal
FH SS 18	FHL-08	0.2	13.3	15.6	16.9	15.8	12.4	16.5	4.9	4.5	0.0	100.0	Polymodal
FH SS 19	FHL-08	0.0	3.6	12.0	9.4	8.2	9.7	17.0	17.4	17.1	5.5	100.0	Polymodal
FH SS 20	FHL-08	0.0	5.6	11.7	7.0	10.2	15.9	21.5	20.3	7.9	0.0	100.0	Polymodal
FH SS 21	FHL-09	0.0	0.0	8.1	10.1	16.1	24.5	37.2	3.8	0.0	0.0	100.0	Polymodal
FH SS 22	FHL-09	0.0	0.0	0.0	0.0	11.7	28.1	41.7	18.5	0.0	0.0	100.0	Trimodal

Note: VFS: very fine silt; FS: fine silt; MS: medium silt; CS: coarse silt and VCS: very coarse silt. VFSa: very fine sand; FSa: fine sand; MSa: medium sand; CSa: coarse sand; VCSa: very coarse sand.

4.1.1.1. Lithological classification of the sediments

Most of the sediment samples on <2000µm size ranges were characterized by distribution of grain size from very fine silt to very coarse sand size sediments throughout the profile/section (Table 4.5). The mean values range from 11.97µm at lithofacies FHL-01 to 140µm at lithofacies FHL-09 (Table 4.3). Generally, most of the samples are poorly to very poorly sorted (standard deviation values range from 2-4µm) and has polymodal distribution whereas the sediment samples FH SS 22 from lithofacies FHL-09 is characterized by a moderately sorted and trimodaly distributed sediments.

Based on the field description (lithofacies) and the statistical grain size analysis (particle size distribution classification based on the proportion of silt and sand size) of the sediments, the profile (section) could be classified into seven lithological units from top to bottom as: lithological unit-01 (silt), lithological unit-02 (sandy silt with charcoal), lithological unit-03 (sandy silt), lithological unit-04 (charcoal with sandy silt sediments), lithological unit-05 (sandy silt with gravel), lithological unit-06 (silty sand), and lithological unit-07 (silty sand with gravel) (Fig. 4.2).

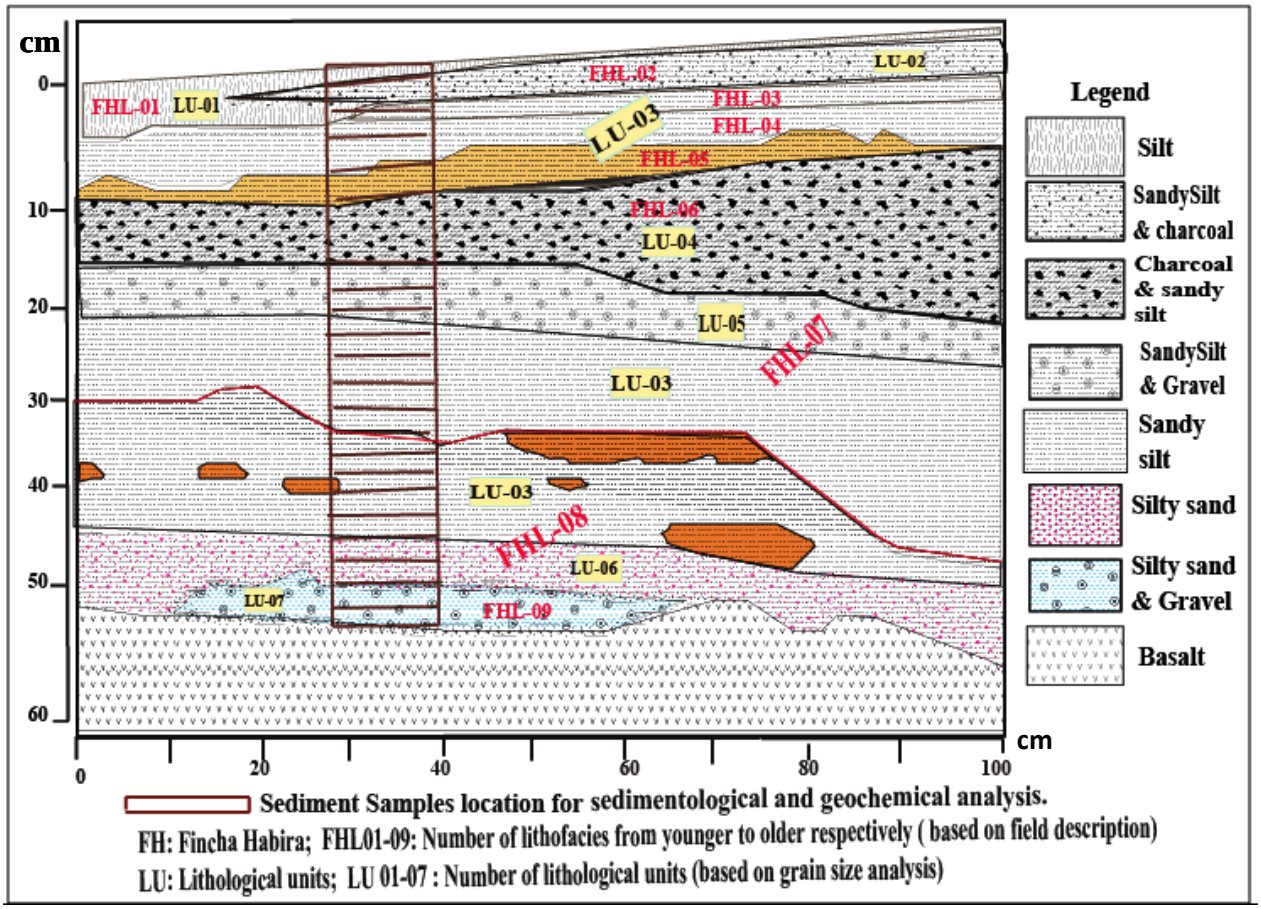

Figure 4.2. Lithostratigraphic section of sediments at Fincha Habera section, Bale Mountain, southeastern Ethiopia. The orange color indicates the inclusion of brown color, sandy silt size sediments in the deposit, red color (contact layer): the disconformity between lithofacies FHL-07 and lithofacies FHL-08: yellow color: the brown color sandy silt size sediments with maximum amount of burned shells.

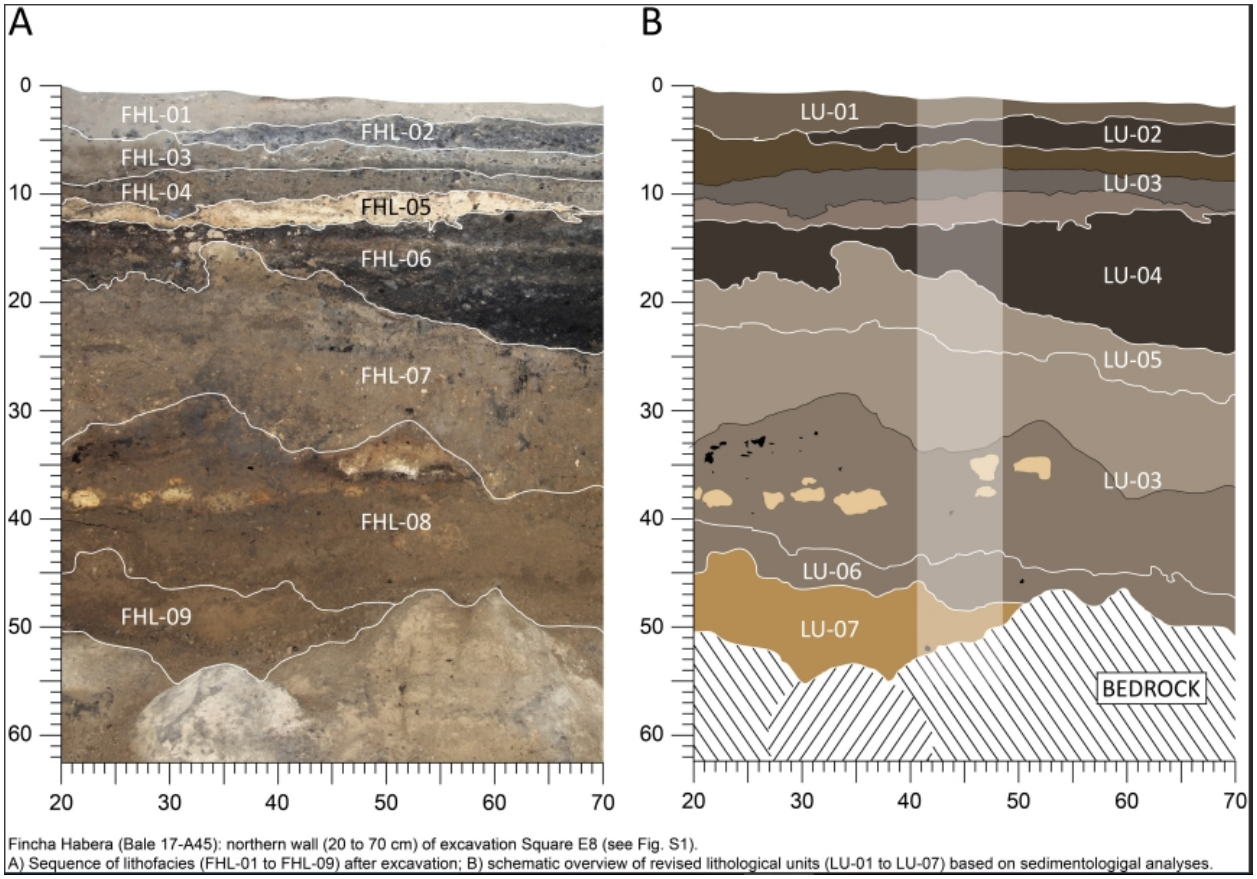

Figure 4.3. Lithofacies association and lithostratigraphic section of the profile (drawing by Goetz, 2018).

Lithological unit-01 (LU-01)

This unit includes the lithofacies FHL-01 is the top most litho-unit of the section with a topsoil of 0-2cm thickness at the top. This layer is characterized by dark grayish brown color, poorly sorted with standard deviation (SD_G) of 2.383µm, more or less symmetrical medium silt sediments with skewness (SK_G) of -0.004µm, and mesokurtic (K_G: 0.92µm). The grain size distributions are polymodal in nature and ranging from very fine silt to very coarse silt size sediments with lack of sand proportions (Table 4.5).

Lithological unit-02 (LU-02)

This lithological unit is the second unit of the profile and comprises 2-4cm thick, black sandy silt sediments with charcoal (lithofacies FHL-02; sediment samples FH SS 02). The statistical parameter of this unit show the sediments to be poorly sorted with standard deviation (SD_G) of 3.941µm and has a polymodal distribution of grains ranging from very fine silt to coarse sand

size sediments (Table 4.5). Symmetry of the sediments is of coarse skewed (indicates a tail of fine grains) with a value of 0.36µm. The degree of curvature (peakedness) of the sediments near the mode reveals the sediments are mesokurtic (moderately peaked) in nature with a kurtosis value of 1.097µm.

Lithological unit-03 (LU-03)

This unit consists high range of lithofacies groups and is the dominant lithological unit of the profile. The lithofacies grouped in this unit include FHL-03, FHL-04, FHL-05, FHL-07 (sediment samples FH SS 09, FH SS 10, FH SS 11, FH SS 12, and FH SS13) and lithofacies FHL-08 (sediment samples FH SS 14, FH SS 15, FH SS 16, FH SS 17 and FH SS 18). The statistical parameters of these samples indicate that the sediments are poorly to very poorly sorted with a standard deviation value ranging from 2.878µm to 4.983µm at lithofacies FHL-05 and FHL-04, respectively. The mean grain size of this unit ranges from 17.6µm at lithofacies FHL-03 to 45.87µm in lithofacies FHL-06, indicating the presence of coarse sand to coarse silt grade of sandy silt sediments. The skewness of this unit varies from very coarse skewed (highest sekewness value at lithofacies FHL-08, sediment sample FH SS 15, with value of 0.396µm) to symmetrical at lithofacies FHL-06 (skewness value of 0.067µm). The peakdness of the sediments varies from very leptokurtic (excessively peaked; a sample curve is better sorted in the central part than in the tail) to platykurtic (deficiently peaked; the sample is better sorted in the tail than in the central part) (Table 4.3).

Lithological unit-04 (LU-04)

This lithological unit comprises a thickness of 9-17cm (lithofacies FHL-06 and sediment samples FH SS 06) and characterized by availability of sizable quantity of ecofacts/charcoal (i.e., indicate the present of human occupation within the sediment deposits inside the rock shelter site) with highly altered black color sandy silt sediments. The statistical parameters of the sediments show the sediments are very poorly sorted with standard deviation of 4.702µm and are polymodally distributed fine sandy coarse silt size sediments. The skewness value (0.067µm) of the sediments shows the grains are preferentially spread symmetrically. The peakedness of the sediments near the mode reveals the sediments are platykurtic in nature (a sample curve is better sorted in the tails than the central parts) with a kurtosis value of 0.777µm.

Lithological unit-05 (LU-05)

This lithological unit is 17cm to 21cm thick and comprises the top most part of the lithofacies FHL-07 (sediment samples FH SS 07 and FH SS 08). This unit is characterized by polymodal distribution of grains ranging from very fine silt to medium sand size sediments (Table 4.5) with some gravel size rock fragments (recovered from 2mm mesh size). The statistical parameters of the sediments indicate that the fine sandy medium silt sediments are very poorly sorted with a standard deviation value ranging from 4.226µm to 4.381µm in sediment samples FH SS 07 and FH SS 08, respectively. The symmetry reveals that the sediments fall in the coarse skewed group (indicates a tail of fines grains) with a skewness value ranging from 0.284µm to 0.279µm in FH SS 07 and FH SS 08, respectively. The degrees of curvature of the sediments start with mesokurtic in sediment samples FH SS 07 with a value of 0.931µm followed by platykurtic nature in sediment samples FH SS 08 with value of 0.895µm.

Lithofacies unit-06 (LU-06)

This lithological unit includes the bottom part of lithofacies FHL-08 (FH SS 19 & FH SS 20) and comprises the thickness from 45cm to 49cm. This unit is characterized by silty sand size sediments with a mean value ranging from 121.4µm in sediment sample FH SS 19 to 85.56µm in sediment sample FH SS 20. The sediments show polymodal type distribution which ranges from fine silt to very coarse sand in sediment sample FH SS 19 and from fine silt to coarse sand sizes at sediment sample FH SS 20 (Table 4.5). Here the silty sand sediments are very poorly sorted with a standard deviation value ranging from 5.198µm to 4.292µm in sediment samples FH SS 19 and FH SS 20, respectively. The symmetry reveals that the sediments fall in the very fine to fine skewed group (indicates a tail of coarse grains) with a value ranging from -0.28µm to -0.311µm in sediment samples FH SS 19 and FH SS 20, respectively. The degrees of curvature of the sediments are platykurtic with a value ranging from 0.734 µm in sediment samples FH SS 19 to 0.858µm in FH SS 20.

Lithological unit-07 (LU-07)

The thickness of this lithological unit is ranges from 49 to 53cm and comprises the lithofacies FHL-09 sediment samples FH SS 21 and FH SS 22. This unit is characterized by polymodal-trimodal distribution of grains from medium silt to medium sand and from very coarse silt to

medium sand size sediments in lithofacies FHL-09 (sediment samples FH SS 21 and FH SS 22, respectively) (Table 4.5). Lithofacies FHl-09 includes mixture of different types of gravel size rock fragments (recovered from 2mm mesh size). The statistical parameters of the sediments indicate that the very coarse silty to fine sand size sediments are poorly sorted to moderately sorted with a standard deviation ranging from 2.572µm to 1.829µm in sediment samples FH SS 21 and FH SS 22, respectively. The symmetry reveals that the sediments fall in the fine skewed nature with a skewness value ranging from -0.378µm to -0.145µm in sediment samples FH SS 21 and FH SS 22, respectively. The degrees of curvature of the sediments show platykurtic nature with values ranging from 0.849µm to 0.864µm at sediment samples FH SS 21 and FH SS 22, respectively.

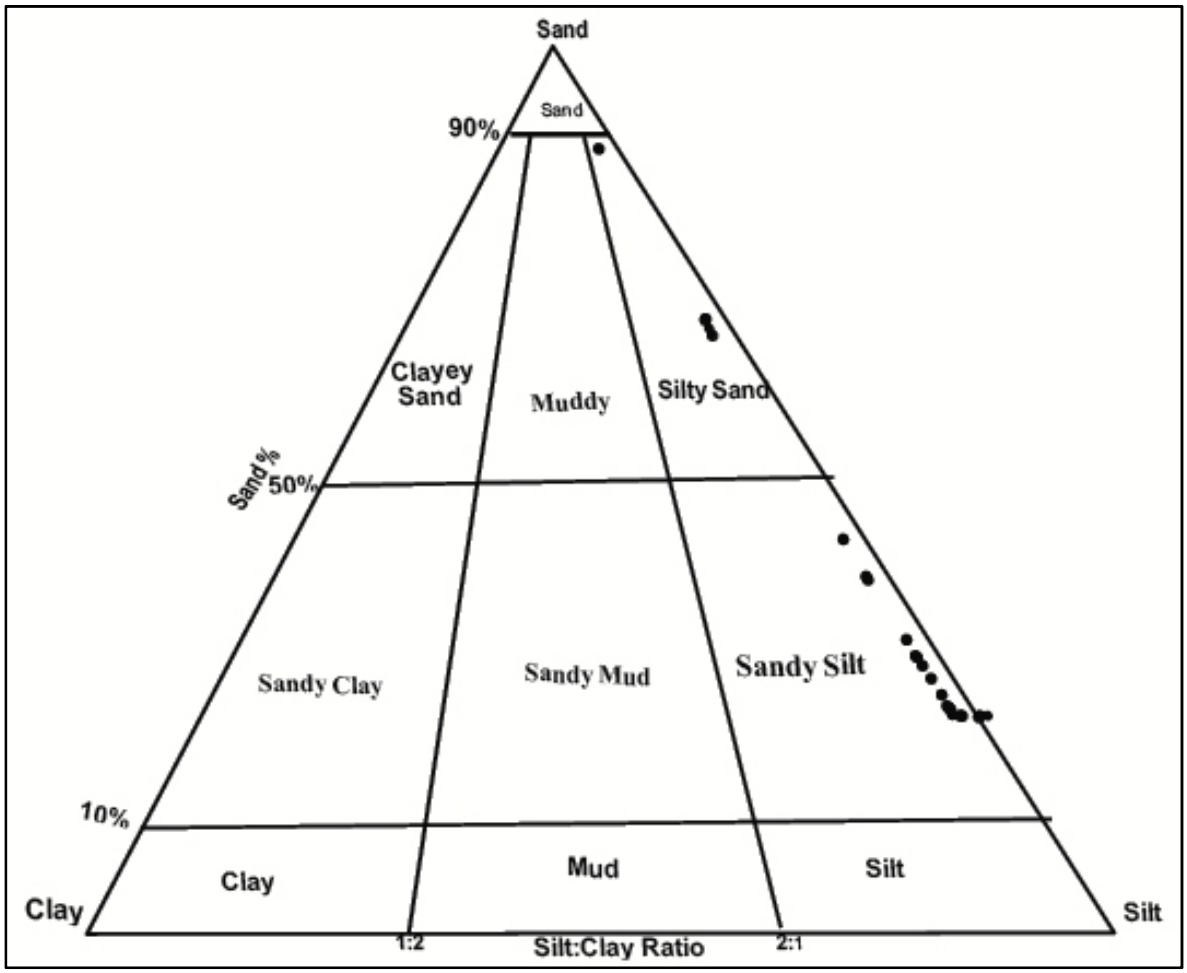

Figure 4.4. Classification of the sediments samples using the Clay-Silt-Sand Ternary diagram.

4.1.1.2. Depth distribution of the grain size parameters

The geometrical measurements of the four grain size parameters (i.e., mean, standard deviation or sorting, skewness and kurtosis) are independent of each other (Fig 4.5) (Folk and Ward, 1957; Swan et al., 1977). Therefore, to understand the sedimentological significance of these statistical parameters it is important to describe and interpret the interrelationship based on the scattering plots of mean versus skewness and kurtosis (Fig. 4.6) and mean versus standard deviation (sorting) (Fig. 4.7).

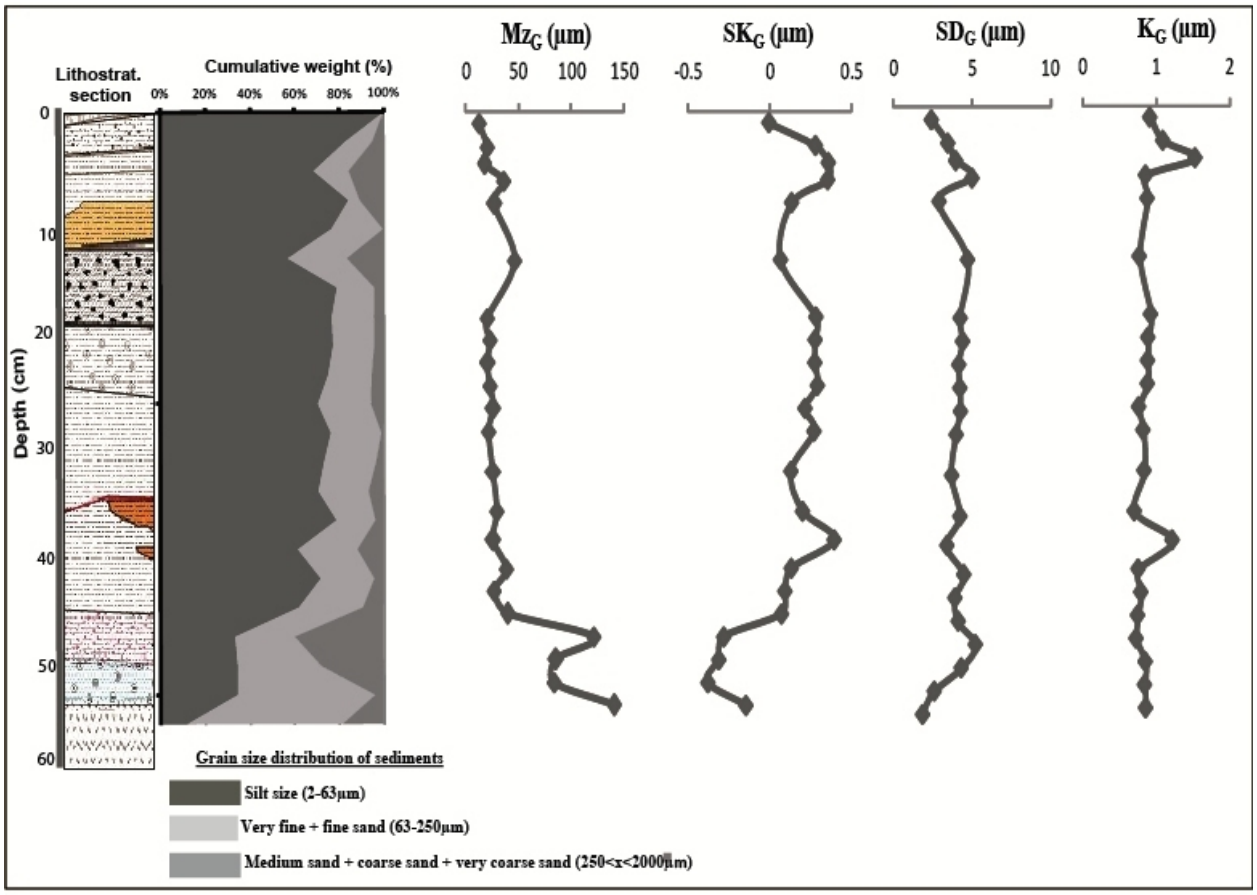

Figure 4.5. Grain size distribution and Depth variations in grain size statistical parameters of sediments, where Mz_G: mean size, SK_G: skewness, SD_G: standard deviation and K_G: kurtosis.

Mean versus skewness

Skewness reflects the sorting of sediments in the tail of the distribution (Boggs, 2009). In the scatter plot of the mean versus skewness the skewness value is strongly related to the function of grain size of sediments. The pure silt size sediments at the lithofacies FHL-01 with skewness

(SK_G) value of -0.004µm and sand: silt proportion of 0:100% produces a symmetrical size curve. The lithofacies FHL-06 (sediment samples FH SS 06) and lithofacies FHL-08 (sediment samples FH SS 17 and FH SS 18) show a symmetrical size curve; however, the addition of some of the percentage of very fine to fine sand size sediments to the medium to coarse silt size sediments causes the curve tending to the positive skewed sizes. The lithofacies FHL-02, FHL-03, FHL-04, FHL-05, FHL-07 and FHL-08 (sediment samples FH SS 14, FH SS 15 and FH SS 16) have a tail to the right with a positive skewness value ranging from 0.131µm at lithofacies FHL-07 (sediment sample FH SS 13) to 0.396µm at lithofacies FHL-08 (sediment sample FH SS 15). These all are characterized by coarse to very coarse skewed size curve with an excess of fine (silt) size sediments. The lithofacies FHL-08 (sediment samples FH SS 19 and FH SS 20) and lithofacies FHL-09 (sediment samples FH SS 21 and FH SS 22) have a tail to the left (i.e., with an excess of coarse (sand) size sediments) with a negative skewness value ranging from -0.145µm at lithofacies FHL-09 (sediment sample FH SS 22) to -0.378µm at lithofacies FHL-09 (sediment sample FH SS 21).

Mean versus kurtosis

Kurtosis indicates the peakedness/sharpness of grain size curves (Boggs, 2009) and an index of the mixing of two normal grain sizes (Folk and Ward, 1957). The pure silt size sediments at lithofacies FHL-01 sediment sample FH SS 01 and the sandy silt size sediments at lithofacies FHL-07 sediment sample FH SS 07 gives nearly normal curves with kurtosis value of 0.92 and 0.931, respectively. The sandy silt size sediments at lithofacies FHL-02 sediment sample FH SS 02 gives a mesokurtic curve size with kurtosis value of 1.097 and this shows the addition of small proportion of sand size sediments into the dominant silt size sediments. The addition of small proportion of sand size sediments at lithofacies FHL-08 sediment sample FH SS 15 and addition of 10.7% of coarse sand size sediments into silt size sediments at lithofacies FHL-03 sediment sample FH SS 03 causes the sorting in the central part to be higher than the sorting in the tail of the curve. Hence, the curve is leptokurtic to very leptokurtic with kurtosis value of 1.225µm and 1.537µm respectively (K_G>1). Most of the sediment samples with the sand silt proportion of 23-33:60-75 or silt sand proportion of 23-33:60-75 shows a platykurtic curve. These show the sorting of the sediments is higher in the tail portion of the curve than in the central part with kurtosis value of less than one (K_G<1).

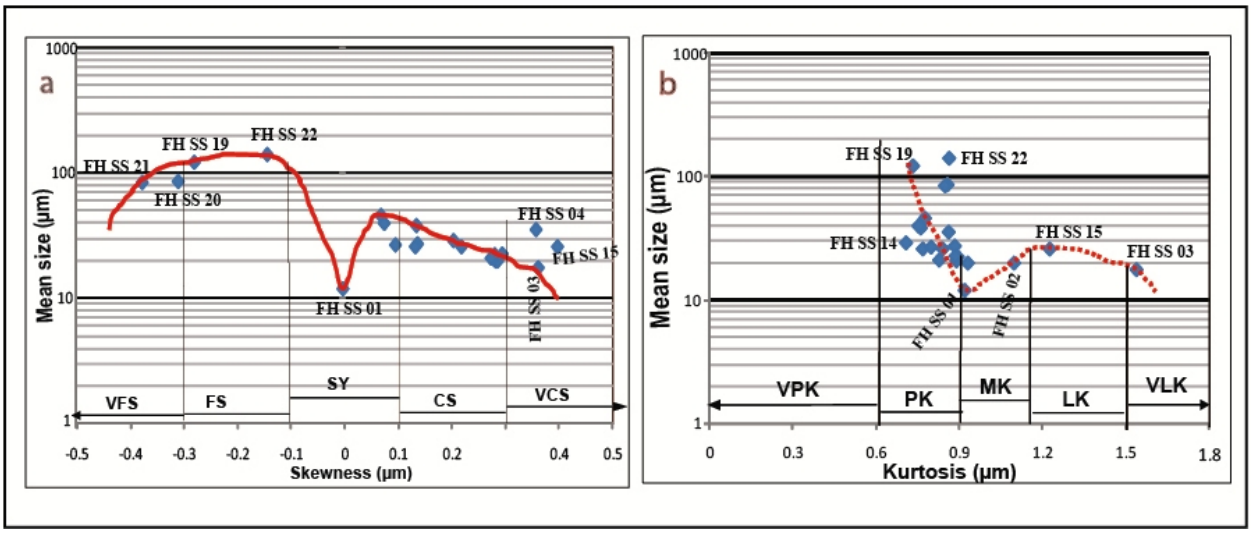

Figure 4.6. Scatter plots of the grain size parameters, where the capital letter acronyms along the x- axis represents the limits of the geometric measurements on skewness and kurtosis values (µm); (a) Scatter plot of mean size versus skewness where VFS: very fine skewed, FS: fine skewed, SY: symmetrical, CS: coarse skewed and VCS: very coarse skewed; (b) Scatter plot of mean size versus kurtosis where VPK: very platykurtic, PK: platykurtic, MK: mesokurtic, LK: leptokurtic and VLK: very leptokurtic (after Folk and Ward, 1957).

Mean versus standard deviation (sorting)

Sorting is a measure of the range of grain sizes present within the sediments and the magnitude of the scatter of these sizes around the mean sizes (Boggs, 2009). The distinct sediment sample (FH SS 22) from lithofacies FHL-09 has moderately sorted and trimodaly distributed (particle distributed from very coarse silt to medium sand size) sediments. At lithofacies FHL-01 sediment sample FH SS 01, the sand silt proportion of the sediments is 0:100 (pure silt) and the standard deviation value is relatively low (SD_G: 2.383 µm). As the sand mode adds to the silt size sediments (e.g., at lithofacies FHL-02) or add silt size sediments to the sand mode sediments (e.g., at lithofacies FHL-09 sediment sample FH SS 21), the samples lie on the poorly sorted size curve with relatively high value of standard deviations (SD_G: 3.432µm and 2.572 µm respectively). When the samples consist all range of grain size distributions (from very fine silt to coarse/very coarse sand sizes) and characterized by highly graded (non-uniform size) sediments, the sorting is very poor with extremely higher value of standard deviation (e.g., in lithofacies FHL-04 sediment sample FH SS 04 (SD_G: 4.983µm) and lithofacies FHL-08 sediment sample FH SS 19 (SD_G: 5.198µm)).

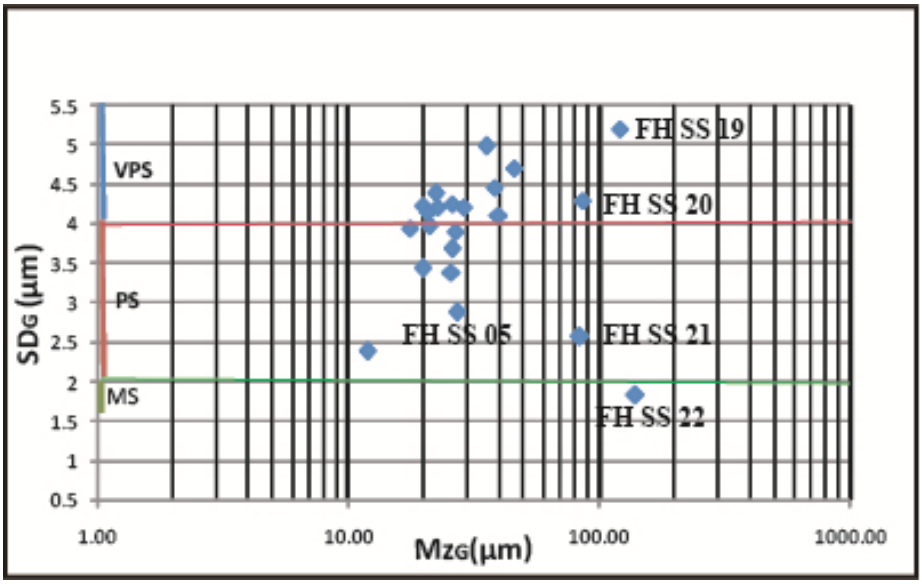

Figure 4.7. Scatter plots of the grain size parameters, where the capital letter acronyms along the margin of y-axis represent the limits of the geometric measurements on standard deviation (sorting) values (µm); MS: medium sorted, PS: poorly sorted and VPS: very poorly sorted sediments (graph after Folk and Ward, 1957).

4.1.2 Magnetic susceptibility

Magnetic susceptibility is a magnetic property of sediments that indicates the strength of the induced magnetism within the samples. Magnetic susceptibility shows the relative incorporation of magnetic minerals into the sediments either by the inherent compositions of the weathered, eroded, and/or transported source material or by pedogenesis and post depositional alteration of the sediments (Boadi et al., 2014; Harrold et al., undated).

The Bartington instrument MS2B dual frequency sensor and MS3 meter was used to measure the magnetic susceptibility of unconsolidated sediments. The accuracy of the sensor is checked by the calibration sample, which exhibits negligible frequency dependence and the magnetic susceptibility value is marked on it. The result of the sample measurement was calculated as mean mass specific susceptibility (*10^{-6}SI) of three successive measurements (Table 4.6 and Fig. 4.8). Low frequency magnetic susceptibility ranges from 1.48×10^{-6} SI in lithofacies FHL-02 (sediment sample FH SS 02) to 10.7×10^{-6} SI in lithofacies FHL-05 (sediment sample FH SS 05). High frequency magnetic susceptibility ranges from 1.36×10^{-6} SI in lithofacies FHL-02 (sediment sample FH SS 02) to 9.73×10^{-6}SI in lithofacies FHL-05 (sediment sample FH SS 05).

Table 4.6. Magnetic susceptibility measurement of sediments (HF & LF).

Sample ID	Lithofacies	Depth (cm)	Mean depth (cm)	(Mean) Ma.Su.Me.in 10^{-6}SI (HF)	(Mean) Ma.Su.Me.in 10^{-6}SI (LF)
FH SS 01	FHL-01	0-2	1	2.8	3.02
FH SS 02	FHL-02	2-4	3	1.36	1.48
FH SS 03	FHL-03	4-5	4.5	2.58	2.79
FH SS 04	FHL-04	5-7	6	2.12	2.31
FH SS 05	FHL-05	7-9	8	9.73	10.7
FH SS 06	FHL-06	9-17	13	1.44	1.53
FH SS 07	FHL-07	17-19	18	1.64	1.73
FH SS 08	FHL-07	19-21	20	1.88	1.98
FH SS 09	FHL-07	21-23	22	1.77	1.86
FH SS 10	FHL-07	23-25	24	1.93	2.04
FH SS 11	FHL-07	25-27	26	2.3	2.44
FH SS 12	FHL-07	27-29	28	2.35	2.47
FH SS 13	FHL-07	29-34	31.5	2.7	2.86
FH SS 14	FHL-08	34-36	35	3.53	3.77
FH SS 15	FHL-08	36-39	37.5	1.74	1.86
FH SS 16	FHL-08	39-41	40	2.87	3.08
FH SS 17	FHL-08	41-43	42	4.51	4.82
FH SS 18	FHL-08	43-45	44	4.54	4.83
FH SS 19	FHL-08	45-47	46	4.83	5.13
FH SS 20	FHL-08	47-49	48	5.02	4.62
FH SS 21	FHL-09	49-51	50	1.64	1.7
FH SS 22	FHL-09	51-53	52	1.68	1.73

Note: FH SS 01-22: Fincha Habera Sediment Sample 01-22; Mean Mass Susc. Meas.: Mean Mass Susceptibility Measurement; LF: Measurement at low frequency (0.465 kHz) and HF: Measurement at high frequency (4.65 kHz).

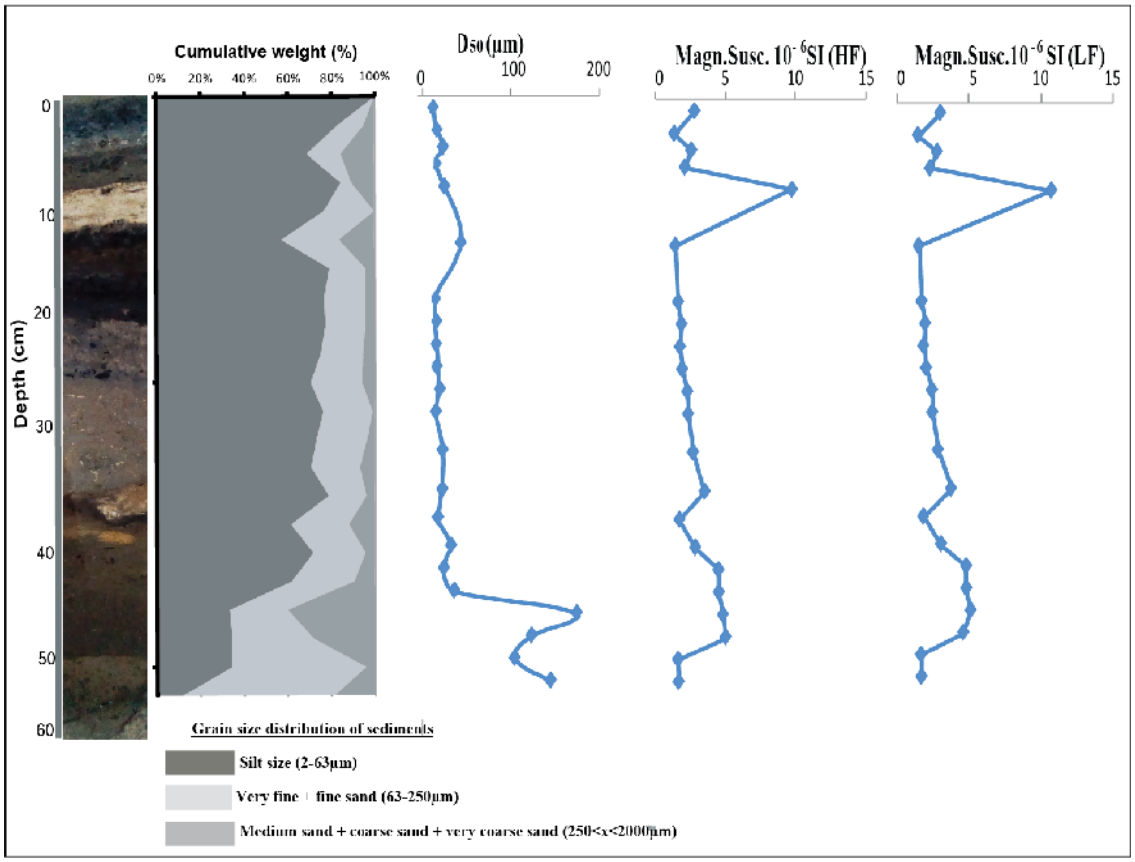

Figure 4.8. Graphic correlation between dual magnetic susceptibility measurements (LF and HF) and grain size distribution of sediments, Fincha Habera Section, Bale Mountain, south eastern Ethiopia.

Generally based on the vertical (depth) variation in magnetic susceptibility measurements of the sediment samples and physical characteristics recorded in the field, the profile can be classified into four zones, zones A to D, from extremely high to very low magnetic susceptibility values (particularly based on the lower frequency value, x_{lf}).

Zone A

This unit (lithofacies FHL-05, 7-9cm) consists extremely high value of magnetic susceptibility (10.7×10^{-6} SI) compared to the other four zones. This zone is distinguished by its brown color sediments and consists of sizable amount of burned and broken shells (i.e., that enhance the magnetic susceptibility value of the sediments).

Zone B

This zone include lithofacies FHL-01 (sample FH SS 01) and FHL-08 (samples FH SS 14, FH SS 16, FH SS 17, FH SS 18, FH SS19 and FH SS 20) is characterized by high value of magnetic susceptibility compared to the lower three zones with maximum value in sediment sample FH SS 19 with value of 5.13×10^{-6}SI, and minimum value in sediment sample FH SS 01 (3.02×10^{-6} SI) and mean value of 4.18×10^{-6}SI (Table 4.7).

Table 4.7. Zone B magnetic susceptibility values.

Lithofacies	**Sample Id**	**depth (cm)**	**Meas Magn. Susc.(10^{-6}) (LF)**
FHL-01	FH SS 01	0-2	3.02
FHL-08	FH SS 14	34-36	3.77
	FH SS 16	39-41	3.08
	FH SS 17	41-43	4.82
	FH SS 18	43-45	4.83
	FH SS 19	45-47	5.13
	FH SS 20	47-49	4.62
Average			**4.18**

Zone C

This zone is characterized by relatively low value of magnetic susceptibility compared to the upper two zones and higher than the lower zone, and ranging from 1.7×10^{-6} SI in lithofacies FHL-09 sediment sample FH SS 21 to 2.86×10^{-6} SI in lithofacies FHL-07 sediment sample FH SS 13 with mean value of 2.14×10^{-6} SI (Table 4.8).

Table 4.8. Zone C magnetic susceptibility values.

Lithofacies	**Sample Id**	**depth (cm)**	**Meas Magn. Susc.(10^{-6}) (LF)**
FHL-03	FH SS 03	4-6	2.79
FHL-04	FH SS 04	6-7	2.31
FHL-07	FH SS 07	17-19	1.73
	FH SS 08	19-21	1.98
	FH SS 09	21-23	1.86
	FH SS 10	23-25	2.04
	FH SS 11	25-27	2.44
	FH SS 12	27-29	2.47
	FH SS 13	29-34	2.86
FHL-08	FH SS 15	36-39	1.86
FHL-09	FH SS 21	49-51	1.7
	FH SS 22	51-53	1.73
Average			**2.14**

Zone D

This zone is characterized by very low value of magnetic susceptibility compared to the upper three zones which ranges from 1.48×10^{-6} SI in lithofacies FHL-02 sediment sample FH SS 02 to 1.53×10^{-6} SI in lithofacies FHL-06 sediment sample FH SS 06 and average value of 1.50×10^{-6} SI (Table 4.9). In the field, these successions are distinguished by availability of higher amount of organic matter (charcoal).

Table 4.9. Zone D magnetic susceptibility values.

Lithofacies	**Sample Id**	**depth (cm)**	**MeasMagn. Susc.(10^-6) (LF)**
FHL-02	FH SS 02	2-4	1.48
FHL-06	FH SS 06	9-17	1.53
Average			**1.50**

4.2. GEOCHEMICAL CHARACTERISTICS OF SEDIMENTS

4.2.1. Elemental composition

The bulk major and trace elemental composition of 22 homogenized and powdered sediment samples was determined by X-ray fluorescence analyzer. A total of 19 elements (8 major and 11 trace elements) were analyzed. These are Si, Ti, Al, Fe, Mn, Ca, K and P (Table 4.10) as well as Rb, Sr, Zr, Nb, Ba, V, Cr, Ni, Cu, and Zn (Table 4.11). A mean value of three successive measurements expressed as ppm was finally recorded for each sample analysis. However, the most common and important light elements (Li, Be, Na, and Mg) are not detected by X-ray fluorescence. And the recognition of Si and Ni with the sediment samples is below the detection limits of the XRF analyzer for many samples and they are only detected in 12 and 17 samples, respectively.

Table 4.10. Major element concentration of the sediments (ppm).

Sample ID	FH SS 01	FH SS 02	FH SS 03	FH SS 04	FH SS 05	FH SS 06	FH SS 07	FH SS 08	FH SS 09	FH SS 10	FH SS 11
Me.dep. (cm)	1	3	4.5	6	8	13	18	20	22	24	26
Si	154061	120571	153352	125811	130877	92897	<LOD	<LOD	<LOD	<LOD	<LOD
Ti	5363.7	3126.8	3707.9	3558.4	4544.7	3517.0	5589.6	5364.6	5161.8	5114.2	5106.0
Al	16216.5	9785.8	15547.9	12798.2	23233.8	11699.5	25477.9	27824.3	26743.6	26419.7	26845.6
Fe	36784.8	23778.3	29141.6	27439.5	34732.9	27835.8	43964.5	43347.0	42006.4	40497.5	40333.6
Mn	1748.5	661.4	7150.9	1286.4	11245.3	963.7	1234.1	2842.3	1855.8	1642.6	1585.6
Ca	17182.8	18237.1	28153.3	27128.8	70191.7	16647.0	41958.0	48349.1	56726.4	79760.9	83605.4
K	13249.3	11292.7	15702.6	14366.1	22694.3	11439.1	22590.7	22386.5	21562.4	19565.4	19195.0
P	12163.0	8523.3	15047.9	11327.6	45819.7	6662.2	28598.6	29892.3	30054.2	24262.4	37496.0
Sample ID	FH SS 12	FH SS 13	FH SS 14	FH SS 15	FH SS 16	FH SS 17	FH SS 18	FH SS 19	FH SS 20	FH SS 21	FH SS 22
Me.dep. (cm)	28	31.5	35	37.5	40	42	44	46	48	50	52
Si	<LOD	<LOD	112904	69262.7	99591.0	<LOD	312090	<LOD	<LOD	284208	329485
Ti	4875.5	4804.8	4685.1	3277.6	4213.5	5478.1	4323.1	5661.7	5325.5	6000.8	6253.1
Al	25832.8	26440.4	25580.2	18507.1	23026.9	30713.9	24082.6	28130.7	28918.5	32308.2	33516.0
Fe	41110.7	41697.7	38867.9	26033.9	33708.6	48990.8	36244.4	47187.9	48922.0	47036.9	47202.3
Mn	1545.8	1409.6	1234.8	1321.2	1481.9	1685.4	1496.2	2911.7	2567.9	1881.9	2098.8
Ca	82958.3	86346.4	107878	190293	134544	52901.3	125913	67084.8	58549.4	14022.1	14010.5
K	19067.2	18351.1	19049.3	11911.7	17348.1	24483.8	17914.5	23347.0	24764.1	28211.2	28333.1
P	37796.2	38446.0	47997.0	86956.5	60130.1	22807.2	56631.3	27205.2	25302.9	8484.7	9370.5

Table 4.11. Trace element concentration of sediments (ppm).

Sample ID	FH SS 01	FH SS 02	FH SS 03	FH SS 04	FH SS 05	FH SS 06	FH SS 07	FH SS 08	FH SS 09	FH SS 10	FH SS 11
Me.dep.(cm)	1	3	4.5	6	8	13	18	20	22	24	26
Rb	62.74	51.16	68.42	63.67	73.96	56.75	94.11	95.93	95.28	88.82	90.00
Sr	137.70	137.72	192.60	194.65	475.48	116.19	225.95	244.85	263.59	309.52	319.18
Zr	348.13	256.75	418.02	374.81	420.97	331.81	618.67	647.82	614.76	592.41	668.97
Nb	52.23	36.46	59.19	54.75	64.90	47.58	92.30	94.60	92.50	89.16	86.28
Ba	416.49	62.65	220.56	126.02	648.84	0.00	534.86	526.81	471.67	442.72	503.04
V	119.40	71.87	91.78	88.59	115.11	77.56	128.56	116.68	110.09	111.02	109.82
Cr	133.68	93.07	108.97	98.74	141.48	100.09	159.11	159.66	147.43	154.28	148.92
Ni	<LOD	<LOD	<LOD	<LOD	37.71	<LOD	59.20	52.20	50.50	57.60	84.50
Cu	38.60	30.46	50.80	38.89	82.84	32.44	37.77	45.08	38.89	39.19	41.09
Zn	197.20	177.50	368.25	283.64	714.96	202.96	287.58	350.10	365.42	366.33	322.59
Sample ID	FH SS 12	FH SS 13	FH SS 14	FH SS 15	FH SS 16	FH SS 17	FH SS 18	FH SS 19	FH SS 20	FH SS 21	FH SS 22
Me.dep.(cm)	28	31.5	35	37.5	40	42	44	46	48	50	52
Rb	88.60	88.19	81.85	56.04	73.77	102.15	77.32	96.43	101.23	116.58	115.82
Sr	318.95	319.79	409.85	493.48	378.87	276.06	382.80	283.63	250.58	119.98	121.52

Zr	599.57	561.39	496.66	350.89	490.17	633.59	491.55	649.39	713.40	876.62	925.85
Nb	86.15	83.52	80.31	52.63	71.80	96.51	73.65	103.66	105.97	128.49	127.89
Ba	457.37	549.88	511.44	429.68	426.93	503.72	453.45	521.65	480.98	382.01	433.87
V	106.08	110.09	94.34	52.92	88.11	127.12	89.38	109.73	120.60	112.01	118.48
Cr	152.87	146.95	141.07	124.70	134.26	168.28	142.41	164.15	154.69	144.14	141.56
Ni	61.80	75.00	93.60	54.90	74.30	87.60	49.20	102.00	88.30	61.50	63.40
Cu	36.25	49.41	74.09	42.58	52.48	62.25	52.44	50.72	49.90	16.84	16.05
Zn	320.75	317.15	387.43	476.12	376.20	295.24	382.52	275.09	253.05	168.42	174.87

The chemical and mineralogical composition of clastic sediments are the net result of different sedimentological processes, including source rock composition, the intensity of the source rock to differential weathering, transporting mechanisms, sorting, and different types of post depositional alterations (Feng and Kerrich, 1990; Johnsson, 1993 cited in Peterson, 2009). Therefore, due to the difficulties of separation of individual minerals from clastic sediments, the bulk chemical analysis of major and trace (K, Ca, Rb, and Sr), and immobile elements (Al, Ti, Zr, and Cr) are employed to determine the chemical composition of the source rocks (Feng and Kerrich, 1990; Phillips et al., 2017).

4.2.1.1. Distribution of major elements

In the sediment deposits the trend on variation diagram of chemical elements are a result of mixing of chemically distinct components and this contributed to the chemical compositions of the sediments (Rollison, 1993). The chemical-depth plot correlation of major elements (Fig. 4.9) shows positive correlations of K with Al and Fe, and Ca with P. Hence, in most of the sediment samples there is no as such depth variation in K, Al, Fe and Ti concentrations. In most of the samples, MnO and TiO_2 contents are <1 wt% except in two samples (i.e., in lithofacies FHL-05 the MnO content is 1.45 wt%, and in lithofacies FHL-09 sediment sample FH SS 21, the TiO_2 content is 1.00 wt % and in FH SS 22, it is 1.04 wt %) (Table 4.12). Generally Si concentration shows an increase trend down depth of the section. The CaO concentration range from 1.96 to 26.63 wt % at lithofacies FHL-09 (sample FH SS 22) and lithofacies FHL-08 (sample FH SS 15) and P_2O_5 value from 1.94 to 19.92 wt % at lithofacies FHL-09 (sample FH SS 21) and lithofacies FHL-08 (sample FH SS 15) respectively.

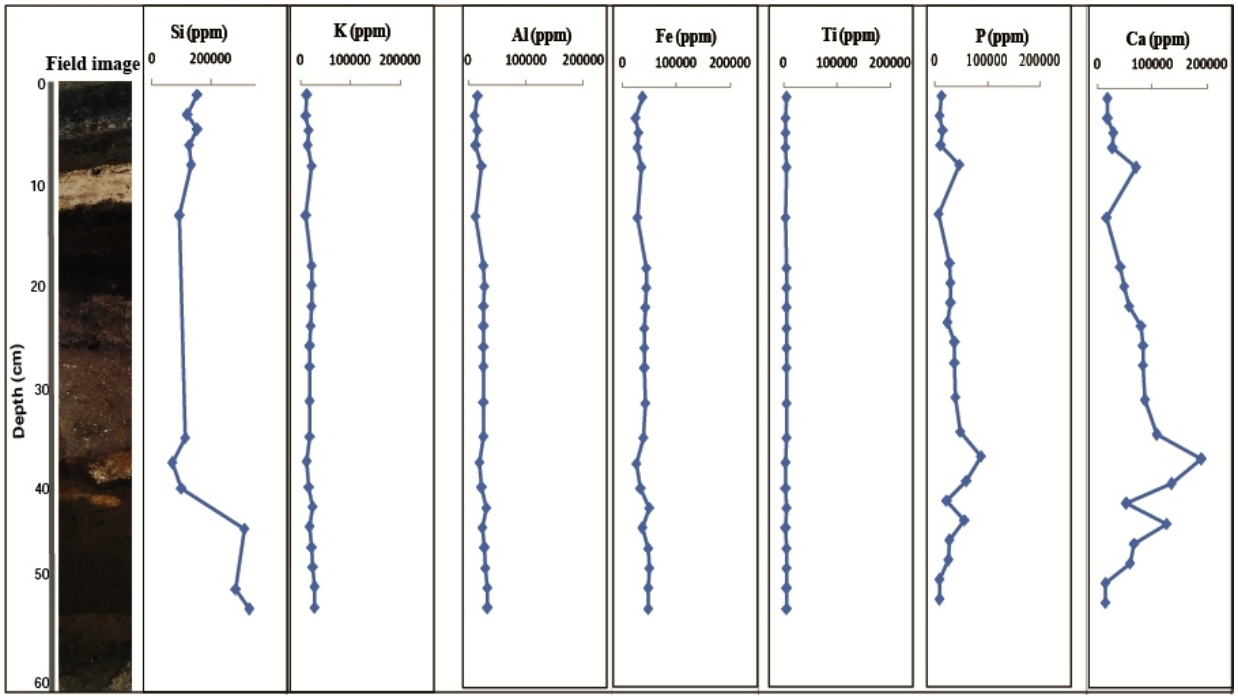

Figure 4.9. Variation diagram of major elements (Si, K, Al, Fe, Ti, Ca and P) concentrations (ppm) with depth.

Table 4.12. Major element concentration of sediments (wt %).

Sample ID	FH SS 01	FH SS 02	FH SS 03	FH SS 04	FH SS 05	FH SS 06	FH SS 07	FH SS 08	FH SS 09	FH SS 10	FH SS 11
Mean depth(cm)	1	3	4.5	6	8	13	18	20	22	24	26
SiO_2	32.96	25.79	32.81	26.91	28.00	19.87	<LOD	<LOD	<LOD	<LOD	<LOD
TiO_2	0.89	0.52	0.62	0.59	0.76	0.59	0.93	0.89	0.86	0.85	0.85
Al_2O_3	3.06	1.85	2.94	2.42	4.39	2.21	4.81	5.26	5.05	4.99	5.07
Fe_2O_3	5.26	3.40	4.17	3.92	4.97	3.98	6.29	6.20	6.01	5.79	5.77
MnO	0.23	0.09	0.92	0.17	1.45	0.12	0.16	0.37	0.24	0.21	0.20
CaO	2.40	2.55	3.94	3.80	9.82	2.33	5.87	6.76	7.94	11.16	11.70
K_2O	1.60	1.36	1.89	1.73	2.73	1.38	2.72	2.70	2.60	2.36	2.31
P_2O_5	2.79	1.95	3.45	2.60	10.50	1.53	6.55	6.85	6.89	5.56	8.59
Al_2O_3/TiO_2	3.42	3.55	4.75	4.07	5.79	3.77	5.16	5.88	5.87	5.85	5.96
$\log(SiO_2/Al_2O_3)$	1.03	1.14	1.05	1.05	0.80	0.95	-	-	-	-	-
$\log(Fe_2O_3/K_2O)$	0.52	0.40	0.34	0.36	0.26	0.46	-	-	-	-	-
Sample ID	FH SS 12	FH SS 13	FH SS 14	FH SS 15	FH SS 16	FH SS 17	FH SS 18	FH SS 19	FH SS 20	FH SS 21	FH SS 22
Mean depth(cm)	28	31.5	35	37.5	40	42	44	46	48	50	52
SiO_2	<LOD	<LOD	24.15	14.82	21.31	<LOD	66.77	<LOD	<LOD	60.80	70.49
TiO_2	0.81	0.80	0.78	0.55	0.70	0.91	0.72	0.94	0.89	1.00	1.04
Al_2O_3	4.88	5.00	4.83	3.50	4.35	5.80	4.55	5.32	5.46	6.10	6.33
Fe_2O_3	5.88	5.96	5.56	3.72	4.82	7.00	5.18	6.75	6.99	6.73	6.75
MnO	0.20	0.18	0.16	0.17	0.19	0.22	0.19	0.38	0.33	0.24	0.27
CaO	11.61	12.08	15.09	26.63	18.83	7.40	17.62	9.39	8.19	1.96	1.96
K_2O	2.30	2.21	2.29	1.43	2.09	2.95	2.16	2.81	2.98	3.40	3.41
P_2O_5	8.66	8.81	11.00	19.92	13.78	5.23	12.98	6.23	5.80	1.94	2.15
Al_2O_3/TiO_2	6.00	6.23	6.18	6.40	6.19	6.35	6.31	5.63	6.15	6.10	6.07
$\log(SiO_2/Al_2O_3)$	-	-	0.70	0.63	0.69	-	1.17	-	-	1.00	1.05
$\log(Fe_2O_3/K_2O)$	-	-	0.38	0.41	0.36	-	0.38	-	-	0.30	0.30

The trend on variation diagram of the concentration (wt %) of major oxides versus SiO_2 (wt %) can be used as proxy for the determination of the change in mineralogical maturity of the sediments (Rollison, 1993). As shown in (Table 4.12) the SiO_2 (wt %) concentration ranges from 14.82 wt % to 70.49 wt % in lithofacies FHL-08 sample FH SS 15 and lithofacies FHL-09 sample FH SS 22, respectively. Most of sediment samples show a general trend of increasing Al_2O_3, K_2O, Fe_2O_3 and TiO_2 with low SiO_2 (wt %) contents (Fig. 4.10), except three samples have anomalous silica contents (i.e., FH SS 18, FH SS 21 and FH SS 22) with high Al_2O_3, K_2O, Fe_2O_3 and relatively high TiO_2 contents. MnO show relatively constant trend with increasing

silica content except in two samples (FH SS 01 and FH SS 03), which show high anomaly of MnO contents. CaO and P_2O_5 show a scattered distribution trend with silica content.

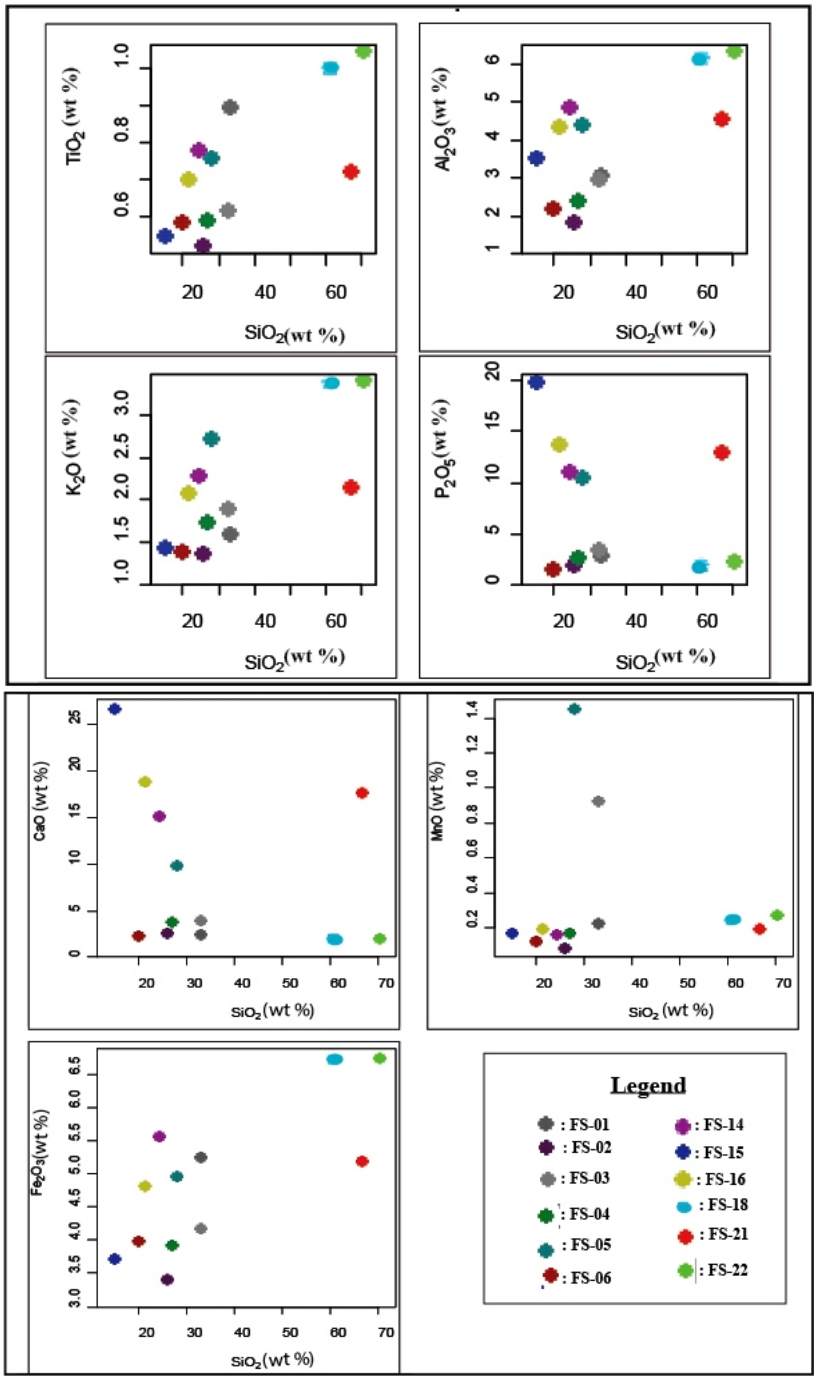

Figure 4.10. Harker variation diagram of the sediment samples shows the variation of TiO_2, Al_2O_3, K_2O, P_2O_5 CaO, MnO and Fe_2O_3 with SiO_2 content. The concentration of major oxides is in wt %.

4.2.1.2. Distribution of trace elements

The chemical-depth plot correlation of trace elements (Fig. 4.11) shows positive correlations of Zr, Rb and Nb, and Cr with V concentrations. However, non of the samples show anomalous concentration of Rb, Nb, Cr and V. Ba concentration range from 62.7 to 648.8 ppm at lithofacies FHL-05 (sample FH SS 05) and FHL-02 (sample FH SS 02) respectively. The concentration of Zr range from 256.7 to 925.8 ppm at lithofacies FHL-02 and FHL-09 (sample FH SS 22) respectively and Sr content range from 116.2 to 493.5 ppm at lithofacies FHL-06 (sample FH SS 06) and FHL-08 (sample FH SS 15) respectively.

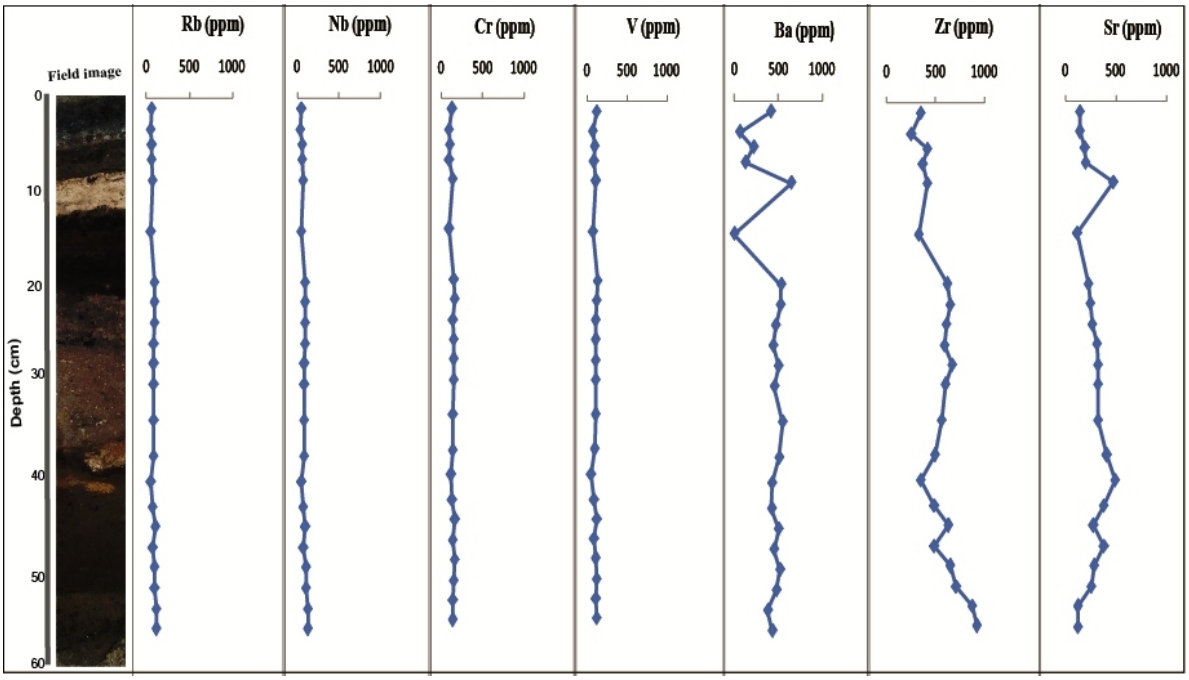

Figure 4.11. Variation in trace element (Rb, Nb, Cr, V, Ba, Zr and Sr) concentrations (ppm) with depth.

The mobile (Sr, Rb, Nb, V and Ba) and immobile (Cr, Zr and Ni) trace element concentration (Rollison, 1993) of the sediment samples are plotted against SiO_2 on Harker variation diagrams (Fig. 4.12) and all of the elements show scattered trends with increasing silica. In addition, the variation diagrams of mobile elements (K, Rb, Sr and Ba) versus Zr (Fig. 4.13) can be used to evaluate the behavior of these elements during weathering because Zr is incompatible and immobile during weathering (Taylor and Mclennan, 1985 cited in Feng and Kerrich, 1990). Accordingly Sr and Ba show a scattered trend with Zr whereas; K and Rb show an increasing trend with Zr.

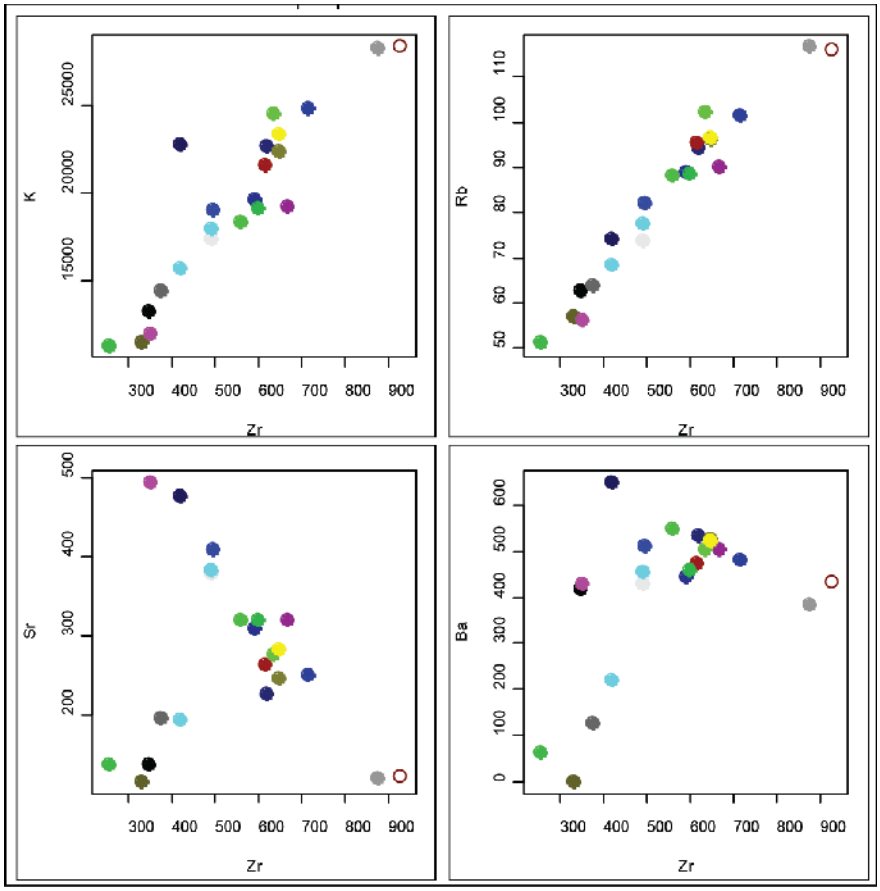

Figure 4.12. Mobile (K, Rb, Sr and Ba) versus immobile (Zr) element variation diagrams. The concentration are expressed in parts per million (ppm).

4.2.2. Mineralogical composition

The quantitative bulk mineralogical analyses of 14 representative unconsolidated sediment samples (i.e., with grain size <2mm) were conducted using X-ray diffraction analyzer. The following samples were selected for the XRD analysis: one sample each from lithofacies FHL-01 to FHL-06, representative samples with less/no organic matter (charcoal) from lithofacies FHL-07 (sediment samples FH SS 07, FH SS 10, FH SS 11 and FH SS 13), lithofacies FHL-08 (sediment samples FH SS 15 and FH SS 18), and lithofacies FHL- 09 (sediment samples FH SS 21 and FH SS 22).

The samples were X-rayed/scanned from 5 to 75 two-Theta degrees with counting time of four second per step. The quantitative X- ray powder diffraction result (intensity) of the sediments (Fig. 4.17) was exported in the form of X-ray diffraction pattern using the MATCH! Phase

Identification software Version 3.6 (Fig. 4.17). The sediments are predominantly composed of feldspars (anorthite and albite) and subordinate quantity of sanidine, quartz, biotite and muscovite minerals.

The mineralogical composition of sediments results from the combined effect of the source rock composition, further modification of the sediments by different sedimentological processes including weathering and transportations (Srodon, 2002), and various post depositional alterations through natural and anthropogenic activities. Hence, the mineralogical compositions of sediments at the Fincha Habera section were highly affected by the availability of sizable quantity of organic matters (i.e., charcoal and bone) which are derived by the anthropogenic and organic activities within the sediment deposits. Though the diffraction patterns of all the samples look similar (Figs. 4.14 and 4.15), there is difference in peak intensity value of each sample (Table 4.13) and the single peak intensity of the diffraction pattern is directly proportional to the concentration of the major minerals found within the sediments (Zou, 2016; and references therein). On the other hand, to estimate the relative abundance and distribution of major minerals down depth of the profile the single-peak intensities of the diffraction pattern of the sediment samples can be used (Stein et al., 2010 cited in Zou, 2016).

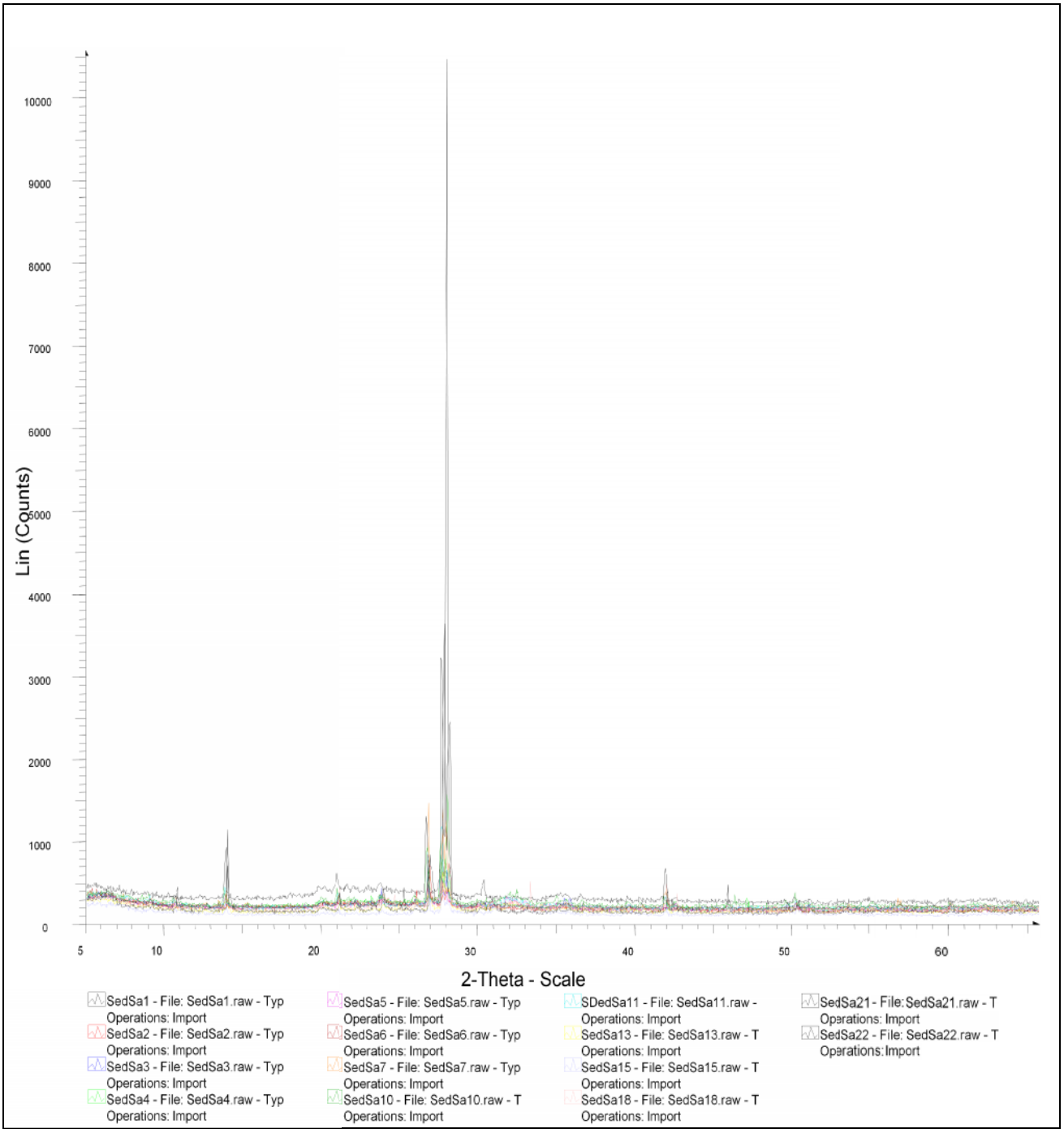

Figure 4.13. X-ray diffraction pattern of selective sediment samples from lithofacies FHL-01 to FHL-09 includes sediment samples FH SS 01, FH SS 02, FH SS 03, FH SS 04, FH SS 05, FH SS 06, FH SS 07, FH SS 10, FH SS 11, FH SS 13, FH SS 15, FH SS 18, FH SS 21, FH SS 22.

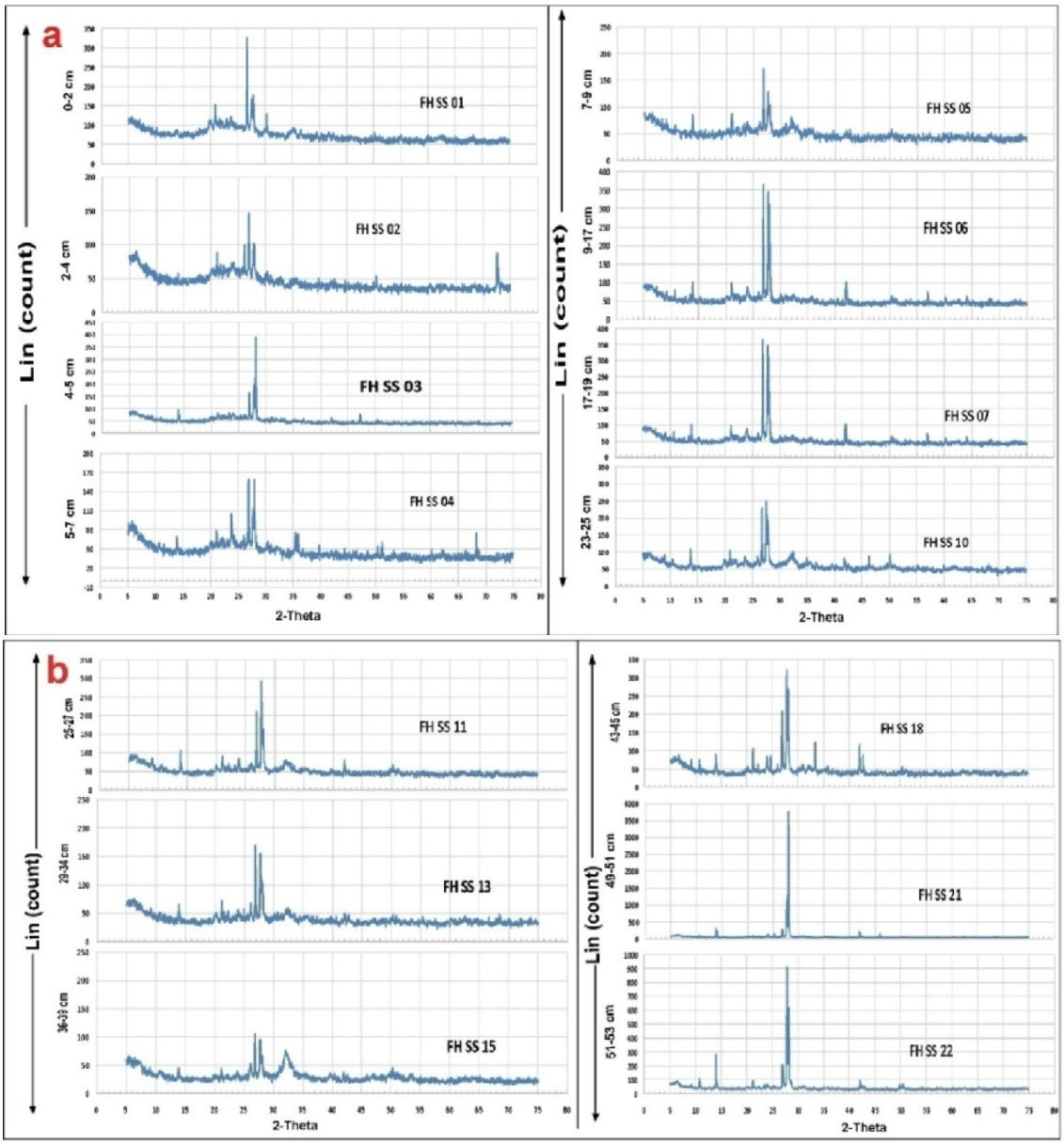

Figure 4.14. X-ray diffraction pattern of selective sediment samples from lithofacies FHL-01 to FHL-09 (a) include sediment samples FH SS 01, FH SS 02, FH SS 03, FH SS 04, FH SS 05, FH SS 06, FH SS 07 and FH SS 10 (b) sediment samples FH SS 11, FH SS 13, FH SS 15, FH SS 18, FH SS 21, FH SS 22.

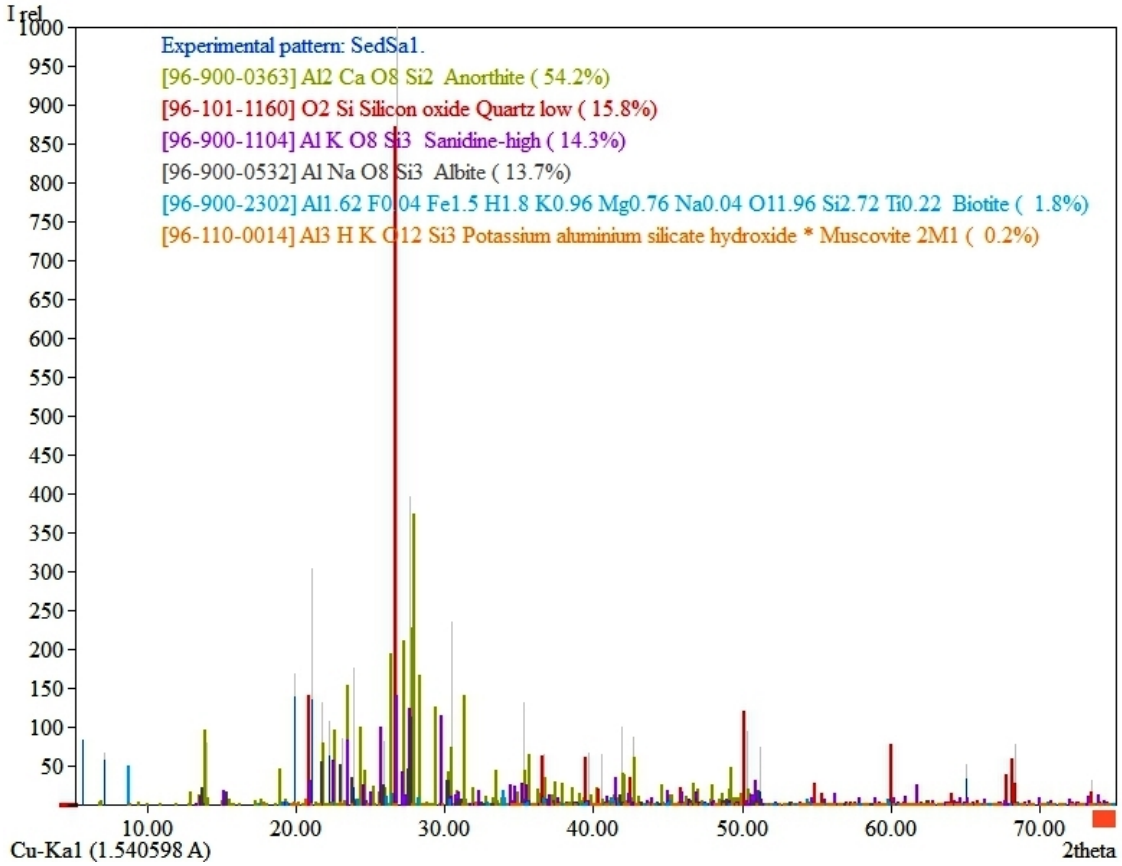

Figure 4.15. Example X-ray diffraction pattern of sediments sample FH SS 01.

After import the 2-Theta degrees and peak intensity raw data value of the sediment samples into the MATCH!(V.3.6) Phase Analysis software the diffraction pattern of the sample and the entry (minerals) that are found within the sediments are exposed automatically (Fig. 4.17). The lists of all minerals that are found within the sediments are listed in the candidate button of the program which is based on their FoM (bottom left side of the fig.). Then search the required expected minerals within the sample either find on the find phase/entries button (on the top-right side of fig.) or on the add entries button (on the upper, middle right side of the fig.) select the elemental composition of the mineral from the periodic table and write the name, formula, and formula sum of the required minerals. Next select the highest concentrated minerals within the sample based on the "figure of merit" (FoM) values from the candidate list of the minerals and by visual agreements from the diffraction pattern (2-Theta value) of the samples (Putz et al, 2018), and drag the corresponding entry from the candidate list to the Match list button (on the bottom-right side of the fig.). Finally, the software gives the semi-quantitative concentration (Quant. (%)) and

the 2-Theta value (i.e. on the peak list button) of the highest dominant minerals found within the sediments (Table 4.14).

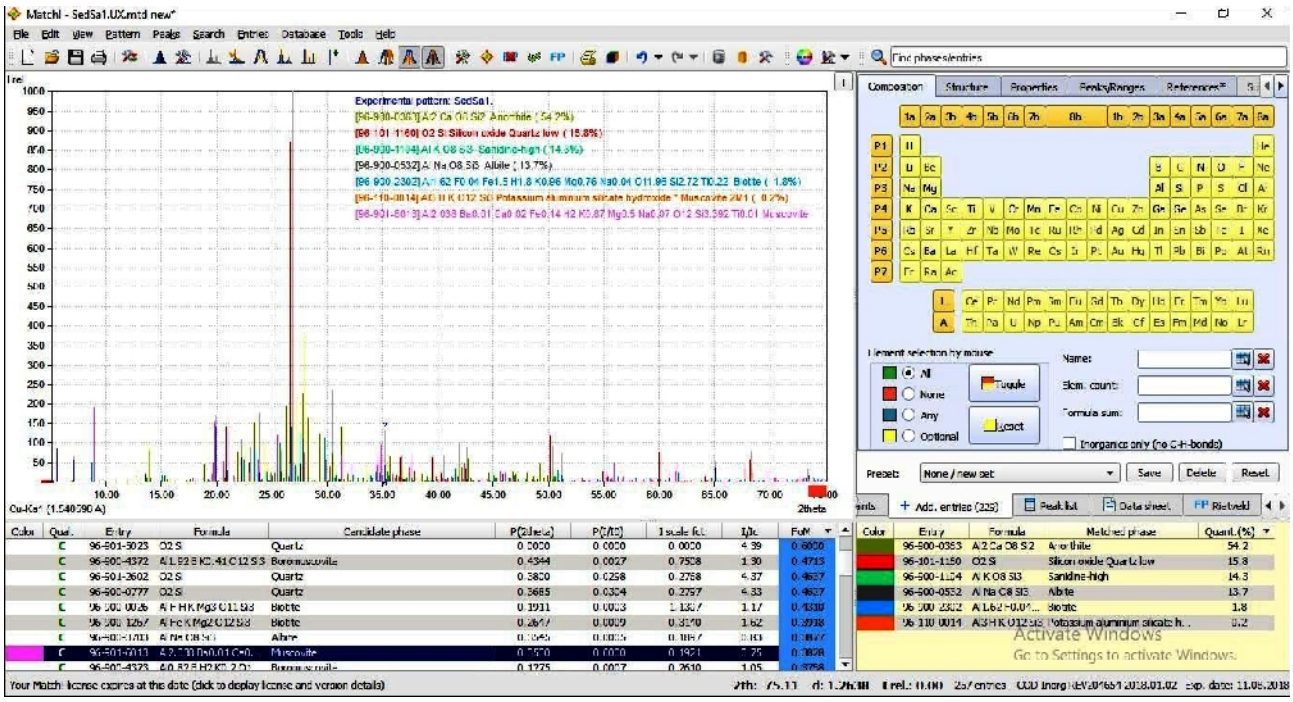

Figure 4.16. The displays view of the Match! Software screen. Where, the upper left side of the image shows the diffraction pattern of the sample, the lower left side is the list of all components found within the sample, ("candidate list") and the "figure of merit" (FoM) values of the minerals, the upper left side of the image include the search (find phases/entries) button and the periodic table which used to write the elemental formula of the required minerals, the lower right side part of the image include the selective minerals with highest concentration.

Table 4.13. Single-peak intensity (Quant. (wt %) and 2-Theta degree) values of silicate minerals.

		Sanidine		Quartz		Muscovite		Biotite		Anorthite		Albite	
Sam. ID	Mean dep.(cm)	Quant. (%)	2Θ	Quant. (%)	2Θ	Quant. (%)	2Θ	Quant. (%)	2Θ	Quant. (%)	2Θ	Quant. (%)	2Θ
FH SS 01	1	14.3	25.87	15.8	26.83	0.2	35.28	1.8	36.66	54.2	27.61	13.7	23.84
FH SS 02	3	5.6	21.14	7	42.76	13.8	23.92	29.3	26.92	29	27.92	15.3	26.09
FH SS 03	4.5	15.8	23.83	5.3	21.05	15.2	23.05	14.3	5.66	49.5	27.96	0	0
FH SS 04	6	13.3	23.75	4.8	26.87	4.4	23.21	5.5	21.06	71.9	28.05	0	0
FH SS 05	8	9.4	26.83	8.7	21.06	7.7	23.15	2.2	8.96	35.1	27.6	37	23.77
FH SS 06	13	7.9	26.04	10.5	21.1	22.4	20.74	0	0	36.9	27.84	22.3	28.18
FH SS 07	18	16.9	25.79	8.4	26.75	0	0	8.7	30.77	59.8	27.72	6.2	22.13
FH SS 10	24	20.6	26.09	13.5	21.11	0	0	26.09	4.6	27.79	38.7	22.7	28.09
FH SS 11	26	41.2	27.68	5	26.78	0.3	20.71	0.7	8.91	52.8	28.01	0	0
FH SS 13	31.5	0	0	1	26.43	30	17.81	12.4	19.22	30.8	26.2	25.7	30.21
FH SS 15	37.5	8.7	23.5	3.1	26.84	0	0	1	19.45	24.6	27.73	62.6	26.05
FH SS 18	44	0.7	27.23	3	20.91	16.4	23.85	0	0	45.4	28.17	34.5	27.9
FH SS 21	50	0	0	0	0	28.7	26.84	0	0	43.4	28.02	27.5	30.98
FH SS 22	52	11.5	23.9	16.1	28.09	1.4	21.1	3.6	36.88	67.4	27.8	0	0

Based on depth distribution (Fig. 4.18) and availability (Fig. 4.19) of some major silicate minerals (feldspars (sanidine, albite and anorthite), quartz, biotite and muscovite) within the sediments the profile (lithofacies) can be described as follows (Table 4.14).

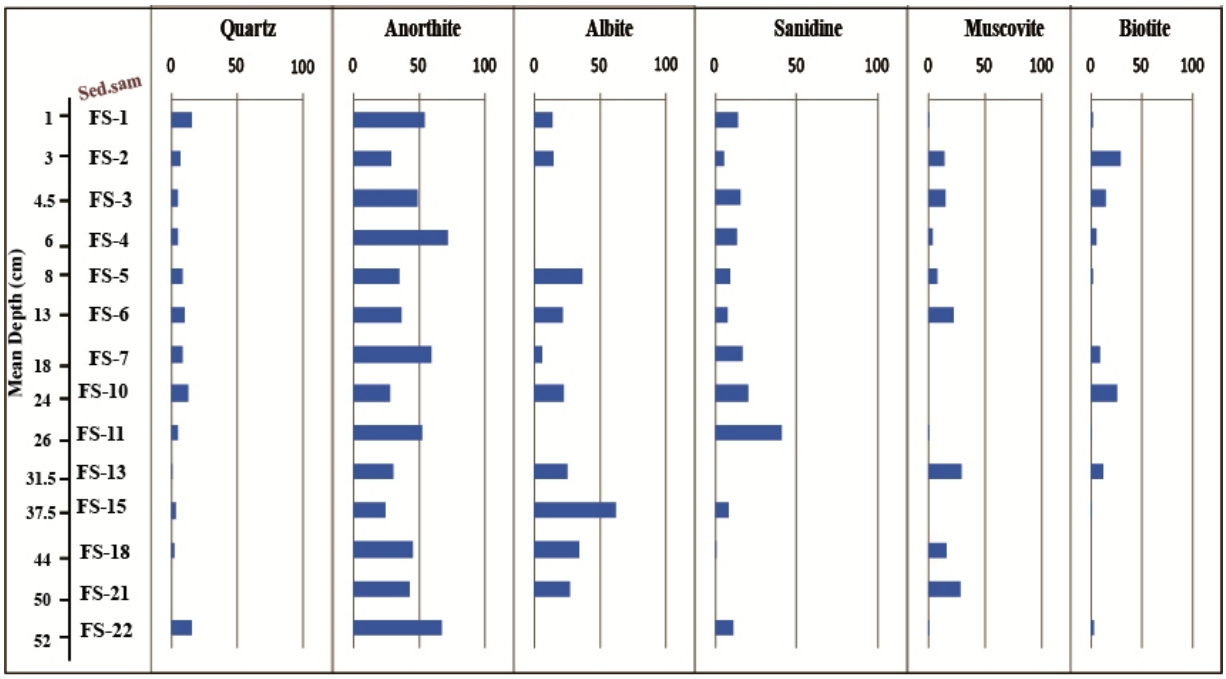

Figure 4.17. Depth- Quant. (%) plot of the single peak intensity variation of silicate minerals.

Table 4.14. Depth distribution and availability of silicate minerals within the sediments.

Sam. ID	Lithofacies	Mean depth (cm)	Available minerals
FH SS 01	FHL-01	1	Very high anorthite, relatively high quartz, sanidine and albite, and extremely low muscovite and biotite minerals.
FH SS 02	FHL-02	3	Relatively high anorthite, very high biotite, albite and muscovite, and low quartz and sanidine minerals.
FH SS 03	FHL-03	4.5	Very high anorthite, high sanidine, muscovite and biotite, and low quartz minerals.
FH SS 04	FHL-04	6	Extremely high anorthite, high sanidine, low quartz, and very low muscovite and biotite minerals.
FH SS 05	FHL-05	8	High anorthite, albite, sanidine and quartz, low muscovite, and very low biotite minerals.
FH SS 06	FHL-06	13	High anorthite, albite, sanidine, quartz and muscovite, and extremely low biotite minerals.
FH SS 07	FHL-07	18	Very high anorthite, high sanidine and quartz, and low biotite and albite minerals.
FH SS 10	FHL-07	24	High anorthite, albite, sanidine and quartz, and very high biotite minerals.
FH SS 11	FHL-07	26	Very high anorthite and sanidine, and low quartz minerals.
FH SS 13	FHL-07	31.5	High anorthite, albite, muscovite and biotite, and extremely low quartz minerals.
FH SS 15	FHL-08	37.5	High anorthite and sanidine, extremely high albite, and very low quartz minerals.
FH SS 18	FHL-08	44	Very high anorthite and albite, high muscovite, and extremely low quartz minerals.
FH SS 21	FHL-09	50	Very high anorthite, albite and muscovite minerals.
FH SS 22	FHL-09	52	Extremely high anorthite, high sanidine and quartz, and extremely low muscovite and biotite minerals.

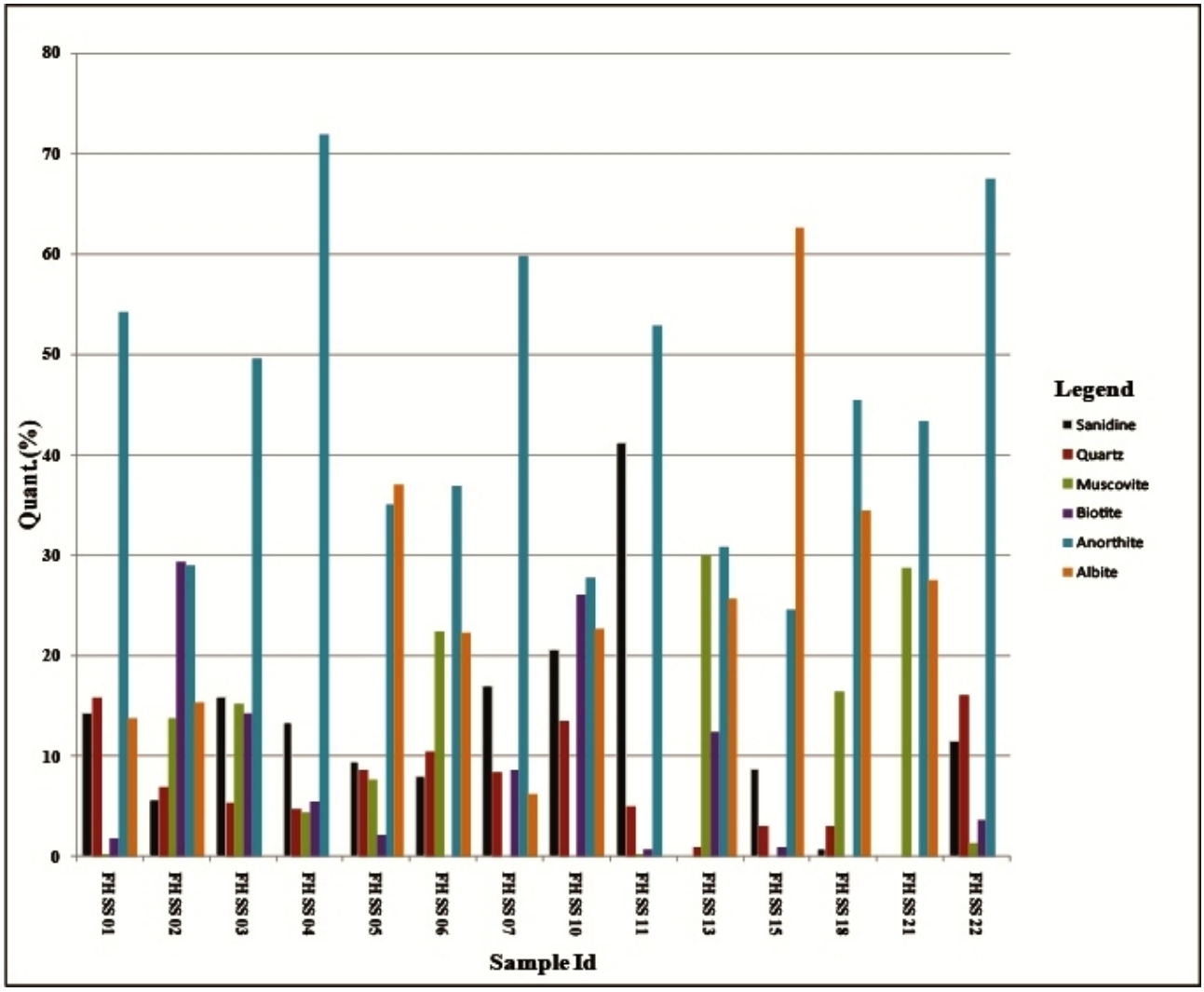

Figure 4.18. Distribution and availability of major silicate (quartz, anorthite, albite, sanidine, muscovite and biotite) minerals within the sediment samples.

CHAPTER FIVE

DISCUSSION AND INTERPRETATIONS

5.1. Depositional histories of the unconsolidated sediments

5.1.1. Transportation media and transportation mechanisms

Water flows are able to transport larger and mixed clasts at the velocity/energy recorded in the river systems (Nicolas, 2009). The nature of the unconsolidated sediments forming the deposits in the rock shelter is very varied in terms of origin, size, shape, sorting, grain size distribution, and compositions. This all may happen due to varying transport conditions of materials/sediments into the depositional setting (the rock shelter). There are black colored and fine grained volcanic rock fragments (basalts) resulting from the breakdown of the underlying bedrock of the shelter at lithofacies FHL-09; geogenic sediments which derived from different sedimentological and geological processes, including weathering, erosion and transportation of polymodally distributed, rounded particles by water from distant source areas (i.e. at lithofacies FHL-07 sediment samples FH SS 07 and FH SS 08 and lithofacies FHL-09 sediment samples FH SS 21 and FH SS 22); and rock fragments as rock fall from the roof of the rock shelter (i.e., basalt) and some light color, fine-grained and angular-shaped volcanic rock fragments (i.e., trachytes/rhyolites) which are transported from the close vicinity of the rock shelter site (i.e., at lithofacies FHL-07 sediment samples FH SS 07 and FH SS 08) (Table 5.1).

The sediment profile also contains anthropogenic deposits, transported and derived from human activities as exogenic inputs (i.e., artifacts/obsidian) and as endogenic products (i.e., ecofacts/charcoal), respectively. There are also biogenic/organic remains (i.e., bones and coprolites) in some levels of the profile.

Based on the particle size distribution of the lithological units, the profile was classified into silt, sandy silt and silty sand size sediments. The ternary diagram of Pejrub (1988) is used to interpret the hydrodynamic energy (i.e., the energy levels during sedimentation) of the sandy silt and silty sand size sediment deposits (Varghese, 2014). The lithological units are all devoid of clay sized sediments, and all the analyzed samples fall into category IV (Fig.5.1), suggesting that the

sediments were transported under energetic (violent) to most energetic hydrodynamic conditions (Pejrub, 1988).

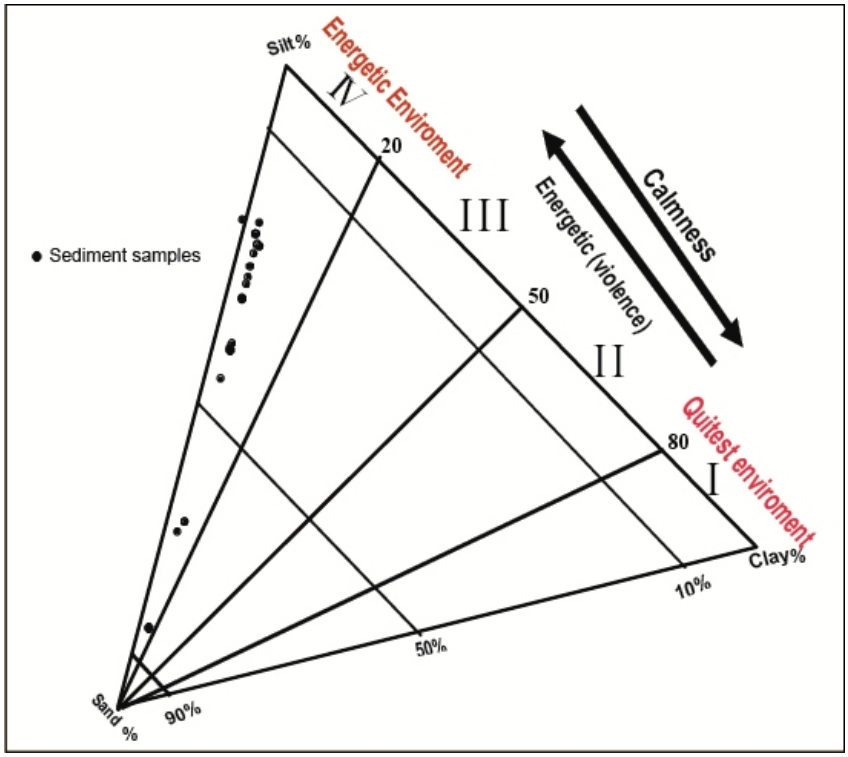

Figure 5.1. Ternary diagram proposed by Pejrub (1988); where the numbers I, II, III and IV indicates that the relative hydrodynamic energy of the environment during sediment transportations (after Varghese, 2014).

Table 5.1. Summary of the depositional history of the sediments, Fincha Habera section.

Lithofacies/ lithological unit	Sample Id	Mean depth (cm)	Mean grain size (µm)	Physical description	Transportation mechanisms	Depositional environments
FHL-01 /LU-01	FH SS 01	1	11.97	Dark grayish brown (10YR4/2), medium silt size sediments	Suspended load fluvial systems	Over bank deposits
FH L-02 /LU-02	FH SS 02	3	19.9	Black (10YR2/1) color, very fine sandy medium silt size sediments with charcoal	Suspended load fluvial systems and anthropogenic activities	Over bank deposits and human occupations
FHL-03 /LU-03	FH SS 03	4.5	17.6	Dark brown (10YR3/3), coarse sandy medium silt size sediments	Suspended load fluvial systems	Over bank deposits
FHL-04 /LU-03	FH SS 04	6	35.41	Dark gray (10YR4/1), coarse sandy medium silt size sediments	Suspended load fluvial systems	Over bank deposits
FHL-05 /LU-03	FH SS 05	8	27.28	Brown (7.5YR5/3), very fine sandy coarse silt size	Suspended load fluvial systems,	Over bank deposits

				sediments with sizable quantity of burned, broken bones, charcoal deposits	biogenic and human induced (anthropogenic) components	
FHL-06 /LU-04	FH SS 06	13	48.87	Black (10YR2/1), charcoal with fine sandy coarse silt size sediments	Suspended load fluvial systems and anthropogenic activities	Over bank deposits and human occupations
FHL-07 /LU-05	FH SS 07 FH SS 08	18 20	19.89 22.37	Light brown (10YR6/2), fine sandy medium silt sediments with gravel and maximum amount of obsidian artifacts, bone, and coprolites	Bed/mixed load fluvial systems and anthropogenic input particles	Channel deposits
FHL-07 /LU-03	FH SS 09	22	20.76	Light brown (10YR6/2), fine sandy fine silt size sediments	Suspended load fluvial systems	Over bank deposits
	FH SS 10 FH SS 11 FH SS 12 FH SS 13	24 26 28 31.5	22.64 25.89 21 25.89	Light brown (10YR6/2), fine sandy medium silt size sediments		
FHL-08 /LU-03	FH SS 14 FH SS 15 FH SS 16	35 37.5 40	28.97 25.86 38.16	Grayish brown (10YR5/2), fine sandy medium silt size sediments	Suspended load fluvial systems	Over bank deposits
	FH SS 17	42	26.74	Grayish brown (10YR5/2), very fine sandy medium silt size sediments	Suspended load fluvial systems	Over bank deposits
	FH SS 18	44	39.74	grayish brown (10YR5/2), fine sandy coarse silt size sediments		
FHL-08 /LU-06	FH SS 19	46	121.4	Grayish brown (10YR5/2), medium silty medium sand size sediments	Bed load fluvial systems	Channel deposits
	FH SS 20	48	85.56	Grayish brown (10YR5/2), medium silty fine sand size sediments		
FHL-09 /LU-07	FH SS 21	50	83.86	Brownish yellow (10YR6/6), very coarse silty fine sand sediments with gravel	Mix load fluvial systems	Channel deposits
	FH SS 22	52	140			

In addition, most of the analyzed samples are characterized by a polymodal nature (highly distributed from very fine silt to very coarse sand size sediments) and consist of poorly to very poorly sorted (texturally unmatured) sediments. These physical (lithological) characteristics and the absence of clay sized (<2µm) sediments suggest that the sediments were carried by a high energy current. The higher flow rates might have caused the pure silt (lithological unit LU-01) and sandy silt (lithological units LU-02, LU-03 and LU-04) size sediments to be kept as suspension load, where as the mixed, poorly sorted and rounded rock fragments with sandy silt (lithological unit LU-05) and silty sand (lithological unit LU-07), and the silty sand (lithological unit LU-06) sediments may have been carried as bed load and mixed load deposits by

rolling/saltation processes (Nicolas, 2009). In sum, this evidence suggests that the sediments may have been carried by the mountain headwater streams (i.e., hence, waterfalls are common) and by the nearby perennial rivers (e.g., the Weyib River), and when the energy of the transportation and elevation of the streams decreased, the sediments started to be deposited at the gentle slope (Gellis et al., 2016) at the mouth of the rock shelter sites.

The sign of skewness (asymmetry of particle distribution) is also related to the variation in energy of transportation/deposition agents (Martins, 2003). The sediments in the shelter show a mixture of positive and negative skewed nature (mixing of fine/silt and coarse/sand size sediments) (Fig.5.2) suggesting an area in a state of flux (Duane, 1964 cited in Martins, 2003). Positive skewness (sandy silt sediments) is attributed to relatively low energy of deposition where the competence of the transportation agent is unidirectional and carries dominantly fine-grained sediments (Martin, 2003). This situation is manifested by the lithological units LU-01, LU-02, LU-03, LU-04, and LU-05. On the other hand, negative skewness implies high energy of transportation and this causes a deposition of dominantly coarse/sand size (silty sand) sediments by the winnowing currents of the water. Lithological units LU-06 and LU-07 are deposited under such conditions.

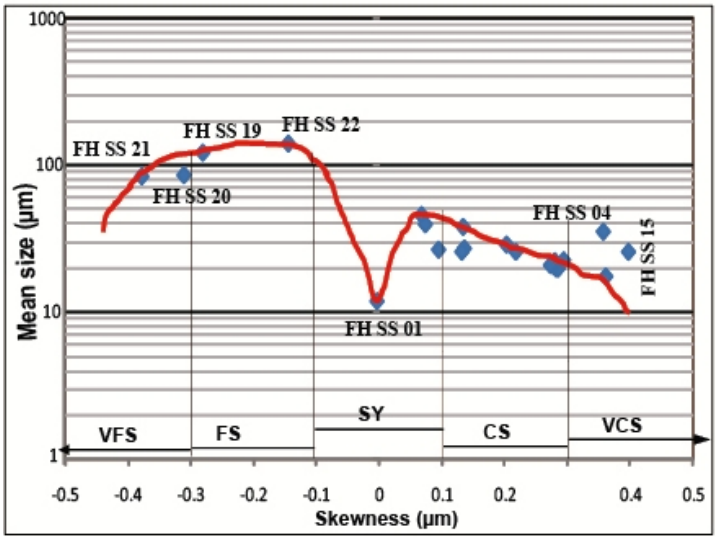

Figure 5.2. Scatter plot of mean size versus skewness; where very fine skewed (VFS) and fine skewed (FS) silty sand sediments at lithological unit LU-06 and LU-07, and symmetrical (SY), coarse skewed (CS) and very coarse skewed (VCS) silt and sandy silt sediments at lithological unit LU-01, LU-02, LU-03, LU-04 and LU-05, are shown.

5.1.2. Depositional environments of the sediments

Combined evidence from the lithofacies association, the geomorphological setting of the study area, the grain size distribution of the sediments along the profile, the scatter diagram of the grain size parameters (mean versus standard deviation or sorting), and the trace element ratio of some selected elements (Zr/Rb and Zr/Ti) versus the D_{50} (median size) of the sediments, show the unconsolidated sediments in the rock shelter have been deposited by fluvial processes.

The bivariate plots of the mean size versus standard deviation value (sorting) in a logarithmic scale (Fig.5.3 and Fig.5.4) can be used to evaluate the depositional environment and the associated energy (hydrodynamic energy) of the deposits (Folk and Ward, 1957; Tanner, 1991; Lario et al., 2000; Watson et al., 2013; Varghese, 2014; Kanhaiya et al., 2017). The scatter plots reveal that all sediments have been deposited in a fluvial depositional environment by high energy channel flows. Both, mean grain size and sorting are hydraulically controlled parameters (Folk and Ward, 1957), and the sediments deposited in the rock shelter are characterized by poor to very poor sorting suggesting that the hydraulic energy was very inefficient to develop sorting during sedimentation in fluvial environments (both floodplain/overbank and channel deposits) (Kanhaiya et al., 2017).

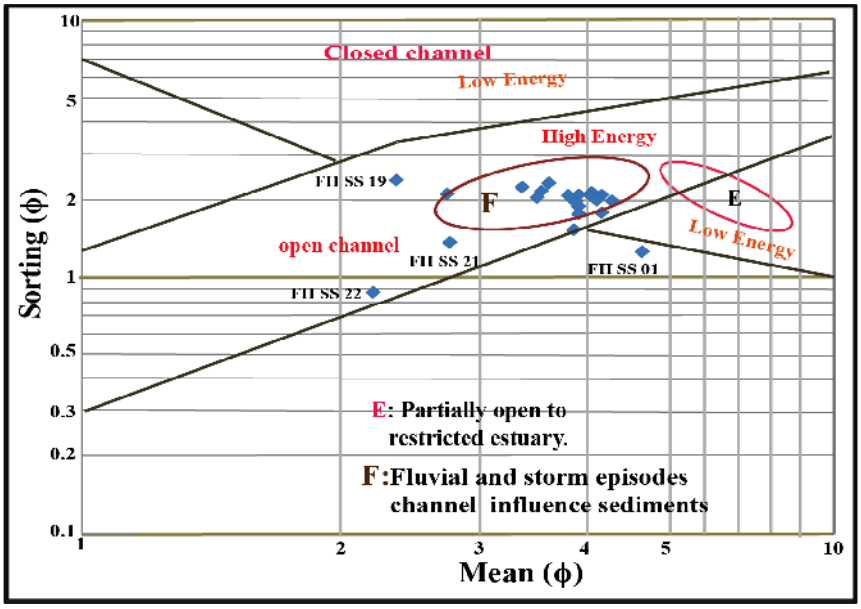

Figure 5.3. Depositional environment and hydrodynamic energy of the unconsolidated sediments based on mean versus sorting scatter diagram (after Tanner 1991 a, b; Varghese, 2014). The phi values of all grain size parameters are presented in Appendix 1.

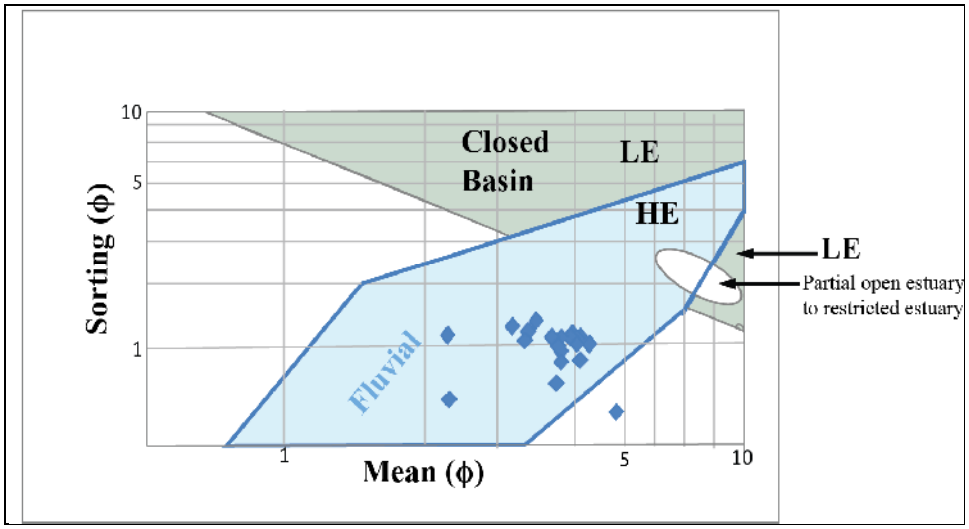

Figure 5.4. Scatter diagram of mean grain size versus sorting of sediments: implication for the interpretation of depositional environment and hydrodynamic energy of sediment deposits (after Lario et al., 2000; Watson et al., 2013). HE and LE are high and low energy, respectively.

During sediment transportation by surface water, the immobile elements (Zr and Ti) are not expected to be strongly fractionated by weathering and other post-depositional sedimentological processes relative to the source region (Taylor and Mclennan, 1985 cited in Feng and Kerrich, 1990) and they are concentrated in particular grain size fractions due to the varying resistance of the minerals in which these elements occur (Turner et al., 2015). The correlation between particular element ratios such as Zr/Rb and Zr/Ti with actual grain size analysis (D_{50}) (Fig. 5.5) can be used as a proxy for the reconstruction of fluvial depositional environments (Turner et al., 2015). Accordingly, Zr is relatively more concentrated in the silty sand/coarse size sediments at lithological unit LU-06 (sediment samples FH SS 19 and FH SS 20) and lithological unit LU-07 (sediment samples FH SS 21 and FH SS 22), while Ti and Rb are relatively more concentrated in the sandy silt/fine size sediments. Generally, the Zr/Rb and Zr/Ti ratios show an increasing trend with increasing grain sizes of the sediments from the top pure silt size sediments at lithofacies FHL-01 (lithological unit LU-01) to the bottom silty sand size sediments at lithofacies FHL-09 (lithological unit LU-07). This all supports the fining upward sequence characteristics of the lithofacies association of the fluvial depositional environments.

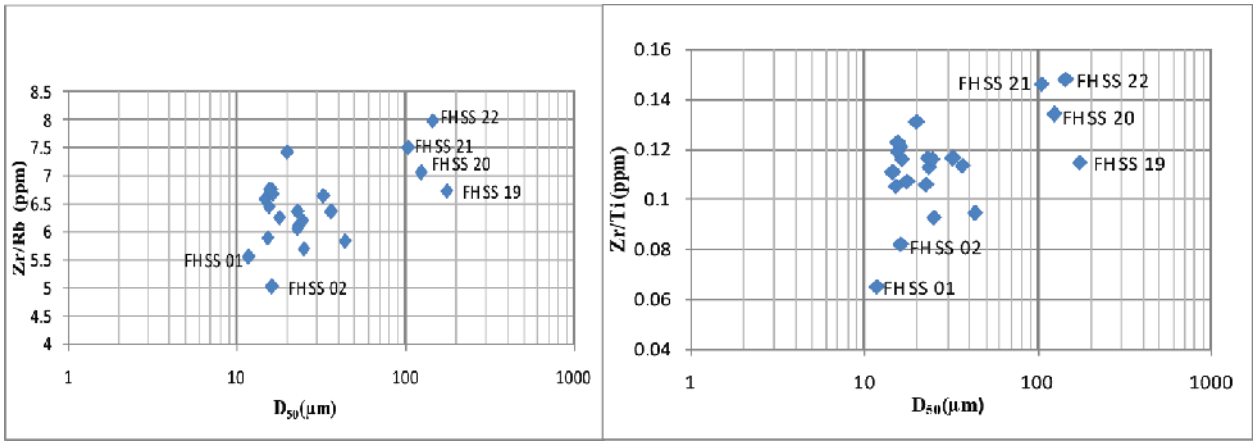

Figure 5.5. Scatter diagram showing the correlation between Zr/Rb and Zr/Ti with actual grain size analysis of sediments D_{50} (median) (after Turner et al., 2015).

The simplified geomorphological setup (Fig.5.6) of the study area and the particle size distribution of the sediments (lithological units) show that sediments were removed from the erosional zones at the source areas (the mountainous zone of the region) by high energy water and transported to the lower slope transfer zones. Deposition barely occurs in the transfer zone due to still high current of water (Fig.5.1), rather the silt and fine sandy silt sediments are carried as suspension load, while the silty sand sediments and the mixture of medium-coarse sand size sediments with the rounded, gravel size and polymodal rock fragments are transported by rolling/saltation as bed/mixed load fluvial systems to the lower elevated zones of the area (rock shelter), where ultimate deposition occurs. When the energy of transportation decreased, the silt and fine sandy silt size sediments (at lithological unitsLU-01, LU-02, and LU-03 including lithofacies FHL-01, FHL-02, FHL-03, FHL-04, FHL-05, FHL-07 [sediment samples FH SS 09,FH SS 10, FH SS 11, FH SS 12 and FH SS 13], FHL-08 [sediment samples FH SS 14, FH SS 15, FH SS 16, FH SS 17and FH SS 18], and lithological unit LU-04 [lithofacies FHL-06; sediments sample FH SS 06]) were possibly deposited beyond the channel of the river as overbank or floodplain deposits (e.g., Kanhaiya et al., 2017). During flood stage the bed load and mixed load sediments were deposited along the channel margins as waters overflow through the confining over bank deposits (e.g., Galloway and Hobday, 1996). Similar to the rock shelter deposits, the silty sand size sediments at lithological unit LU-06 (lithofacies FHL-08 sediment samples FH SS 19 and FH SS 20) and the mixture of the sandy silt and silty sand size sediments with the rounded, gravel size and polymodal rock fragments at lithological unit LU-05

(lithofacies FHL-07 sediment samples FH SS 07 and FH SS 08) and lithological unit LU-07 (lithofacies FHL-09 sediment samples FH SS 21 and FH SS 22) were possibly deposited as channel system when the river was in a flood stage (Galloway and Hobday, 1996; Nicolas, 2009; Kanhaiya et al., 2017).

Generally, the sequence is characterized by the deposition of a mixture of fine and coarse-grained sediments as suspended and bed load levels (i.e., within individual lithofacies). However, the overall succession (i.e., the lithofacies association) of the profile shows a fining upward sequence with retrogradation of grain sizes from silty sand size sediments at the bottom (lithological unit LU-07) to the pure silt size sediments at top of the sequence (lithological unit LU-01) (i.e., the mean grain sizes are fine up section from 140 to 11.97µm respectively). This all suggests that the overall succession of the deposits shows a lateral accretion of depositional environments from channel deposits (typically at lithological unit LU-07) to overbank deposits (at lithological unit LU-01) and aggradations of sediments from silty sand and gravel size sediments at the bottom (lithological unit LU-07) to the silt size sediments at the top of the sequence (lithological unit LU-01). However, the material (i.e., charcoal) deposit found within sandy silt size sediments at lithofacies FHL-02 (LU-02) and FHL-06 (LU-04) indicates that the evidence of human settlement and adaptation of different types of cultural activates.

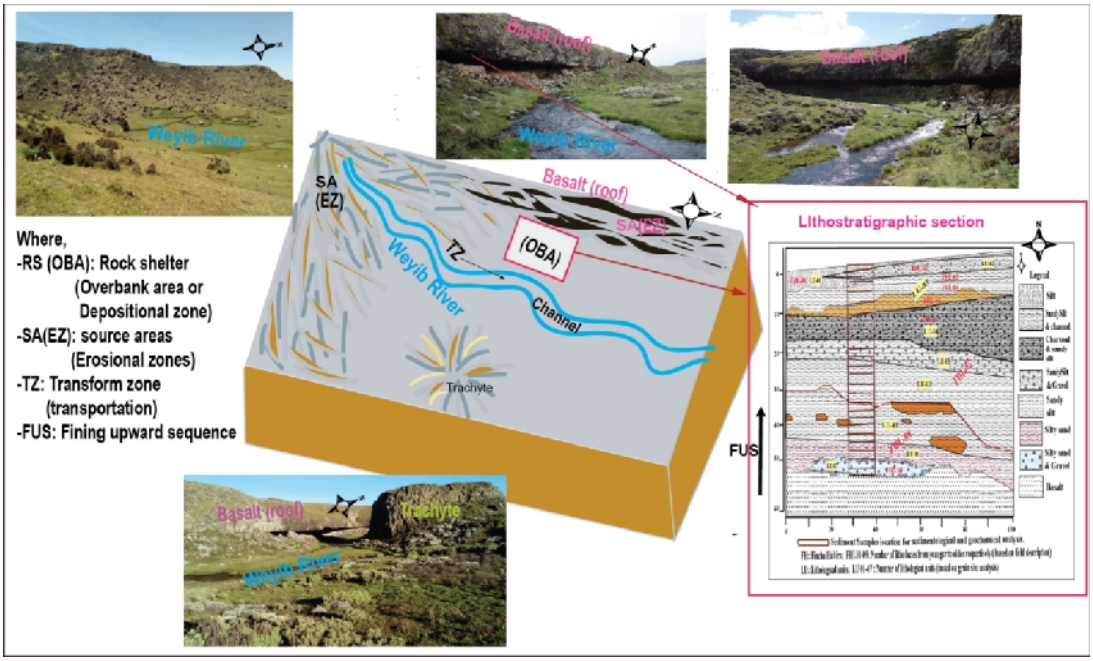

Figure 5.6. Simplified geomorphological setup and lithostratigraphic section of the study area.

5.2. Provenance (source) of the sediments

The macroscopic/field description (lithofacies), grain size analysis, magnetic susceptibility measurement, and elemental and mineralogical compositions of the unconsolidated sediments deposited in the rock shelter show a sediments/materials with very varied in origin (natural or geogenic, biogenic and anthropogenic); size (gravel, sand and silt size sediments); in shape (rock fragments which were recovered from 2mm mesh size); in sorting (poorly to very poorly sorted); distribution (polymodal distribution from very fine silt to very coarse sand size sediments), and in geochemical compositions.

The particle size distribution (poorly- very poorly sorted), on the elemental composition (e.g., the variation diagram of most samples show an increase trend of Al_2O_3, K_2O, Fe_2O_3, CaO, and P_2O_3 with low SiO_2 contents) and mineralogical compositions (i.e., predominantly higher concentration of plagioclase feldspars [anorthite and albite] and minor sanidine, quartz, muscovite and biotite minerals) of sediments suggest that the sediments are under incipient stage of chemical weathering (Maftei et al., 2018) and texturally as well as mineralogically immature.

The heterogeneity/polymodality of the sediments has been a significant challenge in determining the sources of the unconsolidated sediments. However, the integration of data from field description (lithofacies), sedimentological analysis (grain size and magnetic susceptibility measurement), and geochemical analysis (elemental and mineralogical compositions) of the sediments has been used as combined proxy for provenance determination. Accordingly, the integrated data suggest that the materials/sediments that are deposited in the rock shelter have a mixture of three sources: geogenic either as endogenic or exogenic origins; biogenic and human induced (anthropogenic) origins.

5.2.1. Source of geogenic sediments

5.2.1.1. Physical/sedimentological nature of rock fragments

The terrigenous clastic sediments include a mixture of gravel to silt size particles. The gravel size rock fragments (i.e., those recovered from 2mm mesh size) originated either as falls from the roof of the rock shelter (endogenic particles which are typically basaltic in composition) or externally derived by different sedimentological processes including weathering, erosion and

transportation of polymodal mixture of rounded shape gravels via high energy stream flowing into the shelter through the mouth (i.e., as exogenic particles); these are typically found at lithofacies FHL-07 (sample FH SS 07 and FH SS08; lithological unit LU-05) and lithofacies FHL-09 (LU-07). In addition, there are some light color, angular, fine grained trachytic/rhyolitc rock fragments (i.e. exogenic particles) which are transported from close to the rock shelter sites at lithofacies FHL-07 (lithological unit LU-05).

5.2.1.2. Elemental compositions

The sedimentological characteristics of the sand silt and silty sand size sediments (<2mm) are highly variegated. The grain size analysis of the sediments already suggested that the sandy silt and silty sand sediments were transported by high energy stream flows and deposited as open fluvial depositional environments.

The geochemical classification diagram of clastic sediments using the log ratio of major elements (log (SiO_2/Al_2O_3) and log (Fe_2O_3/K_2O)) can be used as an indicator of the chemical maturity and mineralogical stability of the sediments, respectively (Pettijohn et al., 1972; Herron, 1988; Verghese, 2014; Henry and Romanus, 2016). Hence, the major elements ratio of the sediments have log (SiO_2/Al_2O_3) value between 0.5 and 1 and log (Fe_2O_3/K_2O) between 0.2 and 0.6, and all the sediment samples fall in the wacke and litharenite fields (Fig.5.7). Low SiO_2/Al_2O_3 and Fe_2O_3/K_2O ratios indicate that the sediments are chemically/mineralogically immature (Henry and Romanus, 2016) and originated from volcanic rocks with high proportion of rocks forming less stable minerals (i.e., feldspar minerals) and a heterogeneous mixture of volcanic lithic fragments (i.e., wackes) (Henry and Romanus, 2016).

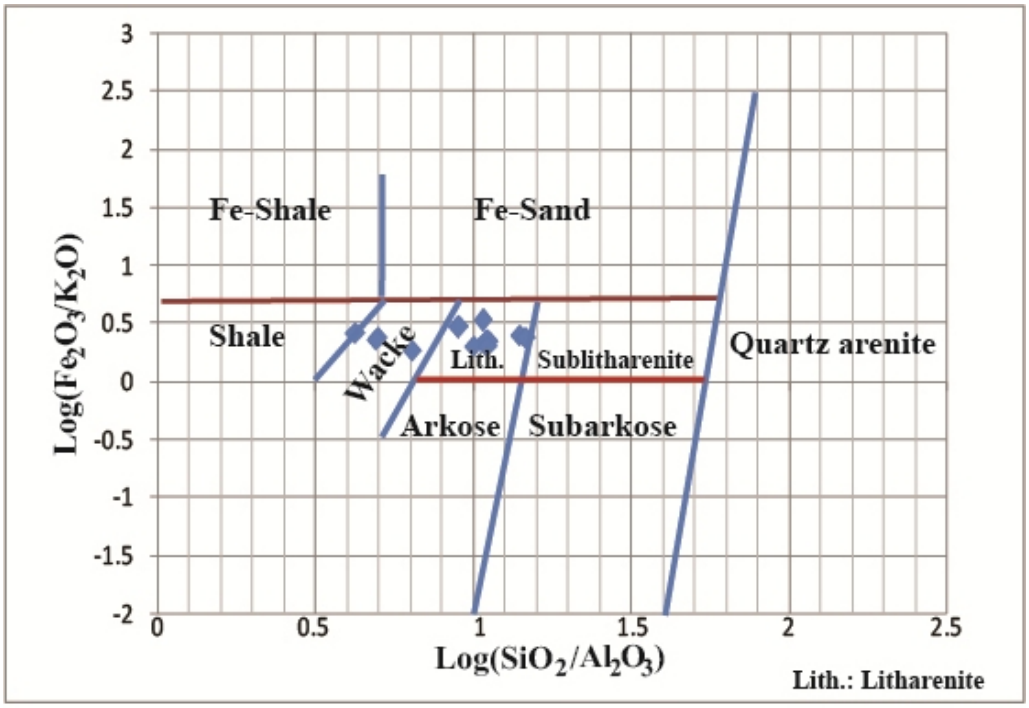

Figure 5.7. Geochemical classification of terrigenous sediments using the log ratio of major elements (after Herron, 1988; Varghese, 2014).

The ratio between less mobile major elements (Al_2O_3 and TiO_2) of clastic sediments could also be used as proxy to infer the chemical composition of the source rocks (Barbera et al., 2006). Accordingly, the Al_2O_3 and TiO_2 ratio of the sediments in Fincha Habera section range from 3 to 6.4 wt % (see Table 4.12) and this suggests that the sediments are derived predominantly from mafic source rocks as they consist (Al_2O_3/TiO_2) ratio of lesser than 14 wt % (Barbera et al., 2006; Verghese, 2014).

5.2.1.3. Mineralogical compositions

The sediments are predominantly composed of the major sedimentary rock forming silicate minerals (i.e., quartz, micas and feldspars in increasing proportion): quartz (1.0 -16.1%), muscovite (0.2-28.7%), biotite (0.7-29.3%), sanidine (0.7-41.2%), albite (6.2-62.6%) and anorthite (24.6-71.9%). Most of the samples lie nearly in plagioclase (anorthite + albite) fields in a Qtz-Alk-Pl Ternary diagram (Fig. 5.8), implying that that the geogenic sediments are formed under low degree of chemical weathering and characterized by an input of relatively higher proportion of mafic volcanic rocks.

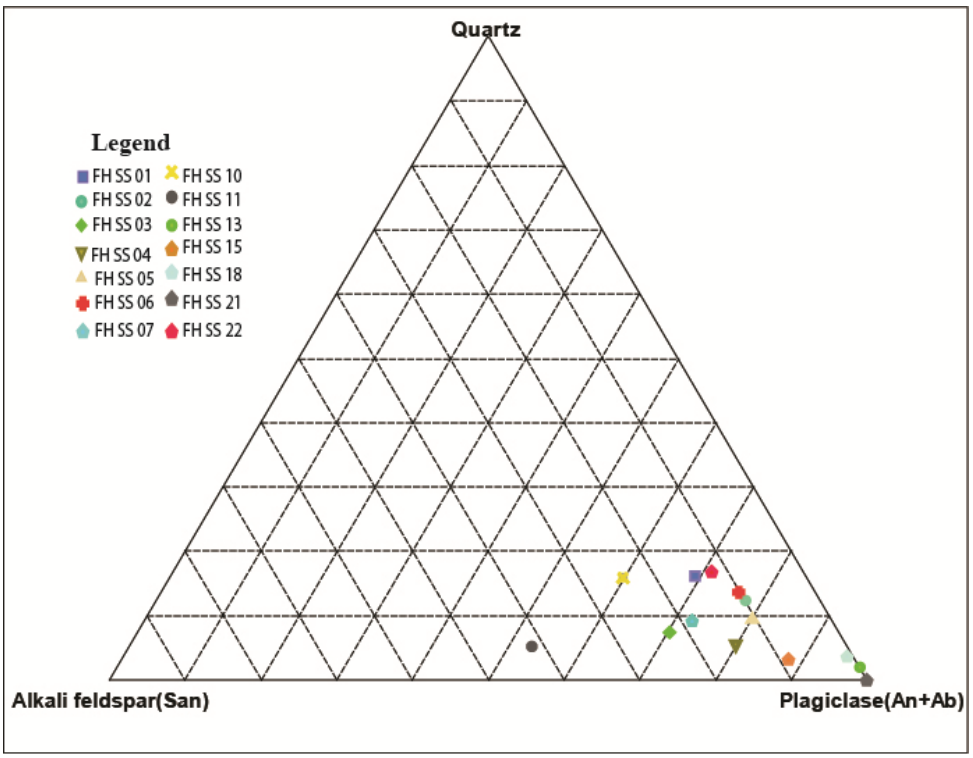

Figure 5.8. Quartz-alkali feldspar-plagioclase plot that shows the distribution of the minerals within the sediments.

However, there are some sediment samples from lithofacies FHL-01 (FH SS 01) which consist of proportionally higher contents of quartz and sanidine minerals; FHL-7 sediment sample FH SS 11 with high content of sanidine minerals; FHL-08 sediment sample FH SS 18 with high content of quartz and muscovite minerals, and FHL-09 sediment samples FH SS 21 and FH SS 22 with high content of quartz. These suggest occasionally higher input of sediments from felsic volcanic (trachy-rhyolitic) source rocks.

5.2.2. Source of biogenic and anthropogenic particles

In addition to the geogenic particles the archeological excavations at Fincha Habera rock shelter (3469 masl), revealed a succession of fluvial sediments with considerable human input and biogenic components of varying extent and nature. Biogenic components which are derived from organic remains (bone and teeth remains of micro-mammals, i.e., rodents, and organic wastes of big mammals, i.e., coprolites) are typically found at the bottom layer of lithofacies FHL-07 and lithofacies FHL-08. The anthropogenic components which originated from human activities

include particle input as exogenic (i.e. artifacts/obsidian) and as endogenic products (i.e., charcoal).

Archeological surveys led to the discovery of five primary obsidian outcrops located almost on top of the prominent Wasama Ridge (Götz et al., 2018). At altitudes between 3959 and 4240 masl, these high-quality raw materials are embedded in ignimbrite rocks. Abundant surface scatters of flaked obsidian artifacts evidence extensive human extraction of obsidian in the past. Obsidian represents the dominantly used raw material (89.8%) at Fincha Habera (Götz et al., 2018). Geochemical analysis reveals high amounts of phosphorus and calcium, indicates availability of high concentration of the remains of herbivores animals (i.e., faces of rodents and hyenas are major input in these layers).

5.2.2.1. Interpretation on the magnetic susceptibility of the sediments

Magnetic susceptibility can be used as a proxy as indicator of source/origin of sediments. All environmental materials have a susceptibility value ranging from <0.001 to >30*10^{-6} m^3kg^{-1} (SI) (Dearing, 1999). In natural environments, the magnetic susceptibility/property ("magnetizability") of the material provides information on the type of the mixtures of ultrafine super paramagnetic minerals which are present within the sediment deposits (Dearing, 1999; Boadi et al., 2014). The mineralogy of the unconsolidated sediments (dominantly plagioclase feldspars [anorthite and albite] and minor sanidine, quartz, biotite and muscovite) in the Fincha Habera section indicates that the sediments are predominantly sourced from mafic rocks. However, in addition to natural magnetization, the magnetic property of sediments can also be affected by various anthropogenic activities (Dearing, 1999; William, 2004). Combustion/heating of the sediments (enhance/increase the magnetic susceptibility value) and occurrence of sizable quantity of organic matter such as charcoal deposits (i.e., low magnetic susceptibility value) can affect the magnetic susceptibility of the sediments. The magnetic susceptibility value can be correlated with the Ca and P concentration (possible indicators of biogenic materials) and the grain size distribution. Accordingly, the section can be divided into 4 magnetic susceptibility zones, some of which are repetitive along the section (Fig.5.9).

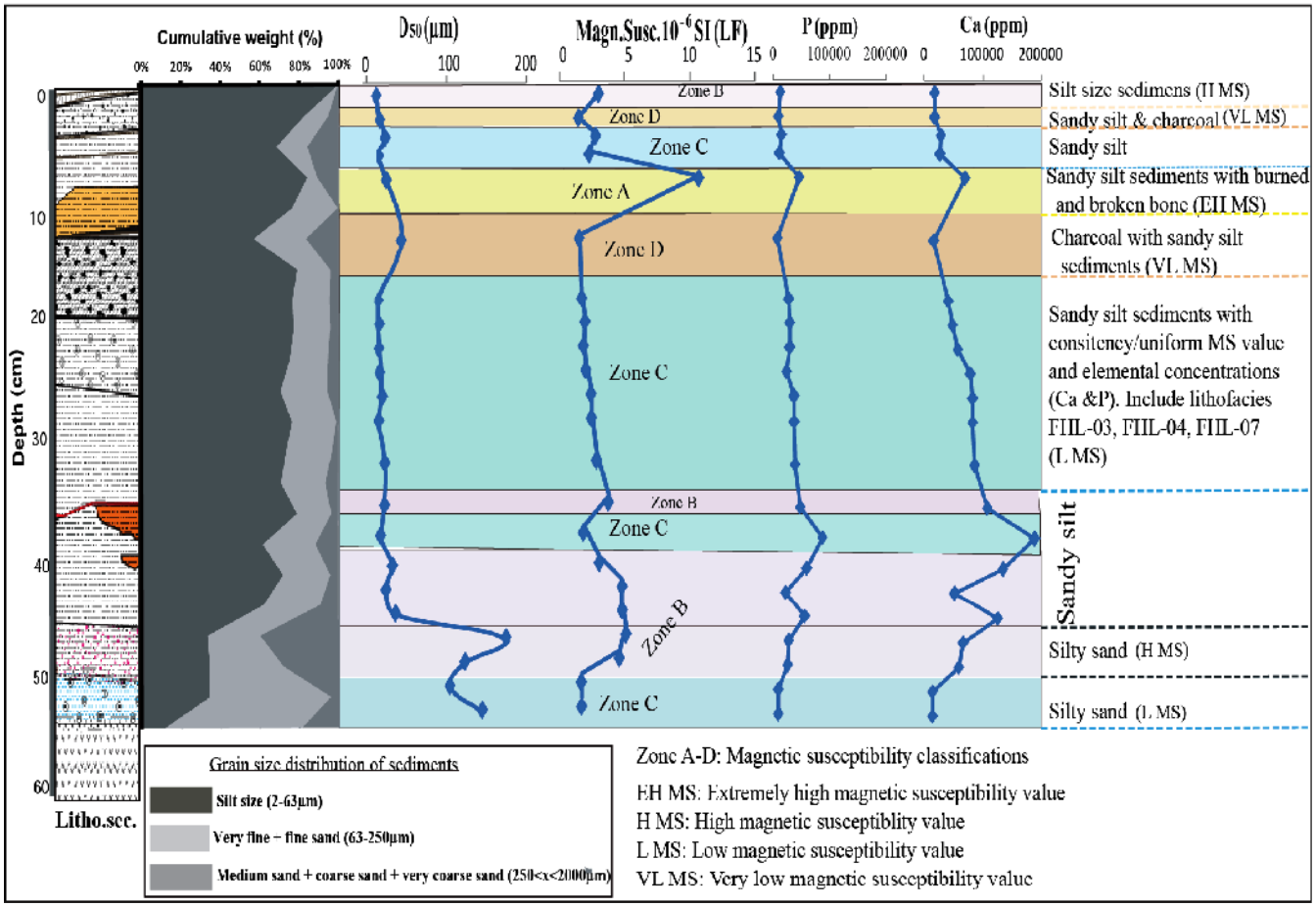

Figure 5.9. Correlation between the grain size distribution of the sediments, frequency dependence magnetic susceptibility measurement (LF), and selected elemental concentrations (Ca and P) (ppm).

Zone A

An elevated value of magnetic susceptibility corresponding to high Ca and P concentration is observed at lithofacies FHL-05, fine/sandy silt size sediments layer (marked zone Zone A in Fig. 5.9) and this could be attributed to the presence of fragments of burned organic remains and organic wastes (bones and coprolites respectively) (William, 2004; Hayes, 2013). Though it is likely that the high Ca content could also be related to the prevalence of plagioclase feldspars, burning of the sediments and the biogenic (bone) fragments could increase the Ca concentration and the magnetic susceptibility.

Zone B

The silt size sediments at lithofacies FHL-01, sandy silt size at lithofacies FHL-08 (sample FH SS 14, FH SS 16, FH SS 17 and FH SS 18), and silty sand sediments at lithofacies FHL-08 (sample FH SS 19 and FH SS 20) are generally characterized by lack of organic matter (charcoal) and low Ca and P concentrations. However, those lithofacies groups (marked Zone B) have elevated positive magnetic susceptibility values ranging from 3.02×10^{-6} SI to 5.13×10^{-6}SI. This could be attributed to the presence of relatively higher concentration of ultrafine super paramagnetic minerals sourced from mafic volcanic rocks.

Zone C

The sandy silt and silty sand size sediments at lithofacies FHL-03, FHL-04, FHL-07, FHL-08 (FH SS 15) and at lithofacies FHL-09, respectively (marked Zone C) have lower but positive magnetic susceptibility values than zones A and B, ranging from 1.7×10^{-6} SI to 2.86×10^{-6} SI. This might suggest that these layers contain small quantities of ultrafine paramagnetic minerals (Dearing, 1999; Plado et al., 2016). Sandy silt size sediments at lithofacies FHL-03, FHL-04 and FHL-07 have uniform/consistent magnetic susceptibility, and Ca and P values, possibly suggesting that these sediments may originate from the same parent material. The sandy silt sediment at FH SS 15 from lithofacies FHL-08 has low susceptibility value due possibly to the high concentration of organic matter (charcoal) in this layer. However, the sample also consists of high and extremely high P and Ca concentrations, respectively, from high content of biogenic fragments/remains (bones and coprolites).

Zone D

Generally, the sandy silt size sediments at lithofacies FHL-02 and FHL-06 (marked Zone D) are characterized by very low magnetic susceptibility values range from 1.48×10^{-6} SI to 1.53×10^{-6} SI, and low Ca and P concentrations. This could be attributed to the sizable quantity of organic maters (anthropogenic ash and charcoal) within these sediments (William, 2004).

CHAPTER SIX

CONCLUSIONS AND RECOMMONDATIONS

6.1. Conclusions

Field (lithofacies), geochemical and sedimentological investigations of sediments at the Fincha Habera section provides valuable information on the provenance and depositional history of the unconsolidated sediments. All datasets allow determining the nature of the geogenic, biogenic and anthropogenic materials, which contribute to buildup of the sedimentation history at the rock shelter site. Based on these studies, the following major conclusions are derived:

- The grain size analyses of the sediments reveal that most of the samples are characterized by poorly to very poorly sorted and polymodaly distributed sediments (i.e., from very fine silt to very coarse sand). These suggest that the sandy silt and silty sand sediments are texturally immature and transported by high-energy stream flows, while the mean versus sorting (standard deviation) relationship of the sediments suggest that they are deposited at open fluvial depositional environments.
- The physical/sedimentological nature of rock fragments which are recovered from >2mm mesh size are highly variegated and either originated as falls from the roof of the rock shelter (endogenic particles which are typically basaltic in composition) or externally derived by different sedimentological processes including weathering, erosion and transportation of polymodal mixture of rounded shaped gravels via high energy stream flowing into the shelter through the mouth (i.e., as exogenic particles).
- On the basis of log ratio of major element (log (SiO_2/Al_2O_3) and log (Fe_2O_3/K_2O)) contents the sediments fall in the wacke and litharenite fields, and in a Qtz-Alk-Pl Ternary diagram most of the samples plot close to the plagioclase (anorthite + albite) fields. These all indicate that the geogenic sediments are formed under low degree of chemical weathering, chemically/mineralogically immature, and characterized by an input of relatively higher proportion of mafic volcanic sources with high proportion of rocks forming less stable minerals (i.e., feldspar minerals). In addition to this, the ratio between less mobile major elements (Al_2O_3 and TiO_2) of sediments range from 3 to 6.4 wt %, suggesting that the sediments are derived predominantly from mafic source rocks as they consist (Al_2O_3/TiO_2) ratio of less than 14 wt %.

- In addition to the geogenic particles, biogenic and anthropogenic components are common particularly in some levels of the sedimentary deposits. The distribution of magnetic susceptibility value of the sediments reflects the anthropogenic input to the deposits. The result indicates that most of the magnetic anomalies are presented in the burned sediments and biogenic (bone) fragments (Zone A). Sediments with higher concentration of organic matter (anthropogenic ash and charcoal) are marked by lower value of magnetic susceptibility (Zone D). The sediments with high concentrations of P and Ca are possible an indicator of occurrences of high content of biogenic fragments/remains (bones and coprolites).

6.2. Recommendations

The recommendations offer that to expand the understanding on the provenance and sedimentation rate of the sediments which are deposited in the excavated archeological sites.

- More and detail major (i.e., Na_2O, MgO) and trace (i.e., rare earth element (REE)) element analysis is required in order to have a better understanding on the provenance of sediments.
- A detail isotope analysis (carbon dating) from each layer (lithofacies) is recommended for better understanding of the relationship of the archeological records with sedimentation rate of the deposits.

REFERENCES

Abbate and Saggri (1979). The volcanites. In Geological map of Ethiopia and Somalia (1973):1:2,000,000 and comment with major land forms, Addis Ababa, Ethiopia, 2-98.

Abbate, E., Bruni, P. and Sagri, M. (2015). Geology of Ethiopia: A Review and Geomorphological Perspectives. *Landscapes and Landforms of Ethiopia*, DOI: 10.1007/978-94-017-8026-1-2.

Addisu Assefa (2011). Mammals of the Bale Mountains National Park, Ethiopia: A Compiled and Annotated Checklist, Walia-Special Edition on the Bale Mountains. *Journal of the Ethiopian wildlife and natural history society.* Addis Ababa, Ethiopia, 350pp.

Anteneh Belayneh, Yohannes.T, and Worku.A (2013). Recurrent and extensive forest fires incidence in the Bale mountain national park, Ethiopia, extent causes and consequences. Addis Ababa, Ethiopia, **1**, 29-39.

Asfawossen Asrat, (2016). The Ethiopia Highlands. In: Anhaeusser, C.R., Viljoen, M.J. and Vijoen, R.P. (eds) Africa's Top Geological sites. Struik Nature, Cape Town, 197-206pp.

Barbera, G., Mazzoleni, P., Critelli, S., Pappalardo, A., Giudice, A.L. and Cirrincione, R. (2006). Provenance of shales and sedimentary history of the Monte Soro Unit, Sicily. *An International Journal of Mineralogy, crystallography, geochemistry, ore deposits, petrology, volcanology, **75,*** 2-3, 313-330pp.

Belay Desta, (1978). Preliminary regional geological report on the Dodola (NB 37-7) 1:250,000 scale map sheet. EIGS, unpublished report, Addis Ababa, Ethiopia.

Belda, M., Holtanová, E., Halenka, T., Kalvová, J. (2014). Climate classification revisited: from Köppen to Trewartha. *Climate research*, **59**: 1–13, Doi: 10.3354/cr01204.

Boadi, B., Preko, K. and Amekudzi, K. (2014). Implication of soil magnetic susceptibility measurements from the waste site deposits of independence Hall, Kwame Nkrumah University of science and technology (K.N.U.S.T), Kumasi. *International journal of scientific research*, **4** (5), 2250-3153.

Boccaletti, M., Mazzuoli, M., Bonini, R., Trua, T. and Bekele Abebe (1999). Plio- Quaternary volcano tectonic activity in northern sector of the Main Ethiopian Rift: Relationship with oblique rifting. *Journals of earth sciences*, **29**(4): 679-698.

Boggs, S.J. (2009). Petrology of sedimentary rocks. *United States of America by Cambridge* University Press, New York, second edition, 612pp.

Blott, S.J. and Pye, K. (2001). GRADISTAT: a grain size distribution and statistics package for the analysis of unconsolidated sediments. *Earth Surface Process and Landforms* **26**, 1237–1248, DOI: 10.1002/esp.261.

Blott, S. (2010). Grain size distribution and statistics package for the analysis of unconsolidated sediments by sieving or laser Granulometer.

Blott, S. J and Pye, K. (2012). Particle size scales and classification of sediment types based on particle size distributions: Review and recommended procedures. *Journal of the international association of Sedimentologists*, **59**, 2071–2096. Doi: 10.1111/j.1365-3091.2012.01335.

Bonini, M., Corti, G., Innocenti, F., Manetti, P., Mazzarini, F., Tsegaye Abebe and Pecskay, Z. (2005). Evolution of the Main Ethiopian Rift in the frame of Afar and Kenya rifts propagation. *Tectonics*, **24**: TC1007. Doi: 10.1029/2004TC001680.

Corti, G. (2009). Continental rift evolution: From rift initiation to incipient break-up in the Main Ethiopian Rift. East Africa. *Earth-Science Reviews*, **96**: 1–53.

Crain, E.R. (2015). X-ray Diffraction Methods. Crain's Petrophysical hand book.

Davies, B.J. (2008). British and Fennoscandian ice-sheet interactions during the quaternary. Durham University, Unpublished PhD thesis.

Dearing, J. A. (1999). Environmental Magnetic Susceptibility Using the Bartington ***MS2*** System. *British library cataloguing in publication data*.

Duane, D. (1964). Significance of skewness in recent sediments, western Pamlico Sound, North Carolina. *Journal of sedimentary petrology***, 34**(4), 864-874.

Eberz, G.W., Williams, E.M. and Williams, M.A.J. (1988). Plio-pleistocene volcanism and sedimentary facies changes at Gadeb prehistoric site, Ethiopia. *Geolodgische Rundschau*, **77**/2, 513-527.

Ebinger, C.J., Tesfaye Yemane, Gidey WoldeGabriel, Aronson, J.L. and Walter, R.C. (1993). Late Eocene Recent volcanism and faulting in the southern Main Ethiopian Rift. *Journal of the Geological Society of London*, **150**: 99–108.

Feng, R. and Kerrich, R. (1990). Geochemistry of fine-grained elastic sediments in the Archean Abitibi greenstone belt, Canada: Implications for provenance and tectonic setting. *Geochemistry of Archean sedimentary rocks*, **54**, 1061-1081.

Folk, R.L. and Ward, W.C. (1957). Brazos river bar, a study in the significance of grain size parameters. *Journals of sedimentary petrology*, **27** (1), 3-26.

Galloway, W.E., and Hobday D.K. (1996). Terrigenous Clastic Depositional Systems Applications to Fossil Fuel and Groundwater Resources. DOI: 10.1007/978-3-642-61018-9.

Gamboa, A., Montero-Serrano, J-C., St-Onge, G., Rochon, A. and Desiage, P.-A. (2017). Mineralogical, geochemical, and magnetic signatures of surface sediments from the Canadian Beaufort Shelf and Amundsen Gulf (Canadian Arctic).*Geochemistry, Geophysics, Geosystems*,**18**, Doi:10.1002/2016GC006477.

Gellis, A., Delaware, M., Fitzpatrick, F., Wisconsin and Berigan, J.S. (2016). A Manual to Identify Sources of Fluvial Sediment. US Geological survey, 117pp.

Gidey WoldeGabriel, G., Aronson, J.L. and Walter, R.C. (1990). Geology, geochronology, and rift basin development in the central sector of the Main Ethiopia Rift. *Geological Society of America Bulletin,* **102**: 439–458.

Gidey WoldeGabriel (2009). Renowned paleoanthropological areas in the Ethiopian Rift basins: Geological and paleo environmental contexts and chronology of hominid fossils and archaeology. In: *International symposium of Africa, Cradle of Humanity*; 1-33.

Gobena Hambisa, Mandefro Belayneh, Tesfaye Kebede, Samson Tesfaye and Amenti Abraham (1997). Geology of Dodola area. Geological survey of Ethiopia. Unpublished technical report, Addis Ababa, Ethiopia, Memoir**, 10**: 150pp.

Harrold, F. B., Ellwood B. B., Thacker, P. T. and Stephen, L. B (undated). Magnetic Susceptibility analysis of sediments at the Middle-Upper Paleolithic transition for two cave sites in northern Spain.

Hayes, K. (2013). Parameters in the use of pXRF for archaeological site prospection: a case study at the Reaume Fort Site, Central Minnesota. *Journal of Archaeological Science* **40** 3193-3211.

Hayward, N.J. and Ebinger, C.J. (1996). Variations in the along-axis segmentation of the Afar Rift system. *Tectonics*, **15**: 244–257.

Henry, Y.M. and Romanus, A.O. (2016). Geochemistry, classification and maturity of the sandstone facies of the Abeokuta formation, south western Nigeria. *European journal of basic and applied sciences*, **3** (2), 2059-3058.

Herron, M.M., 1988. Geochemical classification of terrigenous sands and shales from core or log data. Journal of Sediment Petrology **58(5)**, 820-829, Doi: 10.1306/212F8E77-2B24-11D7-8648000102C1865D.

Hood, D., Hatfield, R. and Patrick, C. (2018). Beta radiocarbon dating. Accredited Testing Laboratory. Iso/IEC 2005:17025.

Johnsson, M. J., 1993, The system controlling the composition of clastic sediments, in Boulder, Colorado, *Geological Society of America Special Paper* **284**, 1-19.

Kanhaiya, S., Singh, B.P., Tripathi, M., Sahu, S. and Tiwari, V. (2017). Lithofacies and particle-size characteristics of late Quaternary floodplain deposits along the middle reaches of the Ganga river, central Ganga plain, India. *Geomorphology*, **284**, 220–228.

Keranen, K. and Klemperer S.L. (2008). Discontinuous and diachronous evolution of the Main Ethiopian Rift: Implications for development of continental rifts. *Earth and Planetary Science Letters,* **265**, 96–111.

Kurkura Kabeto, Sawnda, Y. and Roser B. (2009). Compositional differences between felsic volcanic rocks from the margin and center of the northern Main Ethiopian Rift. *MEJS*, **1**(1): 4-35.

Kurz,T., Gloaguen, R., Ebinger, C., Casey, M. and Bekele Abebe (2007). Deformation distribution and type in the Main Ethiopian Rift (MER): a remote sensing study. *Journal of African Earth Sciences,* **48**: 100–114.

Lario, J., Zazo, C., Plater, A.J., Goy, J.L., Dabrio, C., Bolja, F., Sierro, F.J. and Lllque, L., (2000). Particle size and magnetic properties of Holocene estuarine deposits from the Doñana National Park (SW Iberia): evidence of gradual and abrupt coastal sedimentation. *Z. Geomorphol* **45** (1), 33-54.

Lopez, G. I. (2017). Grain size analysis. *Encyclopedia of Geoarchaeology*, 341-348, DOI 10.1007/978-1-4020-4409.

Mafteia, A.E., Dillb, H.G., Buzatuc, A., Iancuc, O.G., Buzgarc, N. and Andrášd, P. (2018). Chemical and mineralogical composition of fluvial sediments (Bistrita River, Romania): Geogenic vs. anthropogenic input into rivers on its way through mining areas. *Chemie der Erde.*

Martins, L.R. (2003). Recent sediments and grain size analysis. *Sedimentological research group,* **1**, 90-105.

Merla, G., Abbate, E., Azzaroli, A., Bruni, P., Caunti, P., Fazzuoli, M., Sagri, M. and Tacconi, P. (1979). Geological map of Ethiopia and Somalia (1973):1:2,000,000 and comment with major land forms, Addis Ababa, Ethiopia, 2-98.

Munsell, (1994). Determination of soil color. U.S.Dept. Agriculture Hand Book 18-Soil Survey Manual.

Nichols, G. (2009). Sedimentology and Stratigraphy. John Wiley & Sons, Ltd., Second Edition, 432pp.

Opitz, S. (2018). Manual for the determination of grain size distributions by using the Beckmann Coulter LS13320 laser particle size Analyzer. Cologne University, Germany.

Pejrup, M., (1988). The triangular diagram used for classification of estuarine sediments: A new approach. **In**: de Boer, P.L., (Ed.), Tide Influenced Sedimentary Environment and Facies. *Riedal Publishing*, 289-300.

Peterson, J. A. (2009). Geochemical Provenance of Clastic Sedimentary Rocks in the Western Cordillera: Utah, Colorado, Wyoming, and Oregon. *All Graduate Theses and Dissertations*, Paper 439.

Pettijohn, F.H., Potter, P.E., Siever, R., (1972). Sand and Sandstone. *Springer-Verlag,* New York, 618.

Phillips, O.A., Falana, A.O. and Adebayo, A.J. (2017). The geochemical composition of sediment as a proxy of provenance and weathering intensity: a case study of Southwest Nigeria's Coastal Creeks. *Geology, Geophysics and Environment*, **43** (3): 229–248.

Plado, J., Ainsaar, L., Dmitrijeva, M., Põldsaar, K., Ots, S., Pesonen, L.J. and Preeden, U. (2016). Magnetic susceptibility of Middle Ordovician sedimentary rocks, Pakri Peninsula, NW Estonia. *Estonian Journal of Earth Sciences*, **65** (3), 125–137.

Putz, H., Brandenburg K. G. and Kreuzherrenstr (2018). Match! - Phase Identification from Powder Diffraction, Crystal Impact, 102, 53227 Bonn, Germany.

Rollinson, H. R. (1993). Using geochemical data: Evaluation, presentation, interpretation: Longman Group UK Ltd., 97.

Seife Micahel Berhe, Berhe Desta, Nicoletti, M. and Teferra Mengesha (1987). Geology, geochronology and geodynamic implications of the Cenozoic magmatic province in W and SE Ethiopia. *Journal of the Geological Society, London,* **144**: 213- 226.

Siebert, S. (2004). The Bale Mountains of Ethiopia. *Botanizing on the roof of Africa*, Rodes university.

Silva, M.L., Batezelli, A. and Ladeira, F.S. (2017). Micromorphology of Paleosols of the Marília Formation and their Significance in the Paleoenvironmental Evolution of the Bauru Basin, Upper Cretaceous, Southeastern Brazil. *Rev Bras Cienc Solo*., 41:e0160287.

Srodon, J. (2002). Quantitative mineralogy of sedimentary rocks with emphasis on clays and with applications to K-Ar dating. *Mineralogical magazine*, **66** (5), 677-687.

Stein, R., Matthieben, J., Niessen, F., Krylov, A, Nam, S.-i. and Bazhenova, E., (2010). Towards a better (litho) stratigraphy and reconstruction of Quaternary paleoenvironment in the Amerasian Basin (Arctic Ocean). *Polarforschung* **79**, 97-121.

Swan, D., Clague, J.J. and Luternauer, J.L. (1977). Grain size statistics 1: Evaluation of The Folk and Ward Graphic Measures. Geological survey of Canada.

Switzer, A.D and Pile, J. (2015). Grain size analysis. *John Wiley and sons, Ltd.*

Tadiwos Chernet, Hart, W.K., Aronson, J.L. and Walter, R.C. (1998). New age constraints on the timing of volcanism and tectonism in the northern Main Ethiopian Rift-southern Afar transition zone (Ethiopia). *Journal of Volcanology and Geothermal Research,* **80**: 267–280.

Tanner, W.F. (1991a). Suite statistics: the hydrodynamic evolution of the sediment pool. In: Syvitski, J.P.M., (Ed.), Principles, methods and application of particle size analysis, Cambridge, Cambridge University Press, 225-236.

Tanner, W.F. (1991b). Application of suite statistics to stratigraphy and sea-level changes. In: Syvitski J.P.M., (Ed.), Principles, methods and application of particle size analysis, Cambridge, Cambridge University Press, 283-292.

Taylor, S.R. and Mclennan, S. M. (1985). *The* Continekal Crust: Irs Composition and Evolufion. *Geoscience texts*, Blackwell. Oxford.

Tiercelin, J., Gibert, E., Umer, M., Bonne, R., Robert, J., Disnar, (2008). High-resolution sedimentary record of the last deglaciation from a high-altitude lake in Ethiopia. *Quaternary Science Records*, **27** (5-6), 449-467.

Turner, J.N., Jones, A.F., Brewer, P.A., Macklin, M.G. and Rassner, S.M. (2015). Micro-XRF applications in fluvial sedimentary environ-ments of Britain and Ireland: progress and prospects. DOI: 10.1007/978-94-017-9849-5-8.

Udden JA. (1914). Mechanical composition of clastic sediments. *Bulletin of the Geological Society of America* **25**: 655–744.

Umer,M., Lamb,H.F., Bonnefille, R., Lezine, A.M., Tiercelin, J., Gibert, E., Cazet, P. and Watrin, J. (2007). Late Pleistocene and Holocene vegetation history of the Bale Mountains, Ethiopia. *Quaternary Science Reviews* **26** 2229–2246.

Varghese, T.I. (2014). Sedimentology and geochemistry of core sediments from the Ashtamudi estuary and the adjoining coastal plain, central Kerala, India. Unpublished PhD thesis. Kerala, India, 196pp.

Watson ,E.B., Pasternack, G.B., Gray, A.B., Goñi, M. and Woolfolk A.M. (2013). Particle size characterization of historic sediment deposition from a closed estuarine lagoon, Central California. *Estuarine, Coastal and Shelf Science* **126**, 23-33.

Wentworth CK. (1922). A scale of grade and class terms for clastic sediments. *Journal of Geology* **30**: 377–392.

William, R. V. (2004). Application of archaeological geophysical techniques to the investigation of British smelting sites, **2**, Unpublished PhD paper, university of Bradford, 527pp.

Wolfenden, E., Ebinger, C., Gezahegn Yirgu, Deino, A. and Dereje Ayalew (2004). Evolution of the northern Main Ethiopian Rift: birth of a triple junction. *Earth and Planetary Science Letters*, **224**: 213–228.

Workineh Haro, Daba Bulto, Mekonen Bekele, Desalegn Debelo, Muluken Kebede and Mohamed Edris (2014). Geology, geochemistry, and gravity survey of Asela area. Geological survey of Ethiopia, basic geo science mapping directorate. Unpublished technical report, Memoir, **38**: 87.

Wright, D.K., Thompson, J.C., Schilt, F., Cohen, A.S., Choi, J.H., Mercader, J., Nightingale, S., Miller, C.E., Mentzer, M.S., Walde, D., Welling, M. and Chindebvu, E.G. (2017). Approaches to Middle Stone Age landscape archaeology in tropical Africa. *Journal of archaeological science*, **77**, 64-77.

Zou, H. (2016). An X-ray diffraction approach: bulk mineral assemblages as provenance indicator of sediments from the Arctic Ocean. Unpublished PhD paper, 128pp.

Internet sources

http://en.climate-data.org/location/ accessed on 2018, May 17. Oceanic climate. In *Wikipedia, The Free Encyclopedia*. Retrieved from https://en.wikipedia.org/w/index.php?title=Oceanic_climate&oldid=841754520

http://www.crystalimpact.com/match accessed on April 10, 2018.

http://www.researchgate.net. How to convert ppm to weight percentage in case of major elements? Accessed on April 26, 2018.

APPENDIXES

Appendixes 1

Grain size analysis of sediments at Fincha Habera Section (phi scale).

Samp.Id	Dep.(cm)	Lithofa.	$SD_G(\phi)$	Mz_G (ϕ)	SK_G (ϕ)	K_G (ϕ)	D_{50} (ϕ)
FH SS 01	0-2	FHL-01	1.253	6.385	0.004	0.920	6.398
FH SS 02	2-4	FHL-02	1.779	5.651	-0.281	1.097	5.941
FH SS 03	6-7	FHL-03	2.317	4.820	-0.356	0.862	5.408
FH SS 04	4-6	FHL-04	1.979	5.829	-0.360	1.537	6.035
FH SS 05	7-9	FHL-05	1.525	5.196	-0.135	0.884	5.318
FH SS 06	9-17	FHL-06	2.233	4.446	-0.067	0.777	4.515
FH SS 07	17-19	FHL-07	2.079	5.652	-0.284	0.931	6.091
FH SS 08	19-21	FHL-07	2.131	5.483	-0.279	0.895	5.962
FH SS 09	21-23	FHL-07	2.049	5.590	-0.277	0.890	6.012
FH SS 10	23-25	FHL-07	2.074	5.465	-0.293	0.887	5.929
FH SS 11	25-27	FHL-07	2.085	5.271	-0.217	0.769	5.636
FH SS 12	27-29	FHL-07	1.990	5.573	-0.272	0.828	6.001
FH SS 13	29-34	FHL-07	1.881	5.272	-0.131	0.841	5.434
FH SS 14	34-36	FHL-08	2.075	5.109	-0.202	0.709	5.450
FH SS 15	36-39	FHL-08	1.756	5.273	-0.396	1.225	5.812
FH SS 16	39-41	FHL-08	2.156	4.712	-0.133	0.762	4.933
FH SS 17	41-43	FHL-08	1.961	5.225	-0.094	0.799	5.341
FH SS 18	43-45	FHL-08	2.037	4.653	-0.073	0.754	4.778
FH SS 19	45-47	FHL-08	2.378	3.042	0.281	0.734	2.512
FH SS 20	47-49	FHL-08	2.102	3.547	0.311	0.858	3.012
FH SS 21	49-51	FHL-09	1.363	3.576	0.378	0.849	3.253
FH SS 22	51-53	FHL-09	0.871	2.837	0.145	0.864	2.781

Appendixes 2

Formulas used to convert the elemental concentrations of major elements into the oxide forms.

$$Actual\ concentration\ of\ the\ element\ (\%) = \frac{concentration\ of\ the\ element\ (ppm)}{10{,}000}$$

$$\boldsymbol{Oxide\ concen.}\ (\%) = \frac{\boldsymbol{Actual\ concentration\ of\ the\ element}\ (\%)}{\boldsymbol{conversation\ number}}$$

$$\boldsymbol{conversation\ number} = \frac{\boldsymbol{atomic\ number\ of\ the\ element}\ (\boldsymbol{g/mol})}{\boldsymbol{molecular\ weight\ of\ the\ cpd}\ (\frac{\boldsymbol{g}}{\boldsymbol{mol}})}$$

E.g., the concentration of the element (Si) at sediment sample FH SS 01 is 154061.3ppm. In order to convert into oxide forms using the above formulas;

$$Act.\ con.\ ele.\ (\%) = \frac{con.\ of\ the\ ele.\ (ppm)}{10{,}000}$$

$$\frac{154061.3\text{ppm}}{10{,}000} = \mathbf{15.40613}\%$$

$$\boldsymbol{Oxide\ concen.\ SiO2}(\%) = \frac{\boldsymbol{Actual\ concentration\ of\ Si}\ (\%)}{\boldsymbol{conversation\ number}}$$

Where,

$$\boldsymbol{conversation\ number}\ of\ SiO2 = \frac{\boldsymbol{atomic\ number\ of\ Si}\ (g/mol)}{\boldsymbol{molecular\ weight\ of\ the\ SiO2}\ (\frac{g}{mol})}$$

$$conversation\ number\ of\ SiO2 = \frac{28.0848 g/mol}{60.0848 g/mol} = \mathbf{0.4674}$$

Then, $$\boldsymbol{Oxide\ concen.}\ \text{of}\ \boldsymbol{SiO2}(\%) = \frac{15.40613\%}{0.4674} = \underline{\mathbf{36.96\%}}$$

Appendixes 3

X-ray diffraction pattern results

X-ray diffraction pattern of sediments sample FH SS 02

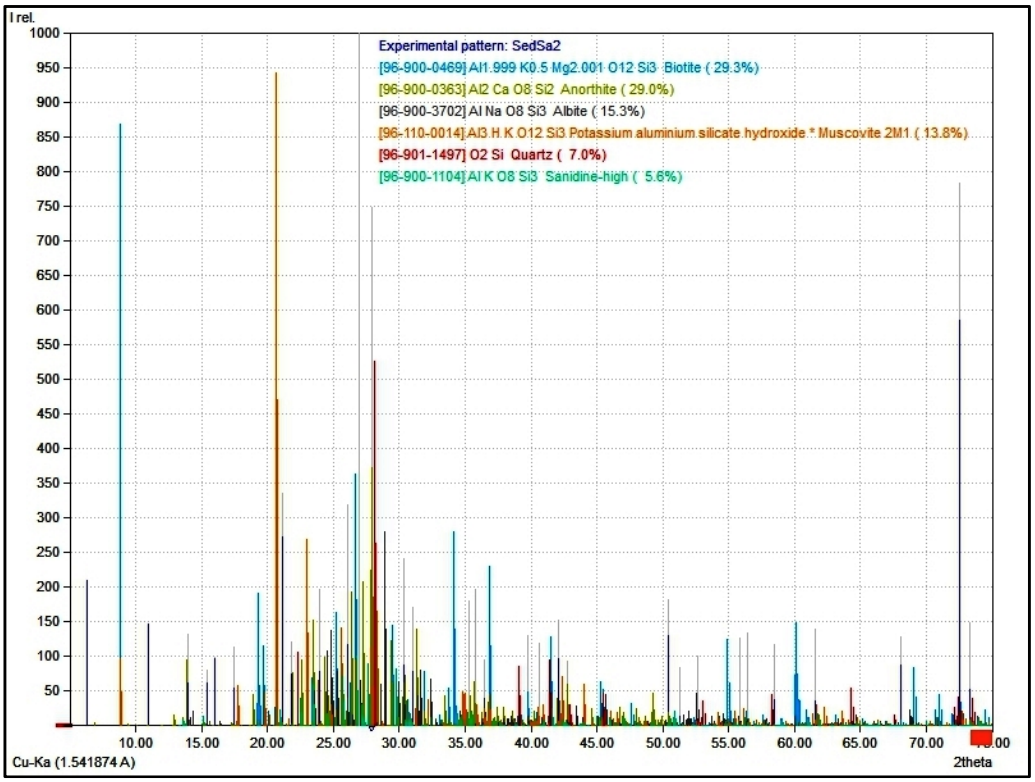

X-ray diffraction pattern of sediments sample FH SS 03

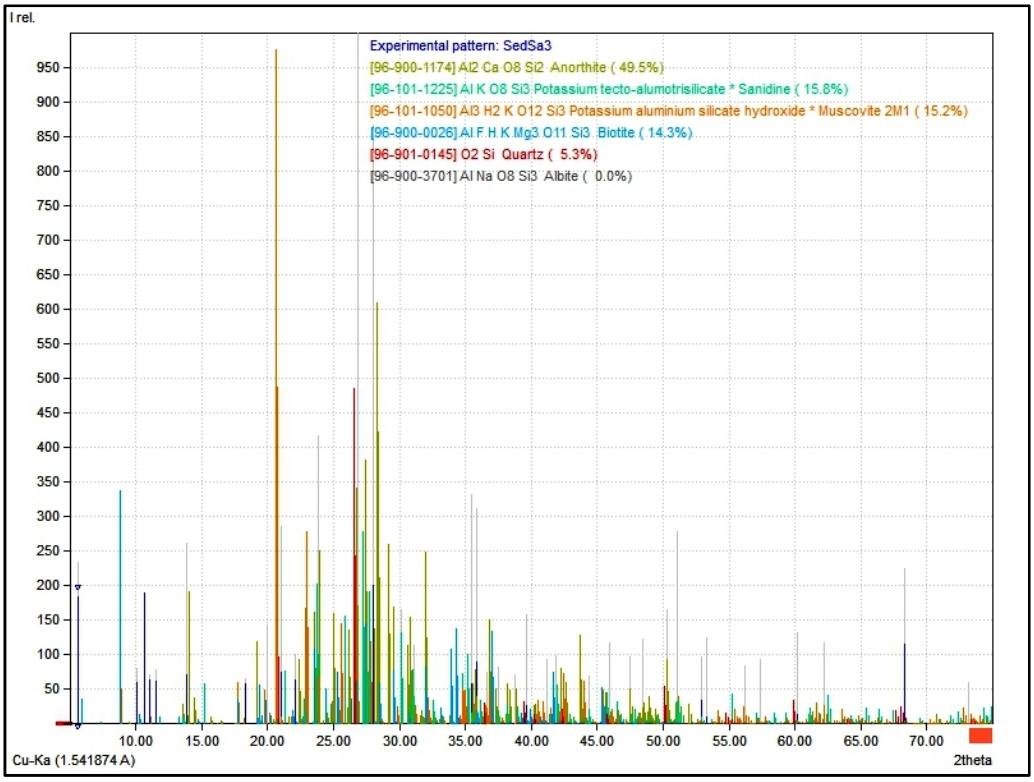

X-ray diffraction pattern of sediments sample FH SS 04

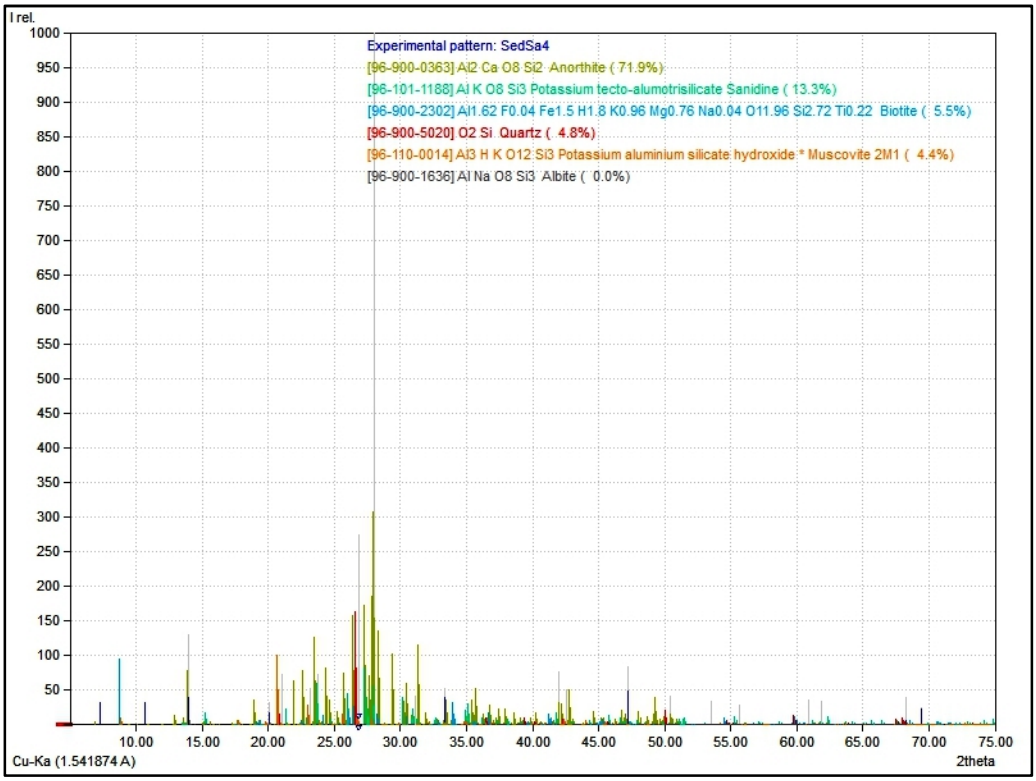

X-ray diffraction pattern of sediments sample FH SS 05

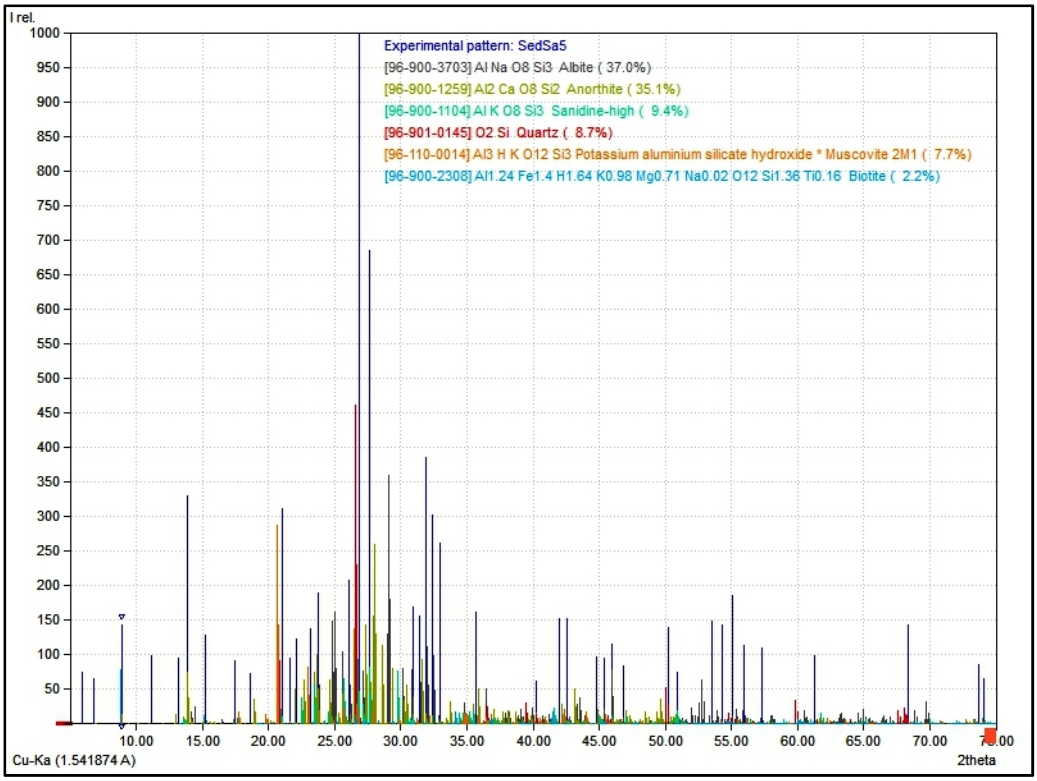

X-ray diffraction pattern of sediments sample FH SS 06

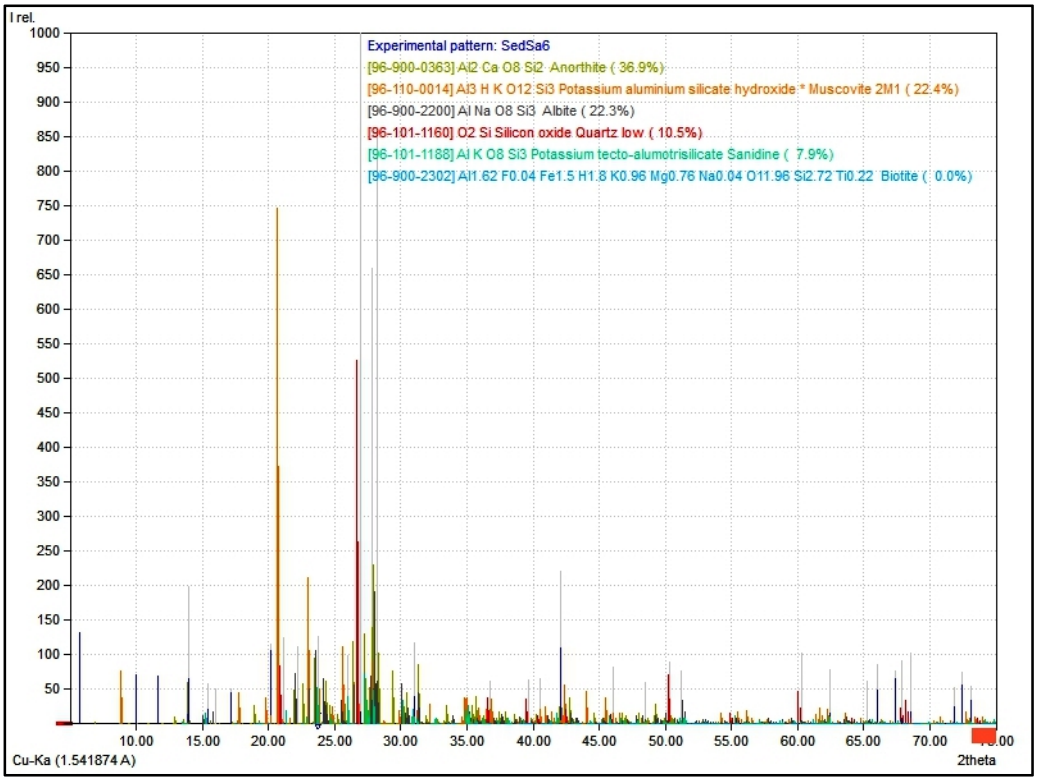

X-ray diffraction pattern of sediments sample FH SS 07

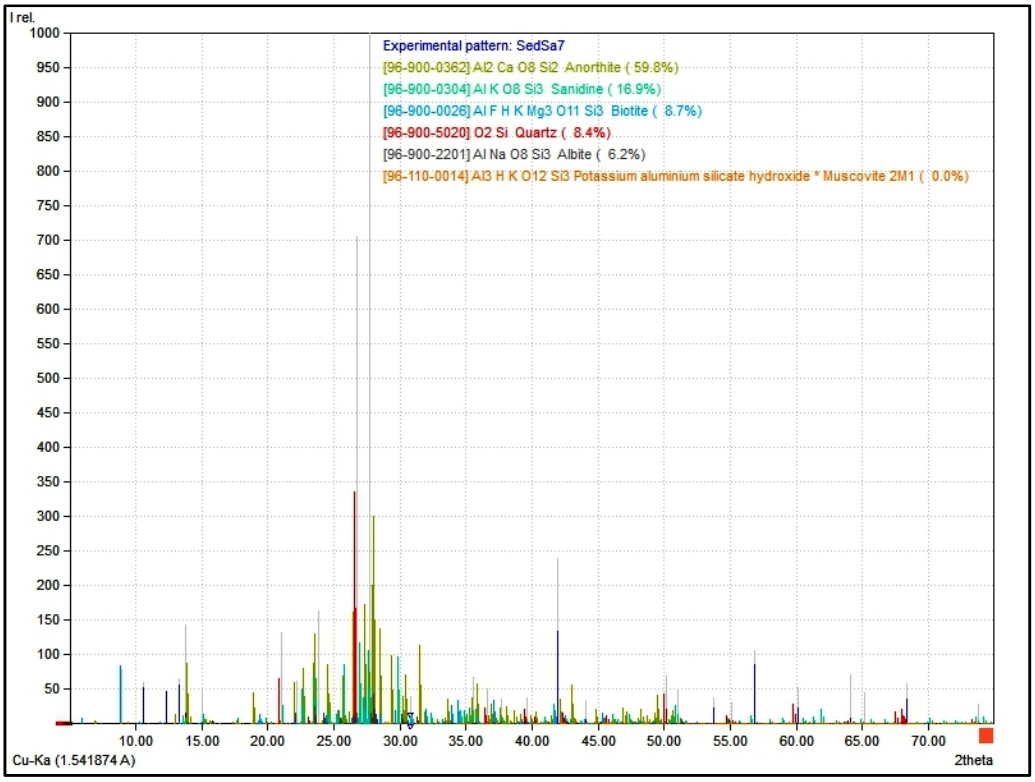

X-ray diffraction pattern of sediments sample FH SS 10

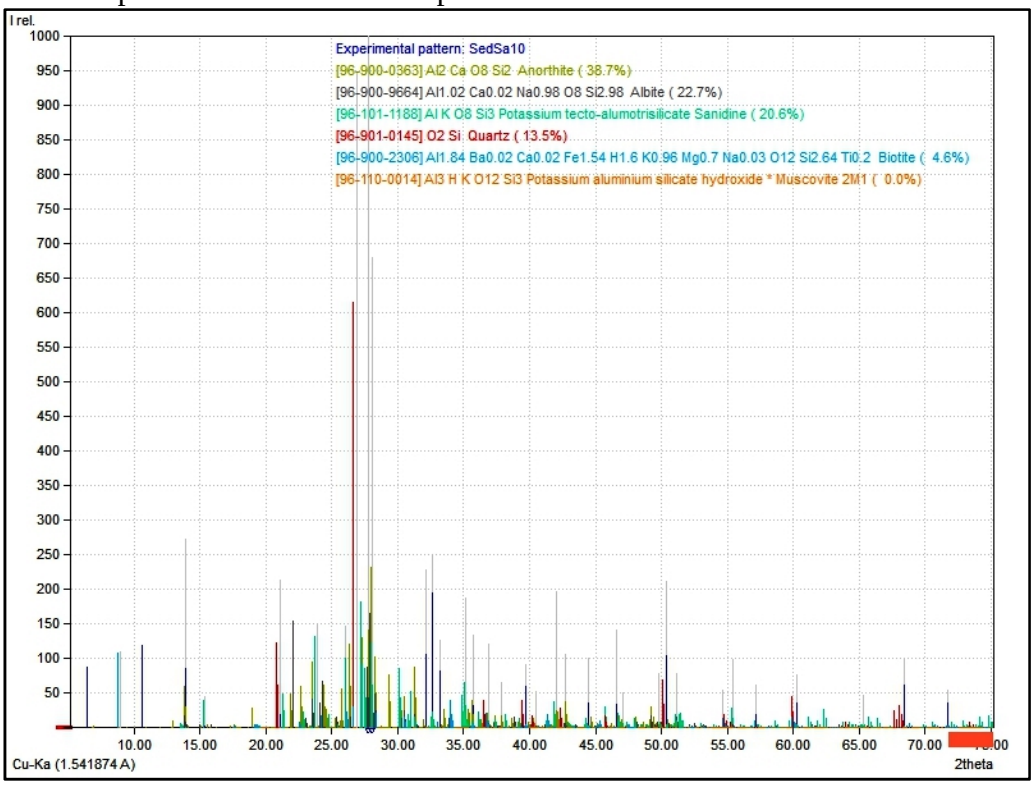

X-ray diffraction pattern of sediments sample FH SS 11

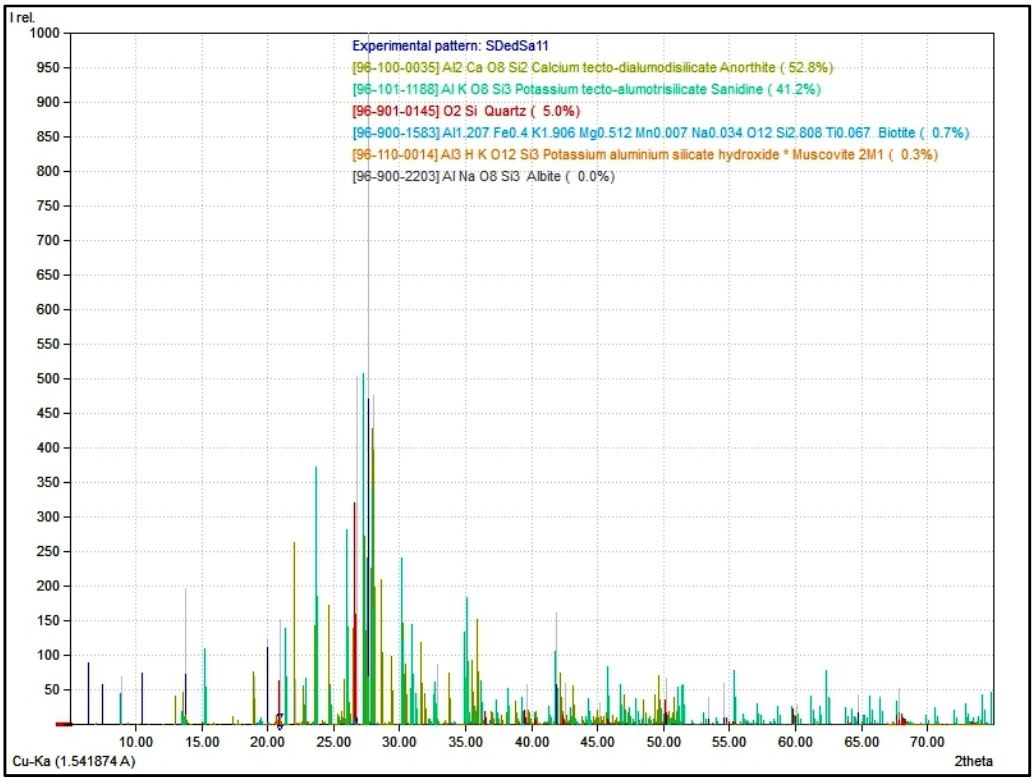

X-ray diffraction pattern of sediments sample FH SS 13

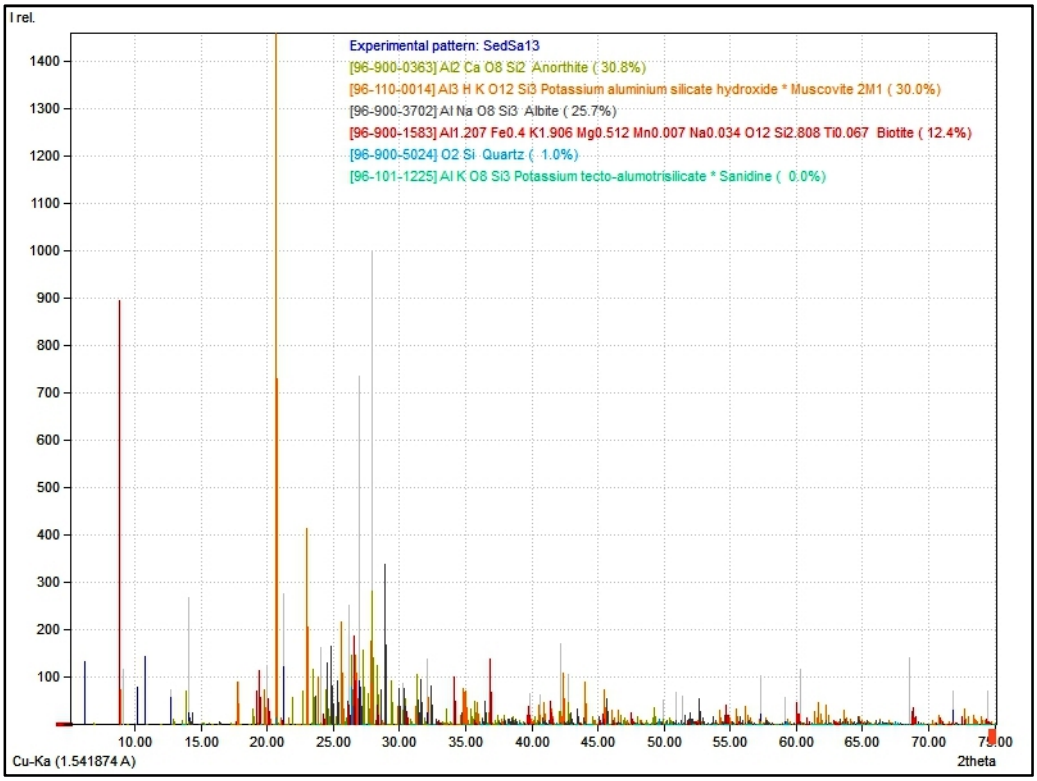

X-ray diffraction pattern of sediments sample FH SS 15

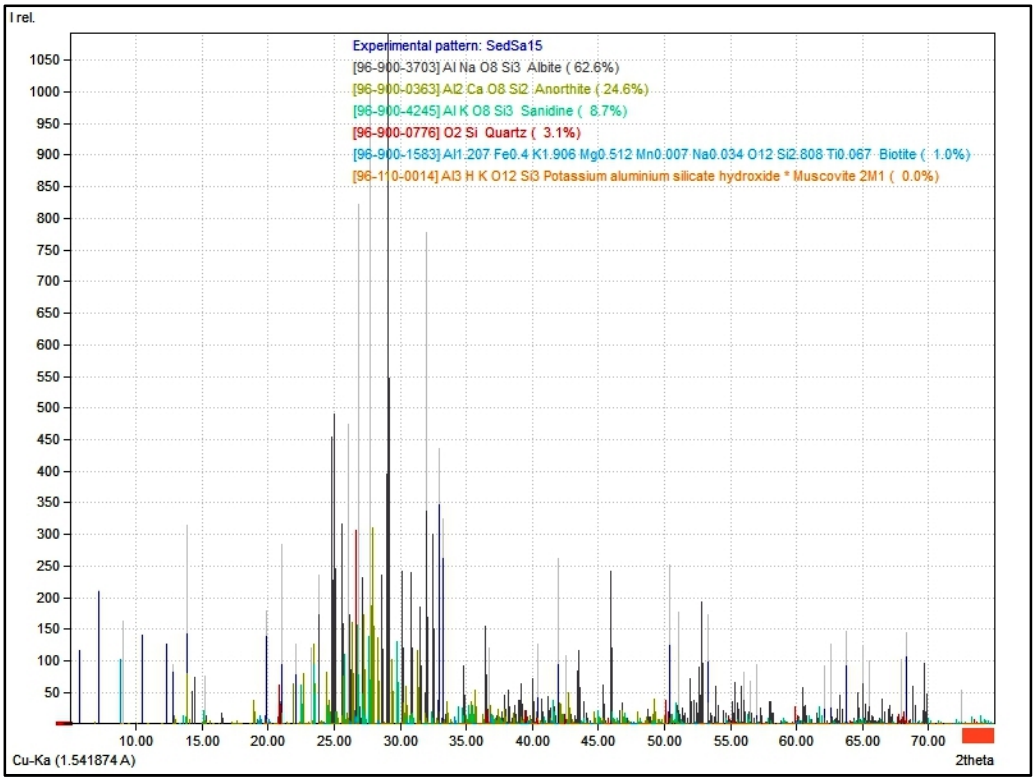

X-ray diffraction pattern of sediments sample FH SS 18

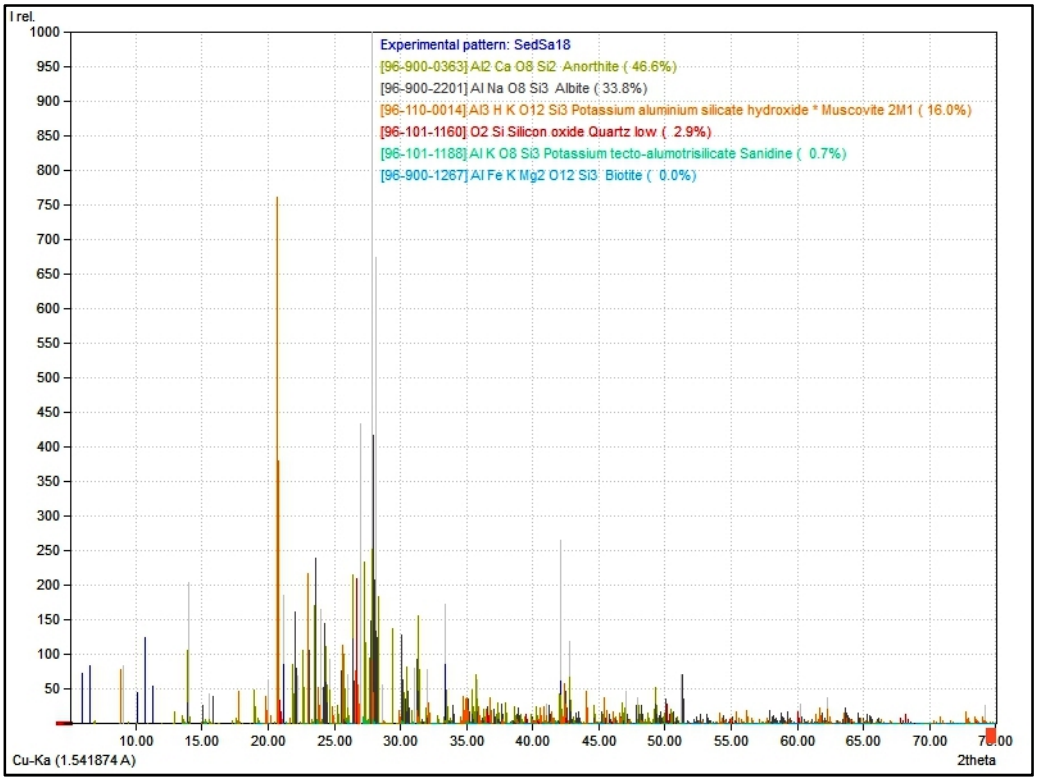

X-ray diffraction pattern of sediments sample FH SS 21

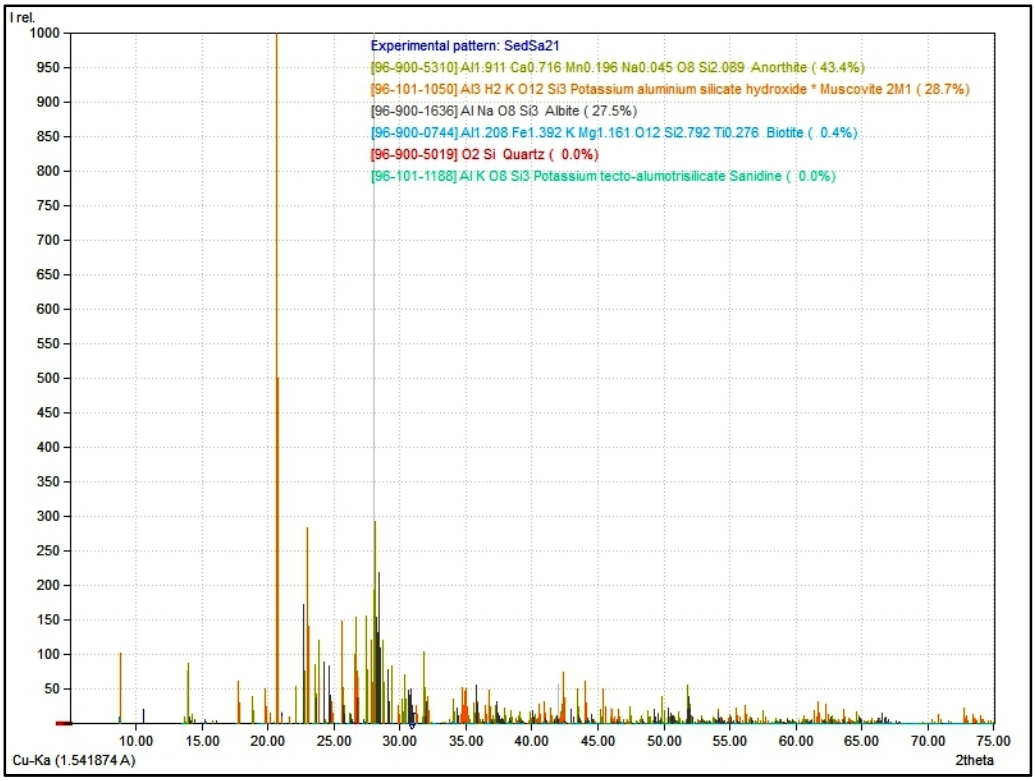

X-ray diffraction pattern of sediments sample FH SS 22